Some Contributions to the Techniques for Testing Compact Heat Exchanger Surfaces

by

John H. Stang

Technical Report No. 74

Prepared under Contract Nonr 225(91)
(NR-090-342)
for
Office of Naval Research

Department of Mechanical Engineering
Stanford University
Stanford, California

December 1970

SOME CONTRIBUTIONS TO THE TECHNIQUES FOR TESTING COMPACT HEAT EXCHANGER SURFACES

Technical Report No. 74

Prepared under Contract Nonr 225(91)
(NR-090-342)

for

Office of Naval Research

Department of Mechanical Engineering
Stanford University
Stanford, California

December 1970

Report Prepared By:

John H. Stang

Approved By:

A. L. London
Project Supervisor

ABSTRACT

Two techniques for testing compact heat exchangers are refined. They are the maximum-slope variation of the single-blow transient technique, and the regular periodic technique.

The maximum-slope method is improved by using an electronic control to produce a very fast heater response, thereby generating a sharper step change in airstream temperature. The design method for the electronic control is presented along with an experimental verification of its function. A 40 to 60 percent reduction in the heater system time constant was achieved. This produced an average increase in experimental heat transfer results of 4 percent, for four glass-ceramic matrix surfaces tested.

The periodic technique is improved by establishing guidelines for use over a range $0.2 < N_{tu} < 50$. Solutions are derived to include the effects of wall longitudinal conduction, both finite and infinite. The finite solution is incorporated into a data reduction program. Experimental heat transfer results obtained using the periodic technique are presented for a new glass-ceramic matrix surface (Core 510) in the test range $2.6 < N_{tu} < 36.6$. This range was limited by test rig capabilities with respect to air flow rate and heater power, not the test technique. Periodic technique results are compared with maximum-slope method results ($3.6 < N_{tu} < 21.3$). The agreement is excellent.

A critical comparison of the periodic and maximum-slope technique is provided. It is concluded that the periodic technique has the major advantages of

1. A very wide useful range, $0.2 < N_{tu} < 50$.
2. Easily generated experimental waves.
3. The accuracy of an integral technique.

In contrast the maximum-slope method possesses the advantages of

1. Being easy and fast to use.
2. Not requiring a digital computer for data reduction.

ACKNOWLEDGEMENTS

This material is being submitted by the author as a thesis for the degree of Engineer.

Support for this project was provided by the Office of Naval Research. The test cores were furnished by Corning Glass Works.

This study is an extension of an investigation started by the late Professor John E. Bush of Marquette University as presented in an earlier report, ref. [4].

TABLE OF CONTENTS

		Page
ABSTRACT		i
ACKNOWLEDGEMENTS		ii
REFERENCES		x
NOMENCLATURE		xii
1.	INTRODUCTION	1
2.	GENERAL OPERATION OF THE TEST RIG	3
	2.1 Introduction	3
	2.2 Heater Control Circuit	4
	2.3 Operation of the Heater Control	5
3.	HEATER ANALYSIS	11
	3.1 Description	11
	3.2 Response of the Heaters to a Simple On-Off Voltage Supply	14
	3.3 Response of the Heaters to a General Time-Varying Voltage Supply	14
4.	STEP-UP DESIGN	16
5.	STEP-DOWN DESIGN	20
6.	HEATER CONTROL PERFORMANCE	24
	6.1 Introduction	24
	6.2 Heater-Response Tests	24
	6.3 Effects on Core Heat Transfer Tests	29
7.	PERIODIC TECHNIQUE	36
	7.1 General	36
	7.2 Solution of the Governing Equations, Including the Effects of Wall Longitudinal Conduction	37
	7.3 Guidelines for Using the Periodic Technique	42

Page

7.4 Sensitivity of the Heat Transfer Results to Errors in Test Core Physical Properties. 43

7.5 Experimental Apparatus 45

7.6 Results of Testing Core 510. 47

8. COMPARING THE PERIODIC TECHNIQUE WITH THE MAXIMUM-SLOPE METHOD 52

8.1 Periodic Technique 52

8.2 Single-Blow Technique, Maximum-Slope Method. 53

8.3 Similarities 53

9. CONCLUSIONS AND RECOMMENDATIONS 55

APPENDIX I. GENERAL TEST RIG INFORMATION 57

Specification of the Test Rig 57

Circuit Layout of the Heater Control 58

Operating Instructions for the Heater Control 58

APPENDIX II. HEATER THERMAL CIRCUIT PARAMETERS AND ECAP INPUT. 62

Thermal Resistance 62

Thermal Capacitance 63

ECAP Input. 63

APPENDIX III. STEP-UP CIRCUIT ANALYSIS 65

Technique Used 65

Sample Calculation 68

APPENDIX IV. STEP-DOWN CIRCUIT ANALYSIS 72

APPENDIX V. DERIVATIONS FOR THE PERIODIC TECHNIQUE 75

Derivation of Equations 76

Solution for Wall Longitudinal Conduction Zero (λ=0). . . . 78

Solution for Wall Longitudinal Conduction Finite. 84

Solution for Wall Longitudinal Conduction Infinite 87

Page

APPENDIX VI. ERROR ANALYSIS FOR THE PERIODIC TECHNIQUE 92

Fluid Temperature Measurement, Sinusoidal Case. 92

Test Core Physical Properties 94

APPENDIX VII. DATA REDUCTION 99

Single-Blow Technique 99

Periodic Technique - Heat Transfer Calculations 103

Friction Factor Calculations. 109

Periodic Technique - Computer Program for Data Reduction. . 109

Input Formats and Nomenclature. 109

Additional Information on the Use of the Periodic-Test-Technique Data Reduction Program. 112

Description of Subroutine CONDCT. 112

Periodic Technique - Output of Test Results 119

LIST OF FIGURES

Figure		Page
2.1	Transient test rig schematic	3
2.2	Heater control power circuit schematic	5
2.3	Heater control firing circuit schematic	5
2.4	Wave shapes of the heater control circuit	8
2.5	Unijunction transistor emitter characteristic curve .	9
3.1	Thermal circuit for heater wires	11
3.2	Thermal circuit parameters used in the design of the heater control	13
3.3	Thermal energy generated as a function of voltage supplied to the heaters	13
4.1	Effects of overshooting on airstream temperature response	17
4.2	Aided step-up heater time constants from design calculations	19
5.1	The step-down response of the airstream	21
5.2	Aided step-down heater time constants from design calculations	23
6.1	Thermal circuit for a thermocouple suspended in the airstream	24
6.2	Thermocouple time constants extracted from the responses to unaided step-changes in airstream temperature	26
6.3	Aided heater time constants extracted from the responses to aided step-changes in airstream temperature	30
6.4	Comparison of aided and unaided maximum-slope results for 505A	31
6.5	Comparison of aided and unaided maximum-slope results for 505B	31

Figure		Page
6.6	Comparison of aided and unaided maximum-slope results for 505C	32
6.7	Comparison of aided and unaided maximum-slope results for 510	32
6.8	Maximum-slope correction for the experimental fluid temperature change	35
7.1	Influence of wall longitudinal conduction on the experimental amplitude attenuation	40
7.2	Influence of wall longitudinal conduction on the experimental phase shift	41
7.3	Recommended nondimensional periods for best test accuracy	44
7.4	Core 510 surface characteristics	49
7.5	Core 510 experimental adherence to the guidelines for testing	51
I-1	Backside of the heater control front panel	60
I-2	Heater control firing circuit board	60
I-3	Heater control power board	61
I-4	Schematic diagrams of banks of capacitors C_2 and C_3	61
II-1	ECAP representation of the thermal circuit	64
III-1	Approximation of the heater control circuit, step-up case	65
III-2	Effective heater control output voltage variation with triggering time	67
III-3	Heater control output voltage	67
III-4	Input to the heater wires, w = 590 lbm/hr	70
III-5	Response of the heater wires calculated using ECAP	70
IV-1	Approximation of the heater control circuit, step-down case	72

Figure		Page
V-1	Segment of an idealized heat exchanger	75
V-2	Phase shift for the fluid temperature response, $x^* = 1$, $\frac{1}{\tau} = 1.0$	86
V-3	Phase shift for the fluid temperature response, $x^* = 1$, $\frac{1}{\tau} = 2.0$	80
V-4	Phase shift for the fluid temperature response, $x^* = 1$, $\frac{1}{\tau} = 3.0$	81
V-5	Phase shift for the fluid temperature response, $x^* = 1$, $\frac{1}{\tau} = 4.0$	81
V-6	Amplitude attenuation for the fluid temperature response, $x^* = 1$, $\frac{1}{\tau} = 3.0$	82
V-7	Amplitude attenuation for the fluid temperature response, $x^* = 1$, $\frac{1}{\tau} = 4.0$	82
V-8	Amplitude attenuation for the fluid temperature response, $x^* = 1$, $\frac{1}{\tau} = 5.0$	83
V-9	Amplitude attenuation for the fluid temperature response, $x^* = 1$, $\frac{1}{\tau} = 6.0$	83
V-10	Sample of the time-varying temperatures at the test matrix exit, $x^* = 1$	89
V-11	Sample of the temperature profile along the test matrix longitudinal axis at time, $\theta^*/\tau = 0$	89
V-12	Sample of the time-varying temperature difference $(T_f^* - T_w^*)$ at the test matrix exit, $x^* = 1$	90
VI-1	Error in N_{St} or N_{tu} relative to an error in core specific heat	98

LIST OF TABLES

Table		Page
2.1	Components used in the electronic heater control	7
6.1	Heat transfer data curve fits, for aided and unaided step-change comparison	34
7.1	Amplitude spectrum of the input temperature wave, normalized to the first harmonic, w = 312 lbm/hr	46
7.2	Core 510 surface geometry and weight	47
7.3	Summary of basic heat transfer and flow friction characteristics for core 510	50
I-1	Stanford transient test rig specifications	57
I-2	Capacitor settings	59
II-1	ECAP program input sample.	64
V-1	Constant ϵ_1 in the solution for the periodic technique with finite wall longitudinal conduction	85
V-2	Constant ϵ_2 in the solution for the periodic technique with finite wall longitudinal conduction	86
VII-1	Nomenclature for single-blow heat transfer results . . .	100
VII-2	Single-blow heat transfer results	101
VII-3	Periodic transient test technique data reduction program	113
VII-4	Nomenclature for periodic technique results.	119
VII-5	Periodic technique experimental results	120

REFERENCES

1. Locke, G. L., "Heat Transfer and Flow Friction Characteristics of Porous Solids," Report No. TR-10, Dept. of Mechanical Engineering, Stanford University, Stanford, California, 1950.

2. Bell, J. C. and Katz, E. F., "A Method for Measuring Surface Heat Transfer Using Cyclic Temperature Variations," Heat Transfer and Fluid Mechanics Institute, Berkeley, California, 1949.

3. Kohlmayr, G. F., "Extension of the Maximum Slope Method to Arbitrary Upstream Fluid Temperature Changes," Trans. ASME, J. of Heat Transfer, Vol. 90, 1968, p. 176.

4. Stang, J. H. and Bush, J. E., "The Periodic Technique for Testing Compact Heat Exchanger Surfaces," Report No. TR-67, Dept. of Mechanical Engineering, Stanford University, Stanford, California, 1968.

5. Wheeler, A. J., "Single-Blow Transient Testing of Matrix-Type Heat Exchanger Surfaces at Low Values of N_{tu}," Report No. TR-68, Dept. of Mechanical Engineering, Stanford University, Stanford, California, 1968.

6. "SCR Manual," Fourth Edition, General Electric Semiconductor Products Department, Syracuse, New York, 1967.

7. "Specification Sheet No. 60.62," General Electric Semiconductor Products Department, Syracuse, New York, 1963.

8. "1620 Electronic Circuit Analysis Program," Publication No. H20-0170-1, IBM Technical Publications Department, White Plains, New York, 1965.

9. McAdams, W. H., Heat Transmission, Third Edition, McGraw-Hill Book Co., Inc., New York, 1954.

10. "Tables of Thermal Properties of Gases," U.S. Dept. of Commerce, National Bureau of Standards, Circular 564, Nov. 1, 1955.

11. Kohlmayr, G. F. and Lombari, D., "A Short Table of Maximum Slopes for Transient Matrix Heat-Transfer Testing," Trans. ASME, J. of Heat Transfer, Vol. 92, 1970, pp. 558-559.

12. Pucci, P. F., Howard, C. P., Piersall, C. H., "The Single-Blow Transient Testing Technique for Compact Heat Exchanger Surfaces," Trans. ASME, J. of Engineering for Power, Vol. 89, 1967, pp. 29-40.

13. Perry, Chilton, Kirkpatrick, Perry's Chemical Engineer's Handbook, Fourth Edition, McGraw-Hill Book Co., Inc., New York, 1963.

14. Kays, W. M. and London, A. L., Compact Heat Exchangers, Second Edition, McGraw-Hill Book Co., Inc., New York, 1964.

15. London, A. L., Young, W. B. O., Stang, J. H., "Glass-Ceramic Surfaces, Straight Triangular Passages--Heat Transfer and Flow Friction Characteristics," Trans. ASME, J. of Engineering for Power, Vol. 92, Oct. 1970.

16. Scarborough, J. B., Numerical Mathematical Analysis, Sixth Edition, Johns Hopkins Press, Baltimore, Maryland, 1966.

1. Shah, R. K., "Data Reduction Procedures for the Determination of Convective Surface Heat Transfer and Flow Friction Characteristics--Steam-to-air Test Cores," Report No. TR-64, Dept. of Mechanical Engineering, Stanford University, Stanford, California, 1967.

NOMENCLATURE

English Letter Symbols

A	Test core heat transfer area
A, B, a, b	Fourier coefficients
A_c	Test core minimum free-flow area
A_{fr}	Test core total frontal area
A_w	Cross-sectional area for wall longitudinal conduction
C_f	Flow-stream capacity rate (wc_p)
C_w	Wall total thermal capacity ($M_w c_w$)
C	Electrical capacitors
c	Specific heat
c_p	Specific heat at constant pressure
c_w	Specific heat of core solid material
d^*	Cell height/cell width
D_f	Amplitude attenuation of fluid temperature wave
D_h	Hydraulic diameter of internal passage ($D_h = 4r_h = 4A_c L/A$)
D_w	Amplitude attenuation of wall temperature
ECAP	Electronic Circuit Analysis Program
f	Friction factor
G	Mass velocity (w/A_c)
h	Average unit conductance for thermal-convection heat transfer
i	Enthalpy
j	$N_{St} N_{Pr}^{2/3}$
k	Thermal conductivity
K	Number of data points taken in a test

K_c, K_e	Contraction and expansion loss coefficients for flow at exchanger entrance and exit.
L	Total heat exchanger flow length
M	Mass
MS	Maximum slope
N	Cell count for matrix
N_R	Reynolds number ($4r_h G/\mu$)
N_{St}	Stanton number (h/Gc_p)
N_{Nu}	Nussett number ($4r_h h/k$)
N_{Pr}	Prandtl number ($c_p \mu/k$)
N_{tu}	Number of transfer units for an exchanger, (hA/C_f)
P	Pressure
p	Porosity
q	Heat transfer rate
R	Heat transfer thermal resistance or electrical resistor
r_h	Hydraulic radius
SCR	Silicon controlled rectifier
T	Temperature
t	Wall thickness to adiabatic surface
T_m	Mean temperature for system
T^*	Nondimensional temperature
$\dot{U}$	Rate of change of internal energy stored
UJT	Unijunction transistor
V	Voltage
w	Mass flow rate
x	Axial flow coordinate

x^*	Nondimensional axial flow coordinate (x/L)
Z	Generalized space coordinate ($x^* N_{tu}$)

Greek Letter Symbols

α	Ratio of total heat transfer area of exchanger to volume of exchanger
β	A phase shift, defined in Eq. (V-20)
γ	Phase shift of fluid temperature wave
Δ	Small quantity or change
ΔT_o	Temperature amplitude of fluid at inlet
$\epsilon_1 \epsilon_2$	Constants used in the periodic technique finite wall longitudinal conduction solution
$\epsilon_3 \epsilon_4$	Constants used in the periodic technique infinite wall longitudinal conduction solution
μ	Viscosity
ρ	Density
θ	Time
θ_H	Time constant of heaters
θ_{TC}	Time constant of thermocouples
θ_o	Period of oscillation
θ^*	Nondimensional time ($\theta/R\bar{C}_w$)
λ	Wall longitudinal conduction parameter ($k_w A_w / LC_f$)
Φ	Nondimensional period $\left(\frac{1}{2\pi} \frac{\theta_o}{R\bar{C}_w}\right)$
ω^*	$= N_{tu}/\Phi = \left(\frac{2\pi}{\theta_o} \frac{\bar{C}_w}{C_f}\right)$

Subscripts

expr.	Experimentally obtained value
f	Fluid
H	Heater
i	Index subscript
m	Mean value
TC	Thermocouple
w	Wall
1	Upstream, $x^* = 0$
2	Downstream, $x^* = 1$
∞	Free stream value

1. INTRODUCTION

There is currently an increasing emphasis on the development of the regenerative gas turbine engine for vehicular application. One of the many advantages over its piston engine competitor is the potential for low exhaust gas emissions (smog). Several regenerator designs incorporate a periodic flow type heat exchanger with a matrix surface. To size the matrix surface, designers need to know the basic flow friction and heat transfer characteristics of the surface. Heat transfer characteristics can be obtained experimentally from an analysis of the transient response of a test core.

There are several variations of the transient technique which in application require an experimental apparatus and an appropriate mathematical model. The term mathematical model as used in this report consists of the specified idealized system including the boundary conditions and additionally the differential equations, and the solution. Heat transfer characteristics are determined by matching the experimentally established temperature variation of the fluid leaving the matrix with a similar theoretical result from the mathematical model. The mathematical models used commonly are for the step function input proposed by Locke [1][1] and others, and the periodic function input originally considered by Bell and Katz [2]. These models require that the input temperature waveform used in developing the theoretical results, be produced by the experimenter. This is especially difficult in the case of the step function.

There are two ways of correcting for errors in heat transfer results associated with non-step inputs, analytical and experimental. Analytical correction involves changing the test experimental results by an amount corresponding to the deviation from the true step function. Kohlmayr [3] has done this by extending Locke's maximum-slope method to arbitrary

[1] Bracketed numbers refer to references listed on page x.

upstream fluid temperature changes. However his findings presented in [3] have not been experimentally validated. Experimental correction involves developing a test rig which will more closely approach the step function input. This approach is desirable since a somewhat speculative theoretical "correction" does not need to be applied to the test results.

The periodic technique was considered in detail by Stang and Bush [4] for low values of N_{tu} (i.e. $0.4 < N_{tu} < 4.8$). The technique was found to be practical and further development to extend it to higher values of N_{tu} was recommended.

The objectives of this study are to:

1. Design and build a heater control which when connected to the Stanford transient test rig will produce a step in temperature which more closely approaches a true step function.
2. Experimentally validate the operation of the new heater system.
3. Examine possible changes in heat transfer results caused by using the heater control.
4. Further develop the periodic technique so that it will be usable in the test range $0.2 < N_{tu} < 50$.
5. Develop a mathematical model for the periodic technique which will account for the influence of wall longitudinal conduction.
6. Develop a practical data reduction procedure for the periodic technique.
7. Compare heat transfer results obtained using the periodic technique and the maximum-slope method.

2. GENERAL OPERATION OF THE TEST RIG

2.1 Introduction

The transient test technique uses one fluid stream flowing through a test matrix. The general schematic diagram of a transient test rig such as that used at Stanford is given in Fig. 2.1. Details of this design are provided by Wheeler [5]. Appendix I provides detailed specifications for the rig components.

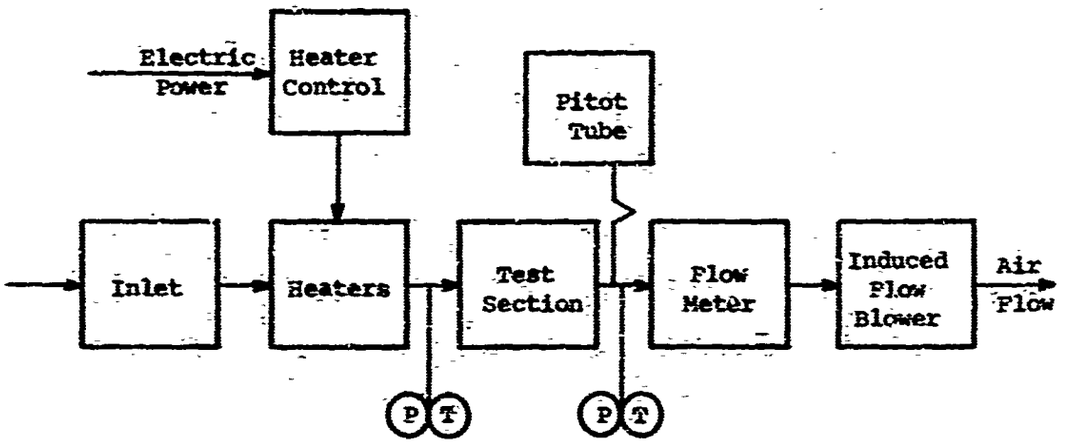

Figure 2.1 Transient Test Rig Schematic

Functions of the various elements are:

1. Inlet - Smooth out variations in fluid velocity and temperature and provide a smooth transition to flow in a duct.
2. Heaters - Provide an input temperature response for the air-stream entering the test section.
3. Heater Control - Regulate electric power to heaters.
4. Test Section - Contains the test matrix.

5. Flow Meter - Measure accurately the air flow rate through the test section.

6. Blower - Induces air flow through the system.

7. (P)(T) - Pressure and temperature sensors.

8. Pitot Tube - Two-dimensional velocity traverse downstream of the test core.

The designs of the inlet, heaters, test section, blower, and pressure and temperature sensors are described in [5].

When the heater is energized it functions so as to produce either a step-change or a cyclically varying temperature in the steadily flowing airstream. The single-blow transient technique employs the step-change. The periodic technique uses the cyclically varying temperature.

An approximate step-change in temperature may be obtained by simply connecting or disconnecting an electric power source. This tends to produce an exponential type of temperature change, pointed out in [5] and shown in Section 3.

Cyclic temperature variation may be obtained by using a DC generator and varying the field strength. Another possibility would be to use a variable transformer, driven mechanically. These could be rather unwieldy and another arrangement using electronic circuitry was employed. The electronic heater control circuit is described in the following section.

2.2 Heater Control Circuit

The circuit in Figs. 2.2 and 2.3 was designed to provide an approximate step-change in temperature which has a short rise-time (< 0.05 sec). The electronic circuitry of Fig. 2.3 accomplishes this by special regulation of the electrical power supplied to the heaters. The basis for the design and its test results are discussed at length in Sections 3 through 6 and Appendices II, III, and IV. The circuit has the additional capability of generating a cyclic temperature variation when an appropriate cyclically-varying resistor is used (Periodic Input. Fig. 2.3).

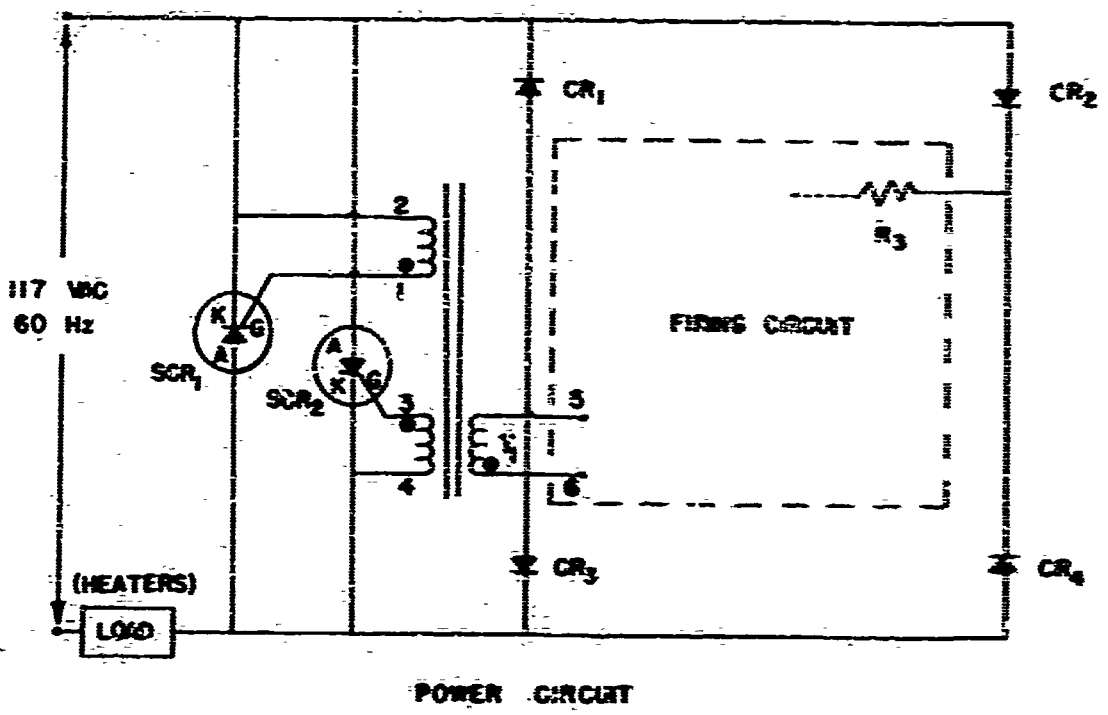

Figure 2.2 Heater Control Power Circuit Schematic.

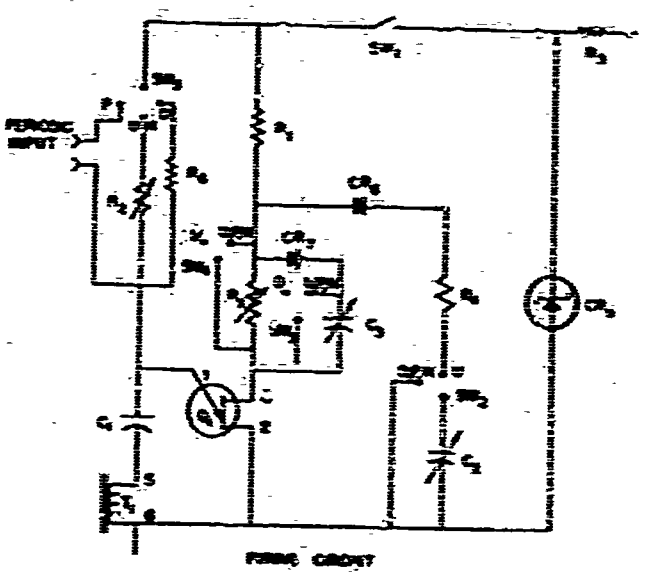

Figure 2.3 Heater Control Firing Circuit Schematic.

A list of the components used in the heater control circuit is given in Table 2.1. Capacitors C_2 and C_3 are banks of fixed capacitors connected using manually set rotary switches. Schematics of the switching diagrams and capacitor banks are included in Appendix I.

The descriptions of the positions of switches 2 through 5 in Fig. 2.3 are:

D - step-down in airstream temperature

U - step-up in airstream temperature

P - cyclic variation of airstream temperature

N - normal airstream temperature response obtained by simply turning the electric power on-off.

Nomenclature for the silicon controlled rectifier (SCR) leads is: K cathode, A anode, and G gate.

2.3 Operation of the Heater Control

Wave shapes, showing the operation of key elements in the heater control circuit, are sketched in Fig. 2.4. They may be used as an aid in understanding the operation of the circuit, or as a guide in troubleshooting or checking-out a newly constructed circuit.

The basic electric supply is 117 volts AC, 60 Hz. This sets a limit on the amount of electric power available to the heaters, which have an electrical resistance of 5 ohms. The basic AC supply is full-wave rectified by CR_1, CR_2, CR_3, and CR_4 and applied to the firing circuit, Fig. 2.3. The voltage applied to the firing circuit is then "clamped" or held almost constant by zener diode, CR_5. The effect of this clamping is to supply the firing circuit with a good approximation of a DC voltage source.

The DC voltage is applied to the series resistance-capacitance network formed by R_2 and C_1. The voltage across C_1 will be a simple exponential function of time, dependent on the magnitude of the manually variable R_2. This voltage formed across C_1 is applied to the emitter of unijunction transistor Q_1 (lead 1).

Table 2.1

COMPONENTS USED IN THE ELECTRONIC HEATER CONTROL

Component	Description
SCR_1, SCR_2	GE C35B, Silicon Controlled Rectifier
CR_{1-4}, CR_6, CR_7	GE 1N1694, Rectifier Diode
CR_5	GE Z4XL22, Zener Diode, 22 volts
Q_1	GE 2N2646, Unijunction Transistor
T_1	UTC H51, Pulse Transformer
R_1	390 Ω, 1 watt
R_2	100 K, Linear Taper Pot
R_3	3300 Ω, 5 watt
R_4	470 Ω, 2 watt
R_5	2000 Ω, Linear Taper Pot
R_6	39 K Ω, 2 watt
C_1	0.22 μF
$C_{2,1}$	6 μF
$C_{2,2} - C_{2,12}$	0.5 μF
$C_{3,1}$	150 μF
$C_{3,2}$	100 μF
$C_{3,3}$	80 μF
$C_{3,4}$	60 μF
$C_{3,5}$, $C_{3,6}$, $C_{3,11}$	40 μF
$C_{3,7}$	25 μF
$C_{3,8}$	20 μF
$C_{3,9}$, $C_{3,10}$	10 μF
SW_1	SPST Toggle Switch
$SW_2 - SW_5$	Rotary Switch, 4-position
SW_{C2}, SW_{C3}	Rotary Switch, modified to function as described in Appendix I.

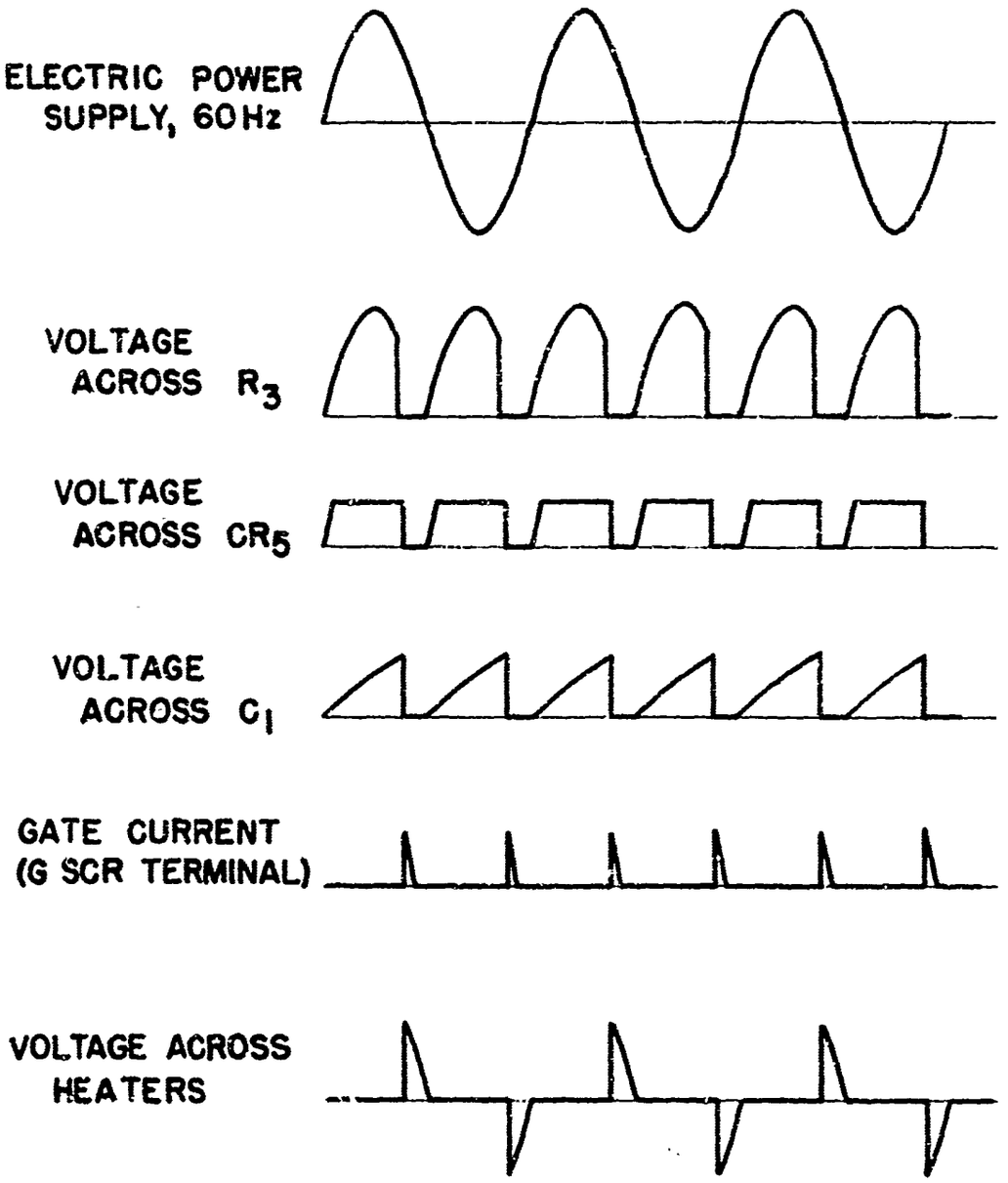

Figure 2.4 Wave Shapes of the Heater Control Circuit.

The unijunction transistor (UJT) has a unique electrical characteristic which is very useful in this application. It has a stable firing voltage, called V_p, which is a fixed fraction of the interbase voltage V_{BB} (lead 4 to 2). This characteristic is shown in Fig. 2.5:

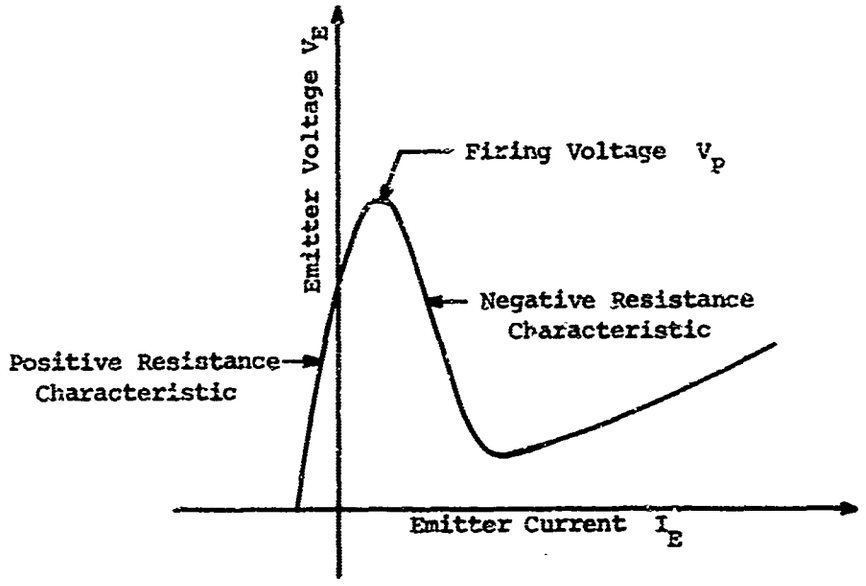

Figure 2.5 Unijunction Transistor Emitter Characteristic Curve

As the emitter voltage V_E (lead 1 to 2) increases from zero, the emitter current I_E becomes less negative and then slightly positive. The emitter in this region behaves much like a high passive positive resistor. When V_E reaches the firing voltage V_p, the UJT fires. This is characterized by the negative resistance region in Fig. 2.5. Firing allows the capacitor C_1 to rapidly discharge through one winding of the pulse transformer T_1. A pulse voltage is then induced across the gates of the SCR's. Fig. 2.4 illustrates the gate current wave shape. The resulting gate current triggers the forward biased silicon controlled rectifier (SCR_1 or SCR_2) into conduction.

The silicon controlled rectifier (SCR) is a unidirectional semiconductor switch, a p-n-p-n device. In its blocking state, current does

not flow in either direction. However, if a small current pulse (typically 3 volts for 10 to 50 microseconds) is applied from the gate G to the cathode K while the device is forward biased, turn-on will occur and the device will become conducting. Conduction will continue until the current drops below about 100 mA or reverses. In the reverse biased direction, the SCR acts like a simple diode and blocks current flow. Because of the very fast turn-on time (can be considered instantaneous), it is possible to trigger an SCR into conducting during an intermediate point on the AC wave. The SCR may be repeatedly triggered, cycle-after-cycle, at a regulated fraction of each AC cycle. The result is a control on electric power, called AC Phase Control. The circuit shown in Figs. 2.2 and 2.3 is a full-wave phase control circuit requiring the use of 2 SCR's. Ref. [6] contains a broad discussion of theory, ratings, and applications of the SCR, including some basic AC phase control circuits.

The unijunction transistor firing voltage V_p is a function of the interbase voltage V_{BB}. The specification sheet [7] for UJT 2N2646 lists this function as typically

$$V_p = 0.65\ V_{BB} + 0.5 \qquad (2.1)$$

The interbase characteristic is very much like a simple resistance if $I_E \approx 0$. The firing voltage function and the interbase characteristic will be used in the analysis of later sections. By regulating V_{BB}, or the time required for the voltage across C_1 to reach V_p, the firing time or phase in each AC wave can be controlled. The resulting AC phase control unit will be used as the heater control. The steady-state output level of the heater control utilizes the time required for voltage across C_1 to reach V_p, to determine its magnitude and is controlled mainly by R_2. An initial power surge (or lack of it in the step-down condition), required to very quickly bring the heaters to steady-state, uses the variable regulation of V_{BB}. This later type of electrical heater power regulation will be termed the AIDED condition in the sections which follow. In summary, the heater control sharpens the step-change by applying an electric power surge (in the aided step-up case) or by delaying the lower level steady-state power (in the aided step-down case).

3. HEATER ANALYSIS

3.1 Description

The low thermal capacitance airstream heaters are described fully in [5]. A brief description follows. The heater system consists of four banks of resistance wires electrically in parallel suspended across the airstream, about 1.3 inches apart in series flow. The wire is 0.003 inch diameter alumel. Each bank has 182 inches of wire in 56 passes, each 3.25 inches long. The wire passes are electrically in series.

Thermal expansion of the wire (about 0.01 inches per 3.25 inch pass) occurs during operation. To take up the slack each pass of wire is looped over an extended cantilever spring support. Spring deflection maintains wire tension in both the heated and unheated states.

Heater wire temperature and heat flow to the surrounding airstream may be analyzed using the thermal circuit in Fig. 3.1.

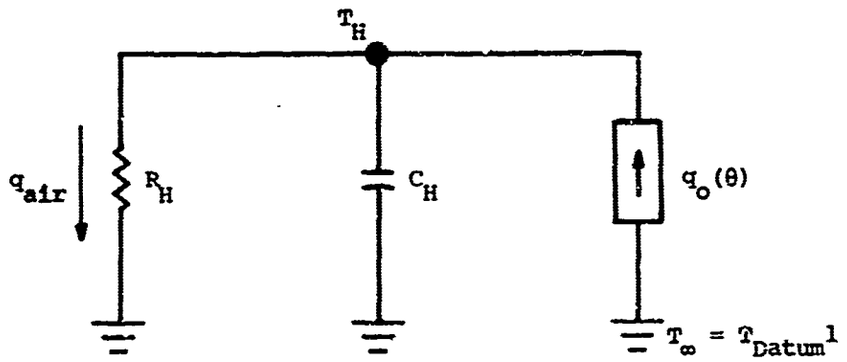

Figure 3.1 Thermal Circuit for Heater Wires

[1] With respect to the T_H variation, the air temperature T_∞ can be treated as constant and used as a datum (see idealization (4) to follow).

Idealizations used in the heater analysis are:

1. Wire temperature is uniform and responds as a single lump.
2. Thermal resistance R_H is a function if air flow rate only.
3. Thermal capacitance C_H is a constant.
4. The airstream temperature change in heating ($\approx 20°F$) is small compared to T_H ($\approx 300°F$ above the air termperature).

The thermal resistance for convective heat transfer from the heater is defined:

$$R_H \triangleq \frac{1}{(hA)_H} \tag{3.1}$$

The thermal capacitance of the heaters is calculated using

$$C_H = (Mc)_H \tag{3.2}$$

Actual values for R_H and C_H are shown in Fig. 3.2 and are calculated in Appendix II.

Thermal energy rate generated by the electrical resistance of the heaters, $q_o(\theta)$, is plotted in Fig. 3.3. The figure shows this energy rate as a function of the voltage impressed by the heater control. In turn the voltage can be regulated to be a function of time.

The heater in Fig. 3.1 has a temperature response, T_H, expressed in equation form as

$$\frac{T_H - T_\infty}{R_H} + C_H \frac{d(T_H - T_\infty)}{d\theta} = q_o(\theta) \tag{3.3}$$

The energy rate (thermal current) flowing through the convective resistance R_H is delivered to the airstream. Air temperature rise across the heater, can then be calculated using the following energy balance on the airstream:

$$wc_p[T_f(0,\theta) - T_\infty] = \frac{T_H - T_\infty}{R_H} \tag{3.4}$$

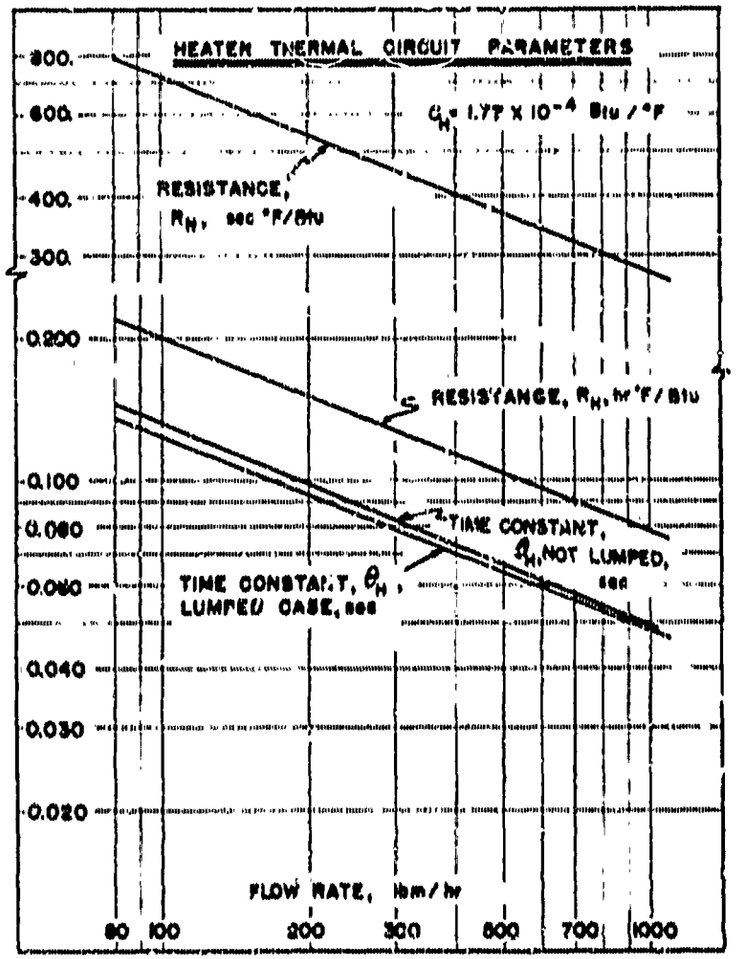

Figure 3.2 Thermal Circuit Parameters Used in the Design of the Heater Control.

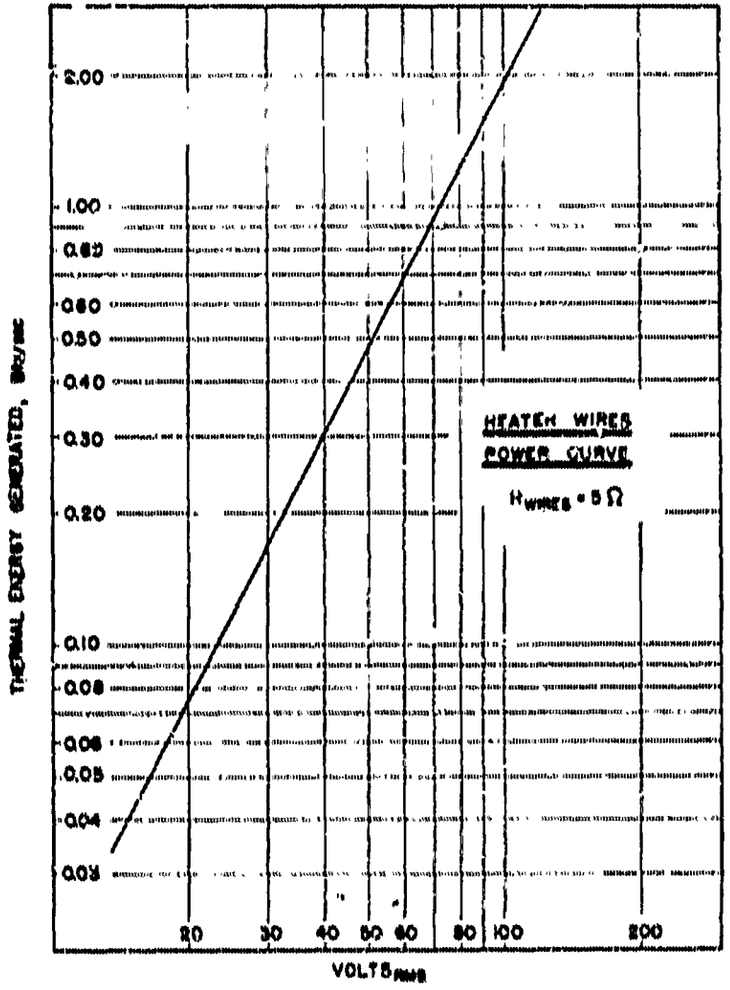

Figure 3.3 Thermal Energy Generated as a Function of Voltage Supplied to the Heaters.

3.2 Response of the Heaters to a Simple On-Off Voltage Supply

If a constant electric voltage, connected to the heater wires, is simply switched on and off, the thermal energy generated, $q_o(\theta)$, will be a step function. The solution to Eq. (3.3), combined with Eq. (3.4), is

$$\frac{T_f(0,\theta) - T_f(0,\infty)}{T_f(0,0) - T_f(0,\infty)} = \exp(-\theta/\theta_H) \qquad (3.5)$$

where $\theta_H \triangleq R_H C_H$. Thus while the $q_o(\theta)$ is a step function, the air response is an exponential. The quantity θ_H is called the time constant of the heaters and is plotted in Fig. 3.2 for the lumped case. As $\theta_H \to 0$, a step-change in temperature is approached.

Fig. 3.2 presents another time-constant curve for the case where the four banks of heater wires are not considered to respond as a lump. The heaters are considered as four distinct banks, sequentially placed in the airstream. Each bank contributes about 25 percent to the total temperature rise of the air. The analysis in this case becomes more complicated. The airstream temperature T_∞ is a time-varying function for the three downstream banks. The first bank of heater wire is still subjected to only a constant incoming airstream temperature. The airstream response was calculated and found to be nearly exponential. Eq. (3.5) was fitted to the calculated response, varying θ_H until a good fit was obtained. The values obtained for the effective θ_H (time constants) are plotted in Fig. 3.2 and are seen to be within 6 percent of the lumped case. For this reason it is believed that the simple lumped treatment is adequate for design purposes.

3.3 Response of the Heaters to a General Time-Varying Voltage Supply

To achieve an extremely short rise time in the heater temperature, the use of a time varying voltage supply is required. Regulation of the supply voltage in time is discussed in Sections 4 and 5 and Appendices III and IV. The thermal energy generated in the heater wires will also be a time-varying function. The solution to Eq. (3.3) is not a simple exponential function and requires the use of a numerical method.

The numerical method used was the IBM Electronic Circuit Analysis Program (ECAP). This program was written to be used by electrical engineers in the design and analysis of circuits. Detailed information on the use of ECAP may be found in the User's Manual [8].

Use of ECAP requires only a description of the circuit, a list of the elements in each branch of the network, a description of circuit excitation or time-varying elements, and a list of the output required.

The time-varying voltage supply to the heaters can be converted into a time-dependent current source for use in Eq. (3.3) by using Fig. 3.2. This current source must be entered into the ECAP program in the form of actual values of the source at specified time steps. The output of the ECAP program was the heater wire temperature $T_H(\theta)$. This, in turn, provided the right hand side of Eq. (3.4) which was then used to establish $T_f(0,\theta)$, the airstream temperature downstream from the heater, as a function of time.

4. STEP-UP DESIGN

Step-up in temperature occurs when voltage is applied to the heaters and the airstream temperature rises. An increase of about 20°F is used for the heater control design and in the experiments. If the heater voltage applied is a constant, and is simply switched-on, the response of the airstream will be exponential and is given by Eq. (3.5). Deviation from a true step-change is governed by the magnitude of the heater-wire time constant θ_H. As $\theta_H \rightarrow 0$, a step-change in air temperature is approached. The value of θ_H has been partially minimized by the use of small diameter wire in the heater [5]. Additional decreases in the value of the heater system effective response time is provided by the electronic control.

If instead of applying a constant level voltage, corresponding to a steady-state heating energy magnitude, a larger voltage is applied. The airstream, of course, will respond faster by tending toward a higher temperature. The process of applying more voltage, than is required for $\Delta T_\infty \approx 20°F$, is termed OVERSHOOTING. Fig. 4.1 shows the overshooting effect on airstream temperature. The part of the step-up response curve of interest, is the initial response characteristic. A small amount of overshooting, say 2X-Overshoot, will reduce by about 60 percent the time required for the airstream to reach 63 percent of the steady-state value of $\Delta T_\infty \approx 20°F$.

An ideal heater control would initially apply a voltage that would produce 2X-Overshoot or more. When steady-state is reached, this applied voltage would revert to a steady-state level. The resulting temperature wave would more closely resemble a true step-change in airstream temperature, with a 90 percent response achieved in only 25 percent of the time required by the normal response of Fig. 4.1.

The heater control circuit, presented in Figs. 2.2 and 2.3, is designed to produce an overshoot very much like that described above. For the step-up case, SW_2, SW_3, SW_4, and SW_5 are set to position U. This has the effect of creating initially a very small interbase voltage V_{BB},

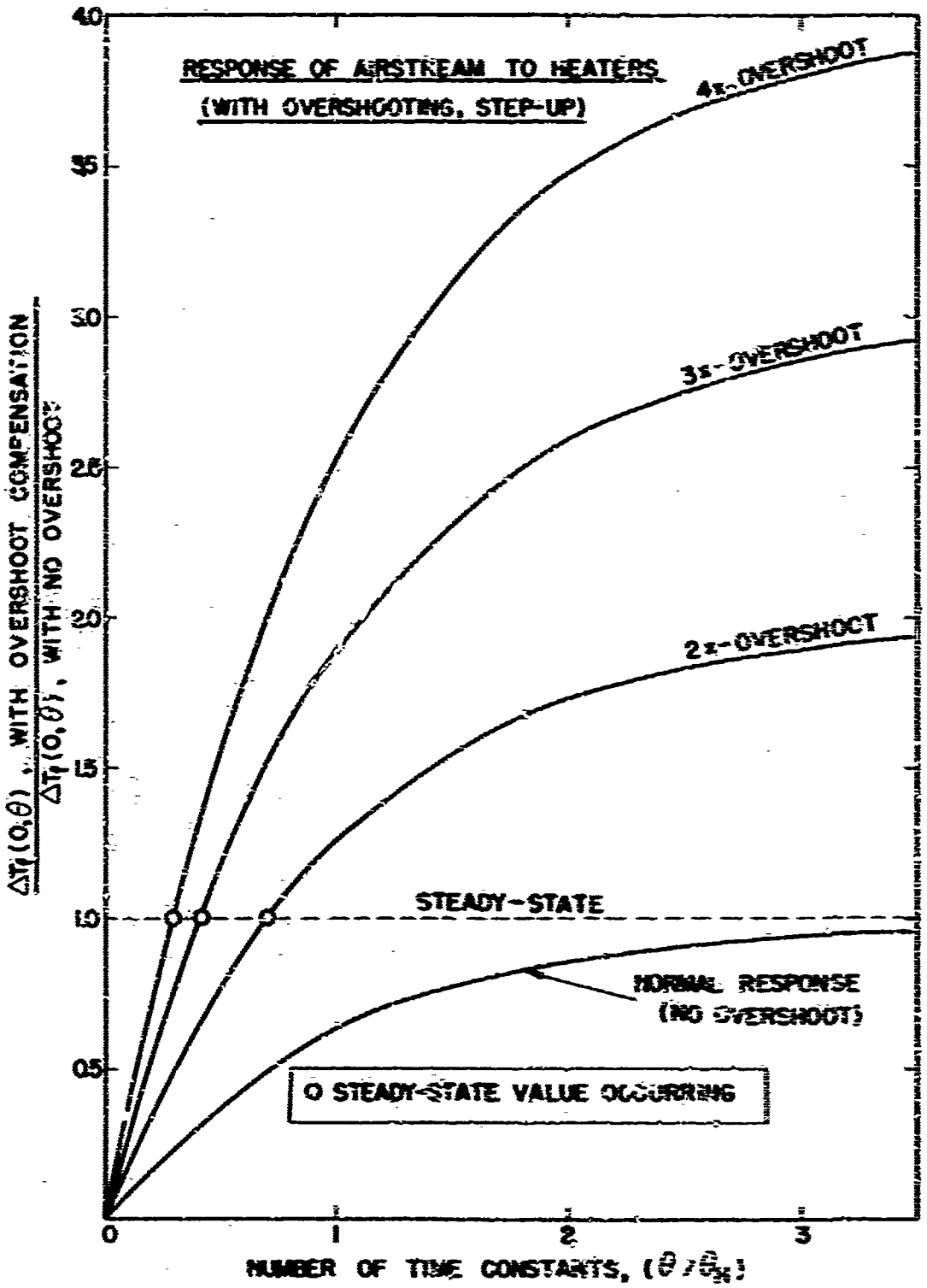

Figure 4.1 Effects of Overshooting on Airstream Temperature Response.

allowing the unijunction transistor Q_1 to fire very early in each AC wave. The net effect is a voltage surge to the heaters. As capacitor C_2 charges, the interbase voltage increases causing the voltage applied to the heaters to taper off to steady-state level. The steady-state level is regulated by the set value of R_2.

An analysis has been done to determine the values for C_2 and R_2 that will produce the desired voltage surge. The circuit-analysis technique used and an example with $w = 590$ lbm/hr are described in Appendix III. The result of the analysis at each flow rate is a temperature response curve for the heater wires. This curve is very nearly exponential and can be fitted using Eq. (3.5), varying θ_H. The calculated time constants of the heater wires are plotted versus air flow rate in Fig. 4.2. At the low flow rates in Fig. 4.2, the time constants are less than at the higher air flow rates. This is the result of more overshooting ability (lower steady-state level) at the lower rates. A comparison of Fig. 4.2 and the time constant curve of Fig. 3.2 indicates the gains realized by the use of the heater control.

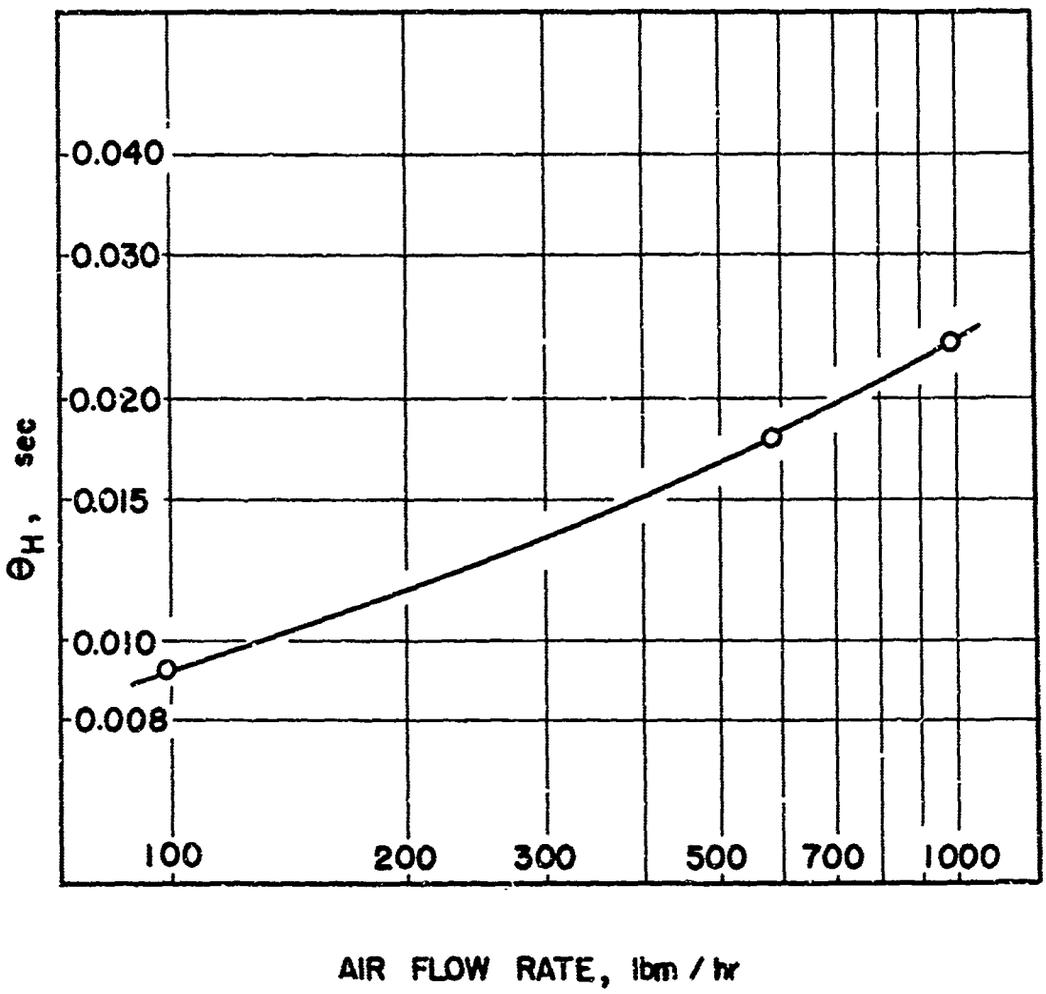

Figure 4.2 Aided Step-Up Heater Time Constants from Design Calculations.

5. STEP-DOWN DESIGN

Step-down in temperature occurs when the voltage applied to the heaters is removed. The airstream temperature drops and the response is given by Eq. (3.5). Deviation from a true step-change is governed by the magnitude of the heater-wire time constant θ_H. As $\theta_H \longrightarrow 0$, a step-change in fluid temperature is approached. The magnitude of θ_H has been partially minimized by using small diameter wire in the heaters [5]. Further decreases require the electronic heater control.

Examining the step-down response curve in Fig. 5.1, the following is noted. The response of the airstream initially is rather quick (steep slope) until about 75 percent of the deflection has occurred. If the response were arrested at about this 75 percent point, as indicated in Fig. 5.1, a response curve more closely resembling a step-change would result. This could be accomplished by removing the voltage to the heaters, and shortly thereafter applying a lower level voltage (enough to produce about 25 percent of steady-state heating).

The heater control circuit, presented in Fig. 2.2 and 2.3, is designed to remove the steady-state voltage and a short time later reapply a lower voltage to the heaters. For the step-down case SW_2, SW_3, SW_4, and SW_5 are placed in the D position. This has two main effects. The resistor in the resistance-capacitance network which supplies the unijunction transistor emitter voltage is increased to a maximum level. The result here is that initially the UJT fires very late in the AC cycle producing almost no power in the heaters. The intexbase voltage then decreases, allowing the UJT to fire progressively earlier in the AC wave until a level of 25 percent of steady-state is reached. Appendix IV includes the circuit-analysis technique used to calculate the response of the heater wires, hence the airstream, for the step-down case. As was also found in the step-up case the response is nearly exponential. The effective time constants to fit Eq. (3.5) are

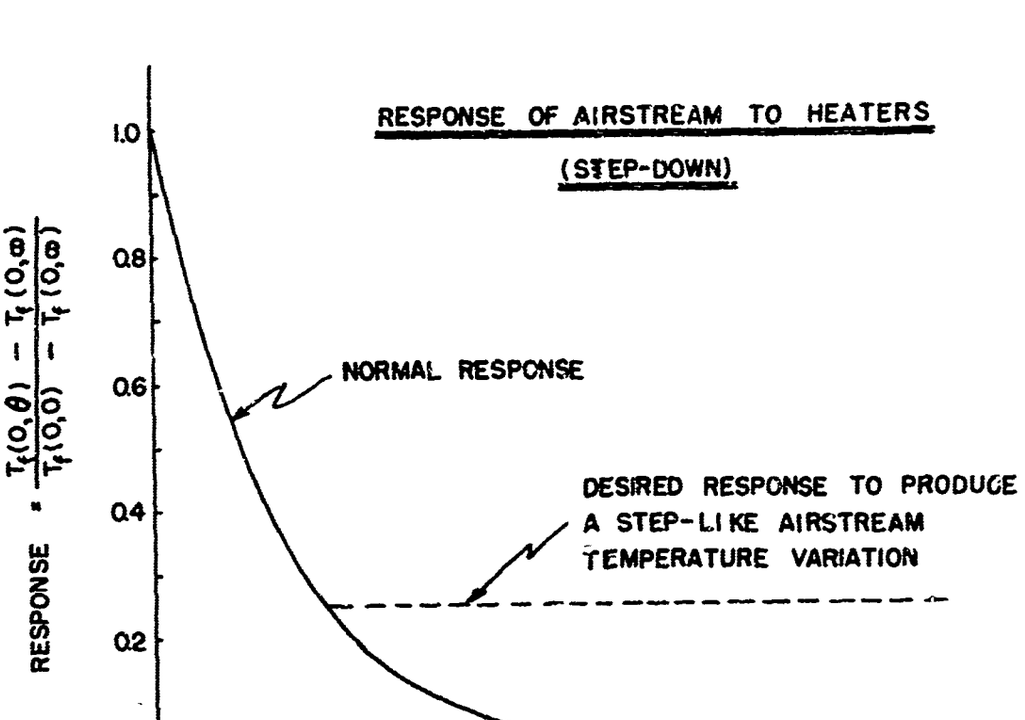

Figure 5.1 The Step-Down Response of the Airstream.

plotted in Fig. 5.2 for air flow rates from 100 to 1000 lbm/hr. These time constants have about the same variation with air flow rate as the unaided case of Fig. 3.2 and a contrary trend as compared to the step-up case. The step-down case does not yield as high a reduction in the effective θ_H as does the step-up case.

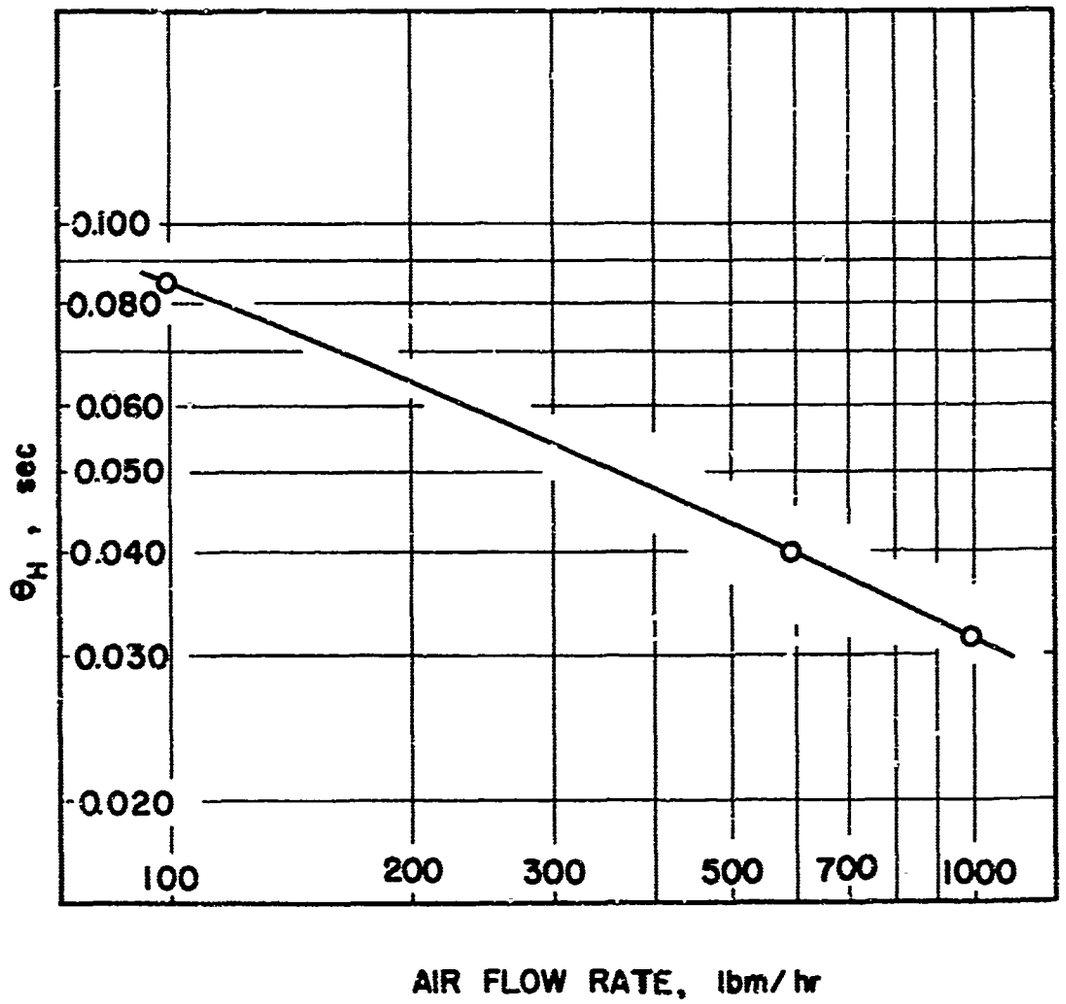

Figure 5.2 Aided Step-Down Heater Time Constants from Design Calculations.

6. HEATER CONTROL PERFORMANCE

6.1 Introduction

Operation of the heater control circuitry was investigated experimentally, as the response predicted by the design in Sections 4 and 5, needed to be validated.

With no core in the test section, the airstream was stepped up and down (both aided and unaided). Temperature response of the airstream was monitored using thermocouples and a fast strip-chart recorder. With a core in the test section, changes in the heat transfer results due to the decreased heater time constants were also investigated. Core heat transfer testing was performed using both the aided and the unaided step-changes in fluid temperature, and the differences in results were evaluated.

6.2 Heater-Response Tests

6.2.1 Unaided - The first set of experiments performed to determine the heater response had no core in the airstream. Since the thermocouples themselves have a bead diameter which is larger than the heater-wire diameter, they will contribute a significant lag to actual airstream temperature measurement. This lag effect must be considered because transient airstream temperature is being measured. A thermal circuit for the behavior of the thermocouples is shown in Fig. 6.1:

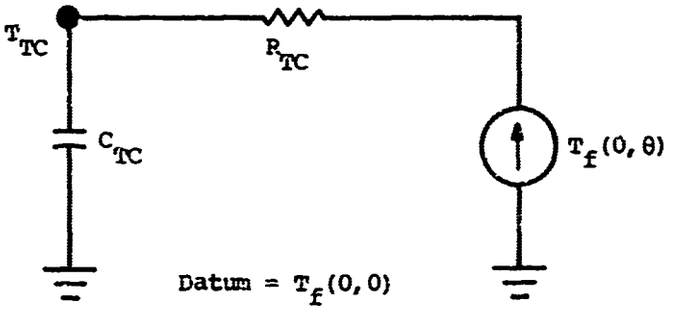

Figure 6.1 Thermal Circuit for a Thermocouple Suspended in the Airstream

Airstream temperature variation in time can be expressed as an exponential function. Using the temperature expression from Eq. (3.5) as the T_f potential source in the thermal circuit of Fig. 6.1, the following solution for the thermocouple temperature $T_{TC}(\theta)$ is produced $(\theta_H \neq \theta_{TC})$[1]:

$$\frac{T_{TC}(\theta) - T_f(0,\infty)}{T_f(0,0) - T_f(0,\infty)} = 1 - \exp\left(\frac{-\theta}{\theta_H}\right) + \left(\frac{1}{\frac{\theta_{TC}}{\theta_H} - 1}\right)\left[\exp\left(\frac{-\theta}{\theta_H}\right) - \exp\left(\frac{-\theta}{\theta_{TC}}\right)\right] \tag{6.1}$$

The three temperatures required in the above equation can all be obtained experimentally from a plot of thermocouple output.

Empirical data from McAdams [9] was used to predict the heater wire time constant θ_H for the unaided case. These results are plotted as a function of air flow rate only, in Fig. 3.2. The thermocouple output was recorded (step-up and step-down) for a series of air flow rates. Eq. (6.1) was then used to obtain $\theta_{TC} (\triangleq R_{TC}C_{TC})$ also as a function of air flow rate. The results are plotted in Fig. 6.2. Exponential curve fits for the thermocouple temperature $T_{TC}(\theta)$ experimental record, are also presented in Fig. 6.2.

The time constant for a 0.005 inch diameter 50 percent copper/50 percent constantan sphere was calculated and is shown in Fig. 6.2 for comparison purposes. The relation used to calculate the convective heat transfer coefficient for the thermal resistance of the sphere was taken from McAdams [9] and is

$$\frac{hD_s}{k_f} = 0.37\left(\frac{GD_s}{\mu_f}\right)^{0.6} \tag{6.2}$$

---

[1] In the special case where $\theta_H = \theta_{TC} \triangleq \theta_c$, the solution is

$$\frac{T_{TC}(\theta) - T_f(0,\infty)}{T_f(0,0) - T_f(0,\infty)} = -\left(1 + \frac{\theta}{\theta_c}\right) \exp\left(\frac{-\theta}{\theta_c}\right)$$

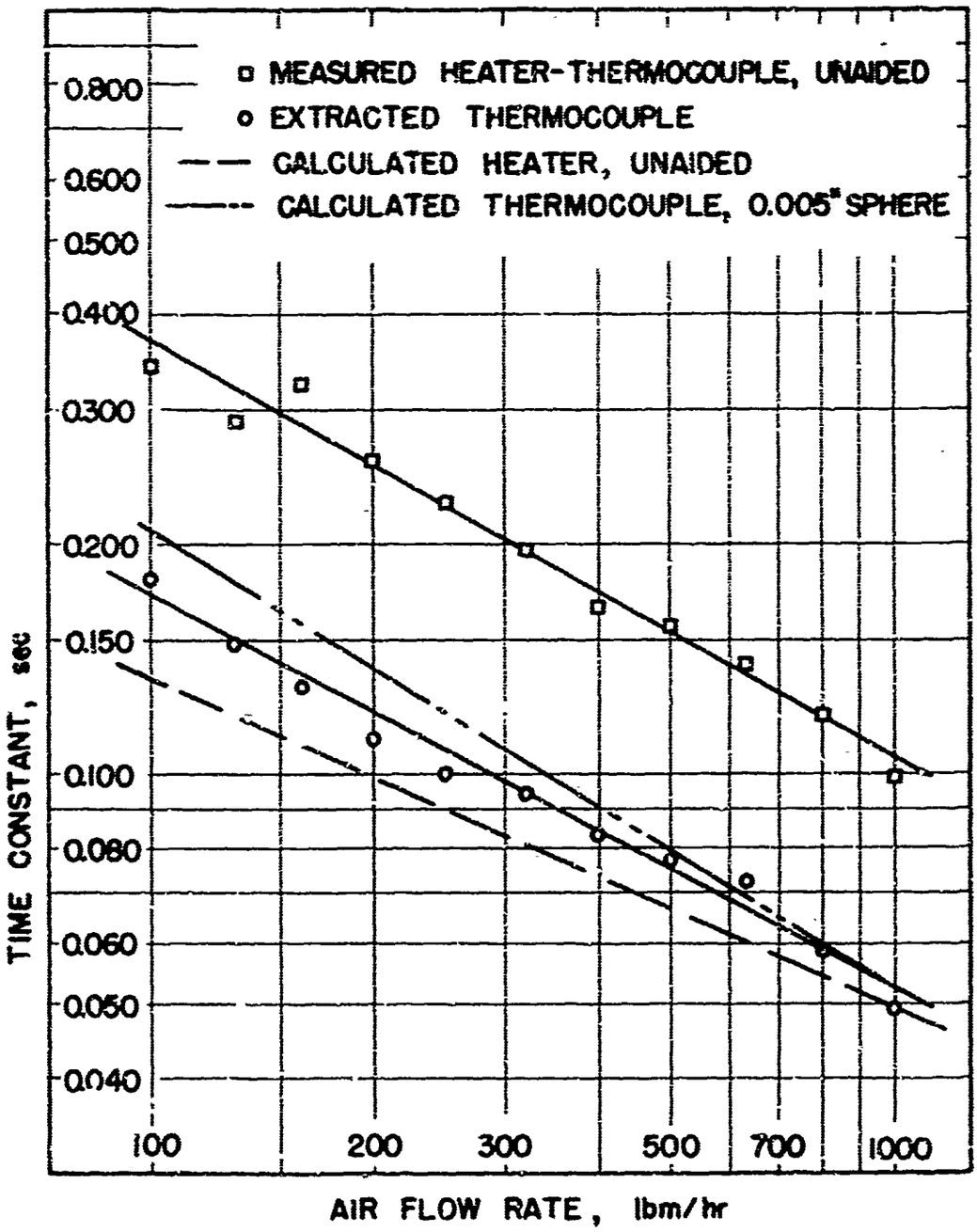

Figure 6.2 Thermocouple Time Constants Extracted from the Responses to Unaided Step-Changes in Airstream Temperature.

where D_s is sphere diameter. The air film properties were taken from Bureau of Standards Sources [10] and are evaluated at 90°F.

The heater-thermocouple response was investigated by Wheeler [5] shortly after the construction of the basic test rig. Results reported are about 30 percent lower than the results shown in Fig. 6.2. The difference is likely caused by the methods of data analysis used. Since the thermocouple output record is not a simple exponential function, see Eq. (6.1), the results of a curve fit will depend on which part of the experimental trace was used in data analysis. Results shown in Fig. 6.2 are averages of several points read over the middle 50 percent of the experimental trace. The calculation in [5] for the expected heater wire time constant (unaided) is about 20 percent lower than the results shown in Figs. 3.2 and 6.2. Here the difference is due to different selections of both gas and solid thermal properties.

To determine what effect the thermocouple time constants, just determined, would have on maximum-slope heat transfer results, the thermal circuit of the thermocouple in Fig. 6.1 is considered with the T_f potential source input

$$T_f(1,\theta) = T_f(1,0) + [T_f(1,\infty) - T_f(1,0)]\,\frac{\theta}{DTAU} \qquad (6.3)$$

where $0 \leq \theta \leq DTAU$

This "ramp" or linear input is used because it resembles the airstream behavior downstream of a test core, especially at the time when the maximum-slope occurs. For the thermal circuit in Fig. 6.1

$$C_{TC}\,\frac{d}{d\theta}\,[T_f(1,0) - T_{TC}(\theta)] + \frac{T_f(1,\theta) - T_{TC}(\theta)}{R_{TC}} = 0 \qquad (6.4)$$

Solving this equation, taking the derivative $dT_{TC}(\theta)/d\theta$, and comparing with $dT_f(1,0)/d\theta$ yields

$$\frac{d\,T_{TC}(\theta)/d\theta}{d\,T_f(1,\theta)/d\theta} = \frac{\frac{1}{DTAU} - \frac{1}{DTAU}\exp\left(\frac{-\theta}{\theta_{TC}}\right)}{\frac{1}{DTAU}} \qquad (6.5)$$

$$= 1 - \exp\left(\frac{-\theta}{\theta_{TC}}\right)$$

The above ratio can be interpreted as the experimentally established slope of the air downstream of the test core (including thermocouple lag) divided by the actual slope of the downstream air (without thermocouple lag). The maximum-slope occurs in the interval $0.3\ DTAU < \theta < 0.5\ DTAU$, [14]. Additionally from measurements presented in Fig. 6.2, $\theta_{TC} < 0.2$ sec. For core 510, $DTAU > 5.0$ sec., so the exponent in Eq. (6.5) is about -10. Consequently it is concluded that thermocouple lag has a negligible influence (much less than 0.1 percent) on maximum-slope heat transfer results. However, lag in the heater wires does have a small but significant effect on the heat transfer results as will be shown in sections following.

6.2.2 Aided - After the thermocouple time constants had been established, the heater system operating in the aided mode was analyzed. Based on the results of the design analysis in Sections 4 and 5 and Appendices III and IV, the heaters can in the aided case also be considered to respond as a simple exponential function. This allows use of Eq. (6.1) to determine the reduced heater system time constant.

Thermocouple time constant θ_{TC} is a function of air flow rate only, and does not depend on the heater control. The values plotted in Fig. 6.2 for the unaided case may be used to extract the heater time constant in the aided case. Eq. (6.1) is again employed. This time the thermocouple trace for aided step-changes in airstream temperature, and θ_{TC} from Fig. 6.2, are used to calculate θ_H. Resulting heater time constants for the aided case are plotted in Fig. 6.3 as a function of air flow rate. The design prediction, obtained by averaging the results of Figs. 4.2 and 5.2, is also included in Fig. 6.3 for comparison.

The results summarized in Fig. 6.3 indicate that a decrease in the heater time constants of about 60 percent at 100 lbm/hr to about 40 percent at 1000 lbm/hr is produced by the heater control circuitry. Also shown in the figure is the good agreement between the design predictions and experimentally determined results.

6.3 Effects on Core Heat Transfer Tests

Heat transfer testing was performed on four test cores: 505A, 505B, 505C, and 510. The maximum-slope method was used with both aided and unaided step-changes in fluid temperature. Experimental heat transfer results for the four cores are plotted in Figs. 6.4 through 6.7. Friction factor results, although they are not affected by the heat transfer technique used, are also plotted as obtained for the aided and unaided cases. This redundancy insures that no errors were made in the air flow rate calculations by providing a cross check, through the friction factor.

Heat transfer results obtained using the aided step-change were generally higher than corresponding results from tests with the unaided step-change. Each point plotted in Figs. 6.4 through 6.7 is based experimentally on the average of two steps-up and two steps-down in air-stream temperature entering the core. Although the change in results can be directly read from the plots (and the tabulated results in Appendix VII) experimental variation from run to run makes it difficult to meaningfully determine the small difference as a function of air flow rate or Reynolds number. Attempts were made to keep test conditions identical in both the aided and unaided cases, varying only the fluid step-change. This was accomplished by performing the aided and unaided tests back-to-back at each flow rate.

So that the differences in heat transfer results could be examined more closely, least-squares curve fits were performed on the maximum-slopes and the N_{Nu}'s of each core versus N_{Re}. This was done for both the aided and unaided cases. The results of the curve fits, evaluated at Reynolds numbers in the respective ranges of testing, are tabulated

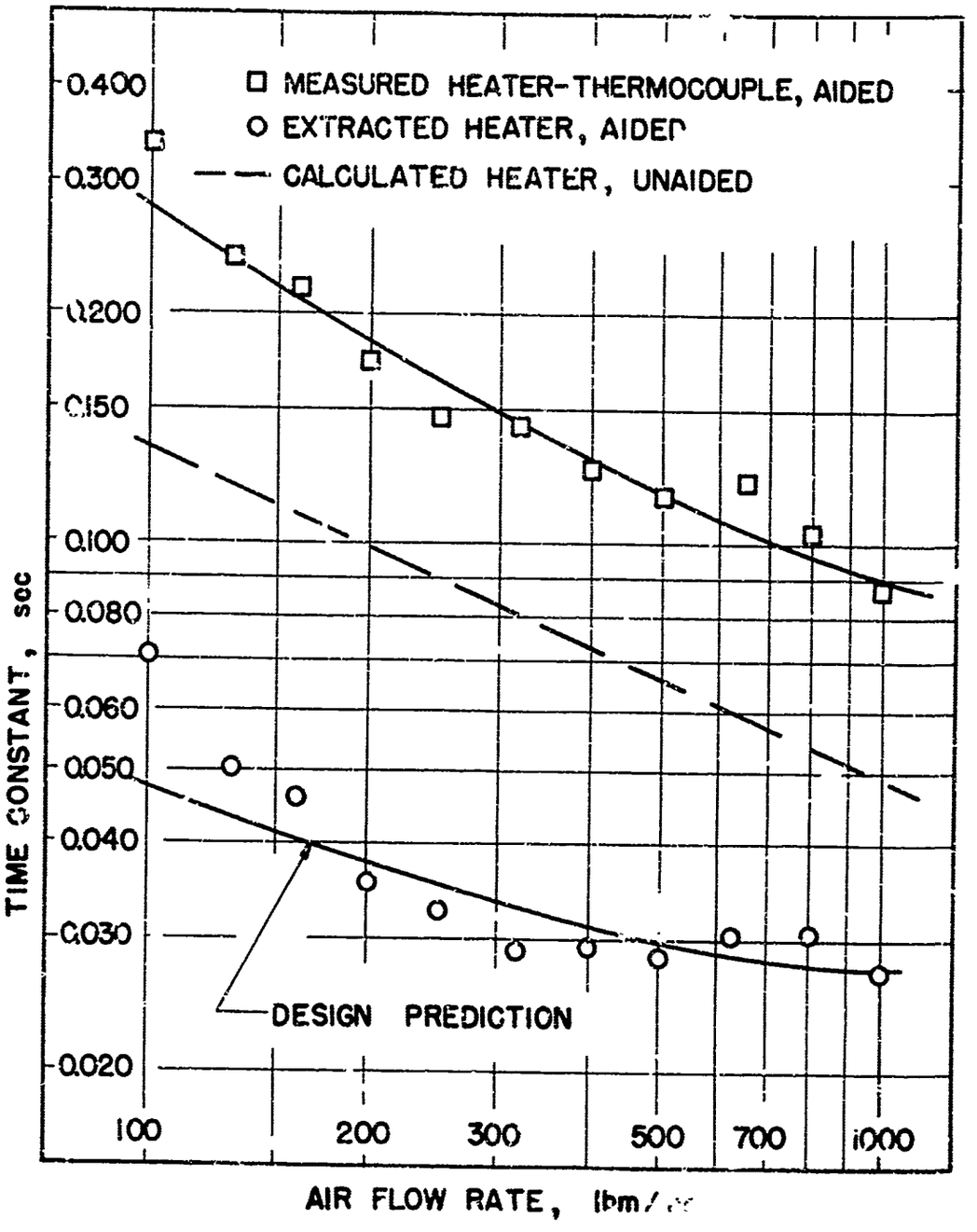

Figure 6.3 Aided Heater Time Constants Extracted from the Responses to Aided Step-Changes in Airstream Temperature.

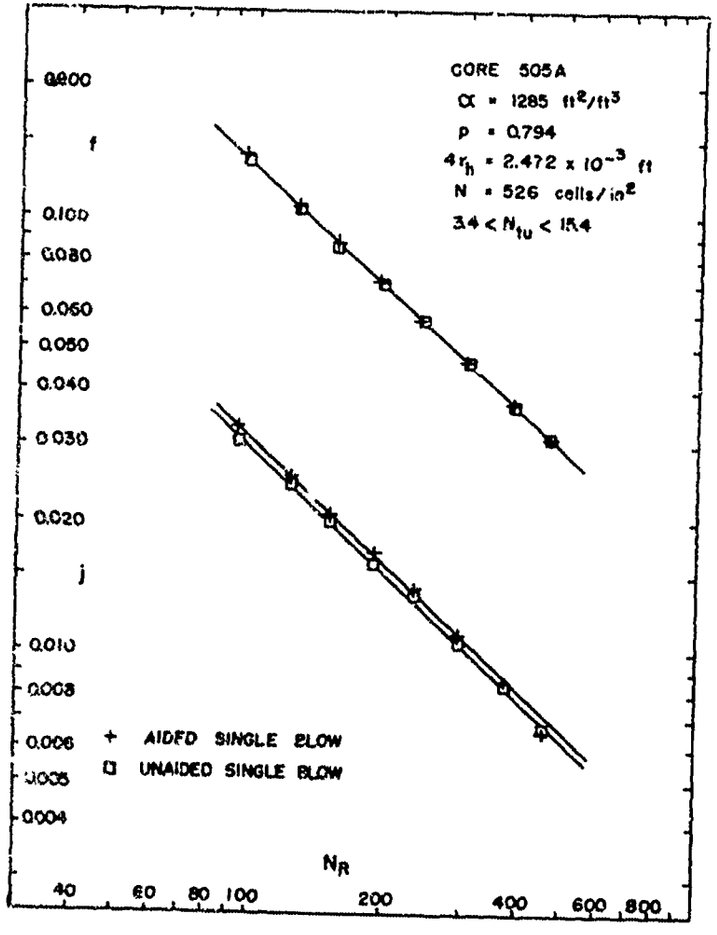

Figure 6.4 Comparison of Aided and Unaided Maximum-Slope Results for 505A

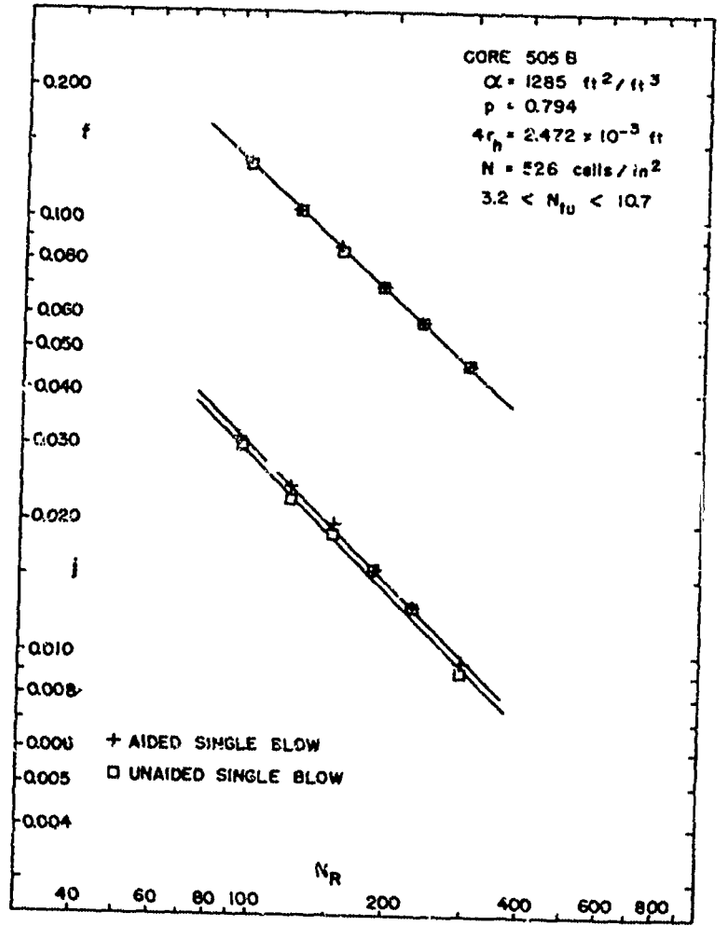

Figure 6.5 Comparison of Aided and Unaided Maximum-Slope Results for 505B.

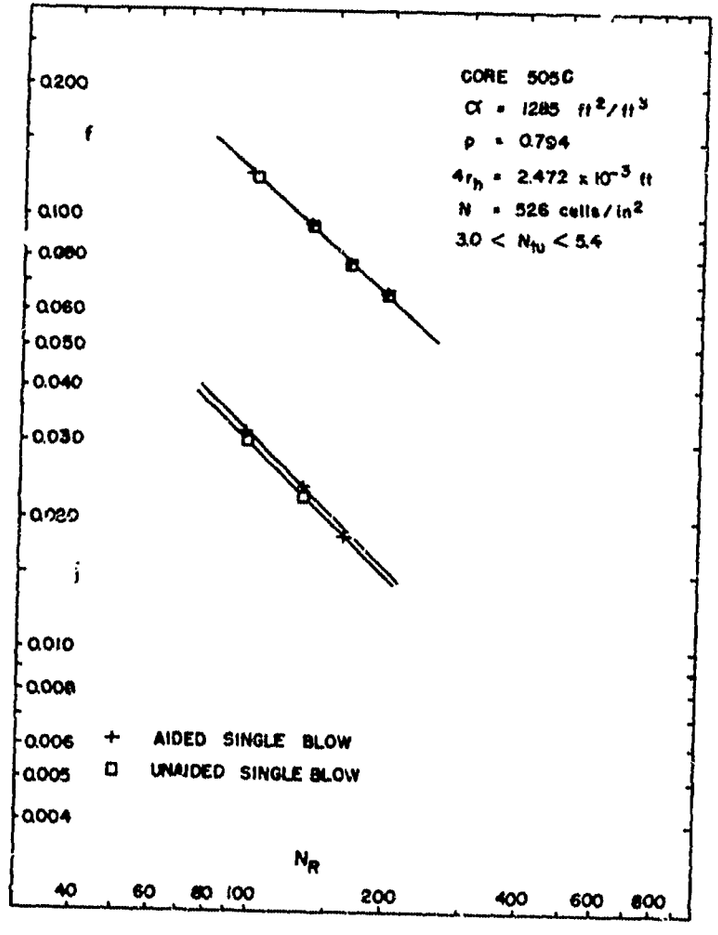

Figure 6.6 Comparison of Aided and Unaided Maximum-Slope Results for 505C.

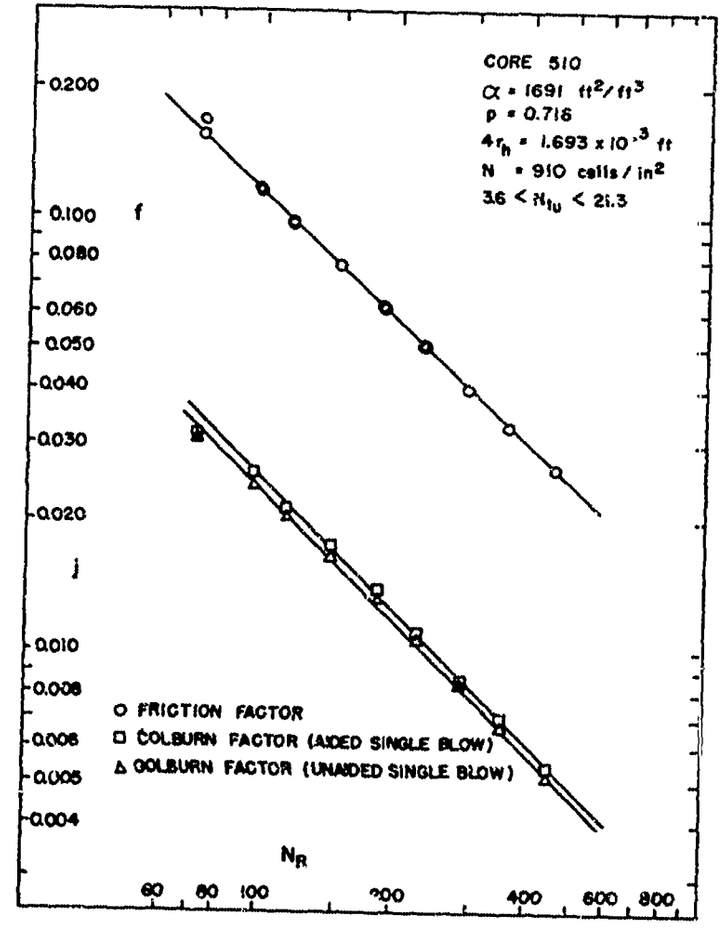

Figure 6.7 Comparison of Aided and Unaided Maximum-Slope Results for 510.

in Table 6.1. From the table's listing, the average change in heat transfer results for the four cores, when using the aided step-change, is 3.8 percent.

Kohlmayr [3,11] has extended the maximum-slope method to include arbitrary upstream fluid temperature changes. In particular he reports tabulations of maximum slope MS with $3 \leq N_{tu} \leq 35$ and $0.02 \leq I \leq 0.50$, for the case of an exponential upstream temperature function. Changes in maximum slope (ΔMS), predicted by [11], are plotted in Fig. 6.8 for $5 \leq N_{tu} \leq 35$ and $0.02 \leq I \leq 0.10$. The parameter I is defined in Table 6.1 and is termed a deviation from the true step-change. For the values of I and N_t in Table 6.1, [11] predicts that the change in maximum slope ΔMS will be less than 0.002, a change under 0.4 percent. Using the sensitivity curves in [12], the heat transfer results will then be changed by less than one percent. However the experimental results in Table 6.1 indicate an average change of 3.8 percent by using the aided heaters (which do not produce a true step-change, only a faster response). The reasons for the disagreement between Kohlmayr's analytical predictions, Fig. 6.8, and the experimental results reported here, are not at all clear. Further work on this question is needed.

Table 6.1

HEAT TRANSFER DATA CURVE FITS, FOR AIDED AND UNAIDED STEP-CHANGE COMPARISON

Core	N_R	W_f lbm/hr	MS aided	MS unaided	ΔMS	N_{tu} aided	N_{tu} unaided	$\frac{\Delta N_{tu}}{N_{tu,aided}}$ %	I
505A	100	107	1.138	1.104	0.034	15.71	14.73	6.3	.0087
	200	214	0.847	0.834	0.013	8.04	7.77	3.4	.0128
	300	320	0.713	0.708	0.005	5.43	5.35	1.5	.0160
	400	426	0.631	0.630	0.001	4.12	4.10	0.2	.0168
505B	100	107	0.919	0.896	0.023	9.86	9.33	5.4	.0131
	200	215	0.686	0.678	0.008	4.89	4.74	3.1	.0192
	300	322	0.578	0.576	0.002	3.24	3.19	1.5	.0243
505C	100	103	0.699	0.688	0.011	5.15	4.96	3.7	.0265
510	100	138	1.160	1.141	0.019	16.34	15.66	4.2	.0081
	200	275	0.865	0.850	0.015	8.53	8.16	4.3	.0120
	300	413	0.728	0.715	0.013	5.83	5.58	4.3	.0151
	400	550	0.645	0.632	0.013	4.42	4.25	4.5	.0175

$$I \triangleq \frac{\theta_H (wc_p)_f}{\bar{C}_w}, \quad \theta_H \text{ is for the unaided case}$$

$$\Delta MS \triangleq MS_{aided} - MS_{unaided}$$

$$\Delta N_{tu} \triangleq N_{tu,aided} - N_{tu,unaided}$$

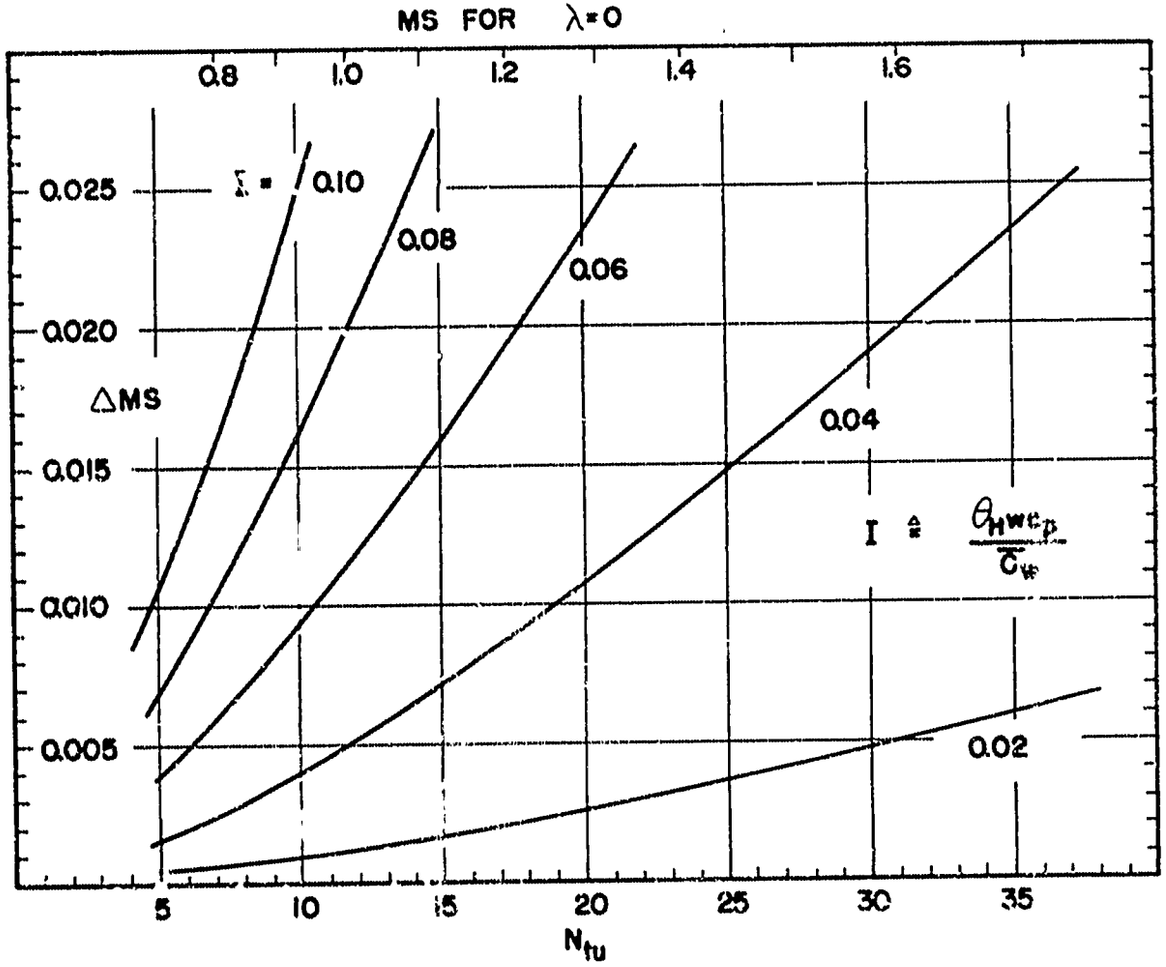

Figure 5.8 Maximum-Slope Correction for the Exponential Fluid Temperature Change (from Kohlmayr [11]).

7. PERIODIC TECHNIQUE

7.1 General

The regular periodic technique for determining the surface average heat transfer coefficient involves imposing a cyclic variation in temperature on the single fluid flowing into the test core and measuring the temperature response of the fluid flowing out of the core after steady-state periodic behavior is established. The measured response will have an amplitude attenuation and a phase shift. As discussed in [4] and in more detail in Section 7.3, both the amplitude attenuation and the phase shift of the fluid temperature response may be used to obtain accurate heat transfer results, but for different N_{tu} ranges; thus the two methods are complementary.

The periodic technique has been improved by the following refinements included in this section:

1. A solution which includes the effects of finite wall longitudinal conduction has been found and is demonstrated to be usable in data reduction.
2. A substantially more simple solution for the case of infinite wall longitudinal conduction is also presented.
3. Guidelines are established for using the periodic technique for $0.2 < N_{tu} < 50$.
4. The uncertainties in heat transfer results associated with core physical properties are discussed.
5. Actual test results for a new test core (510) are presented for $2.6 < N_{tu} < 36.6$ and are compared with the aided single-blow results.

7.2 Solution of the Governing Equations, Including the Effects of Wall Longitudinal Conduction

7.2.1 Finite Wall Longitudinal Conduction - The governing differential equations for the case of finite wall longitudinal conduction are derived in Appendix V and are

$$T_f^* - T_w^* = \frac{\partial T_w^*}{\partial \theta^*} - \lambda N_{tu} \frac{\partial^2 T_w^*}{\partial Z^2} \tag{7.1}$$

$$T_f^* - T_w^* = - \frac{\partial T_f^*}{\partial Z} \tag{7.2}$$

with the following definitions

$$T_f^* \triangleq \frac{T_f - T_m}{\Delta T_o} \quad , \quad T_w^* \triangleq \frac{T_w - T_m}{\Delta T_o}$$

$$\theta^* \triangleq \frac{\theta}{R\bar{C}_w} \quad , \quad \lambda \triangleq \frac{k_w A_w}{LC_f}$$

$$N_{tu} \triangleq \frac{hA}{C_f} \quad , \quad Z \triangleq N_{tu} \frac{x}{L}$$

The wall longitudinal conduction parameter λ, and N_{tu}, in combination as λN_{tu} determine the magnitude of the last term in Eq. (7.1). The boundary condition on the above equation is

$$T_f^*(0, \theta^*) = \sin 2\pi \frac{\theta}{\theta_o} = \sin \frac{\theta^*}{\Phi} \tag{7.3}$$

with $\Phi \triangleq \frac{1}{2\pi} \frac{\theta_o}{R\bar{C}_w}$

The solutions to Eqs. (7.1) and (7.2) are

Fluid Solution

$$T_f^* = \exp(-\epsilon_1 Z) \left\{ \sin \left(\frac{\theta^*}{\Phi} - \epsilon_2 Z \right) \right\} \tag{7.4}$$

Wall Solution

$$T_w^* = \exp(-\epsilon_1 Z)\left\{(1-\epsilon_1)\sin\left(\frac{\theta^*}{\psi} - \epsilon_2 Z\right) - \epsilon_2 \cos\left(\frac{\theta^*}{\psi} - \epsilon_2 Z\right)\right\} \quad (7.5)$$

The terms ϵ_1 and ϵ_2 are functions of ψ and λN_{tu} only and must satisfy the following set of equations

$$\epsilon_1 = \frac{\epsilon_2}{\psi} - \lambda N_{tu}\left(-\epsilon_1^3 + \epsilon_1^2 + 3\epsilon_1\epsilon_2^2 - \epsilon_2^2\right) \quad (7.6)$$

$$\epsilon_2 = \frac{1-\epsilon_1}{\psi} - \lambda N_{tu}\left(\epsilon_2^3 - 3\epsilon_1^2\epsilon_2 + 2\epsilon_1\epsilon_2\right) \quad (7.7)$$

These constants ϵ_1 and ϵ_2 have been calculated and are tabulated in Tables V-1 and V-2. For data reduction the Fortran subroutine CONDCT in Table VII-3 was used to generate the tables and may be used to calculate ϵ_1 and ϵ_2 for intermediate values of ψ and λN_{tu}.

To determine the surface average heat transfer coefficient, Eq. (7.4) is used and the temperature response is measured downstream of the test core where $Z = N_{tu}$. From Eq. (7.4) the amplitude attenuation is

$$D_f \triangleq \exp(-\epsilon_1 N_{tu}) \quad (7.8)$$

the phase shift is

$$\gamma_f \triangleq \epsilon_2 N_{tu} \quad (7.9)$$

In the special case of $\lambda = 0$

$$\epsilon_1 = \frac{1}{1+\psi^2} \quad \text{and} \quad \epsilon_2 = \frac{\psi}{1+\psi^2}$$

The amplitude attenuation D_f and the phase shift γ_f are shown graphically in Appendix V, Figs. V-2 through V-9, as functions of N_{tu}, ψ, and λ. The phase shift is plotted for $0 \leq N_{tu} \leq 10$, $1 \leq \psi \leq 4$, $0 \leq \lambda \leq 0.02$, and $\lambda = \infty$. The amplitude attenuation is plotted for $0 \leq N_{tu} \leq 50$, $3 \leq \psi \leq 6$, $0 \leq \lambda \leq 0.02$, and $\lambda = \infty$. The

ranges chosen for N_{tu}, ϕ, and λ cover those which are likely to be encountered in testing using the two methods.

The influence of λ on experimental amplitude attenuation is shown in Fig. 7.1 and the influence on experimental phase shift is shown in Fig. 7.2. These plots indicate when the effects of longitudinal conduction become significant, compared to other experimental uncertainties. They also can be used to estimate the magnitude of the correction that needs to be applied to the experimental results to obtain the amplitude attenuation and phase shift that do not contain the effects of longitudinal conduction. It should be noted that these plots apply only when the guidelines for testing, set in Section 7.3, are followed.

7.2.2 Infinite Wall Longitudinal Conduction - As the wall longitudinal conduction parameter λ becomes large ($\lambda \rightarrow \infty$), the temperature of the wall T_w becomes a function of time θ only. The fluid temperature T_f remains a function of both time and distance. To account for all of the thermal energy entering and leaving the wall, the entire length of the heat exchanger must be considered. Thermal gradients in the wall do not exist and this is the only means of applying the conservation of energy to the wall; hence the resulting integral Eq. (7.10) below. Eq. (7.11) for the fluid is also presented in intergral form, for consistency reasons. The governing equations are derived in Appendix V and are

$$\frac{-1}{N_{tu}} \int_0^{N_{tu}} T_f^* \, dZ + T_w^* + \frac{dT_w^*}{d\theta^*} = 0 \qquad (7.10)$$

$$\frac{1}{N_{tu}} \int_0^{N_{tu}} \frac{\partial T_f^*}{\partial Z} \, dZ + \frac{1}{N_{tu}} \int_0^{N_{tu}} T_f^* \, dZ - T_w^* = 0 \qquad (7.11)$$

The solutions to the above equations are

$$T_f^* = \exp(-\epsilon_3 Z) \sin \frac{\theta^*}{\phi} + \frac{\epsilon_4^2}{N_{tu}} \cos \frac{\theta^*}{\phi} \qquad (7.12)$$

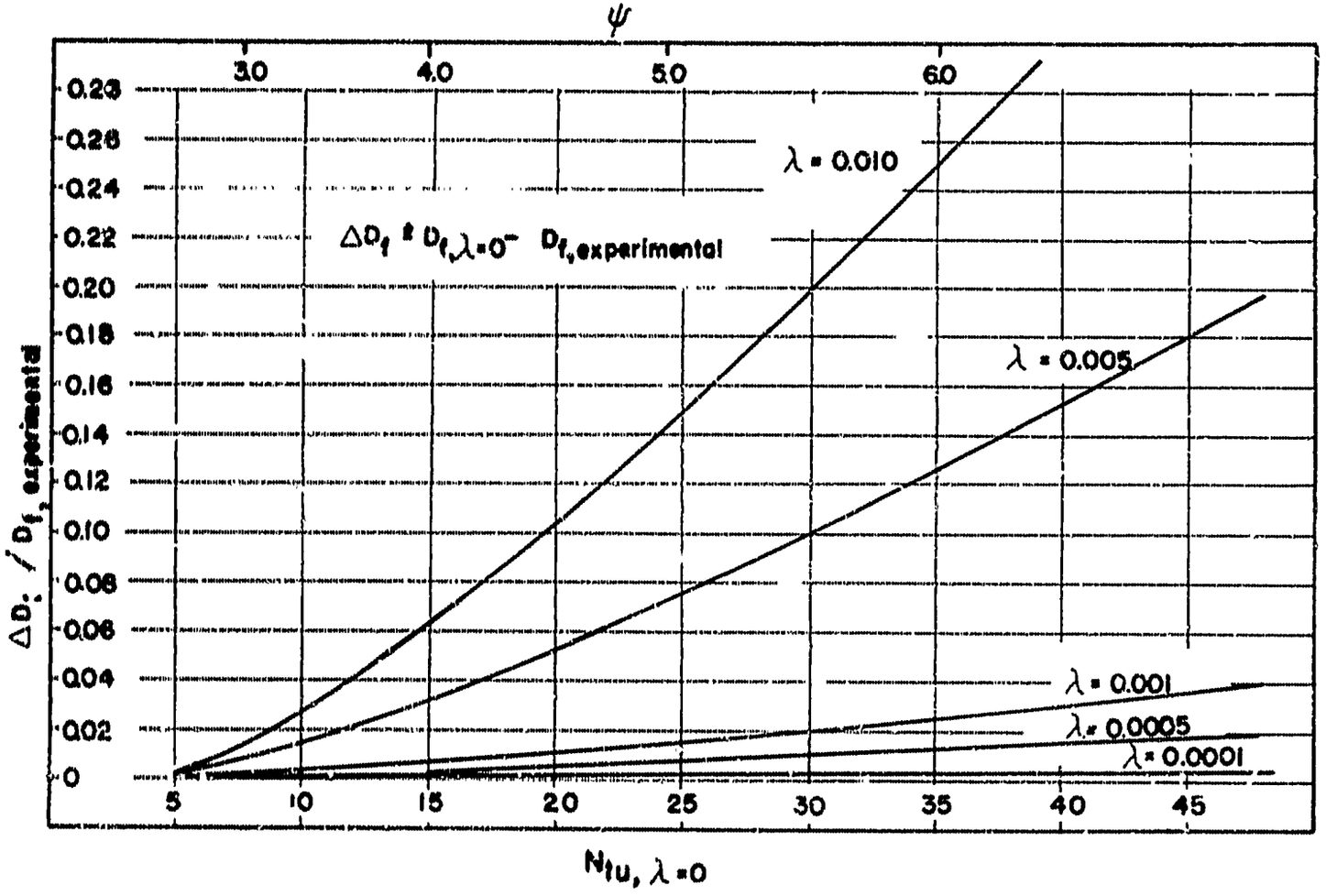

Figure 7.1 Influence of Wall Longitudinal Conduction on the Experimental Amplitude Attenuation.

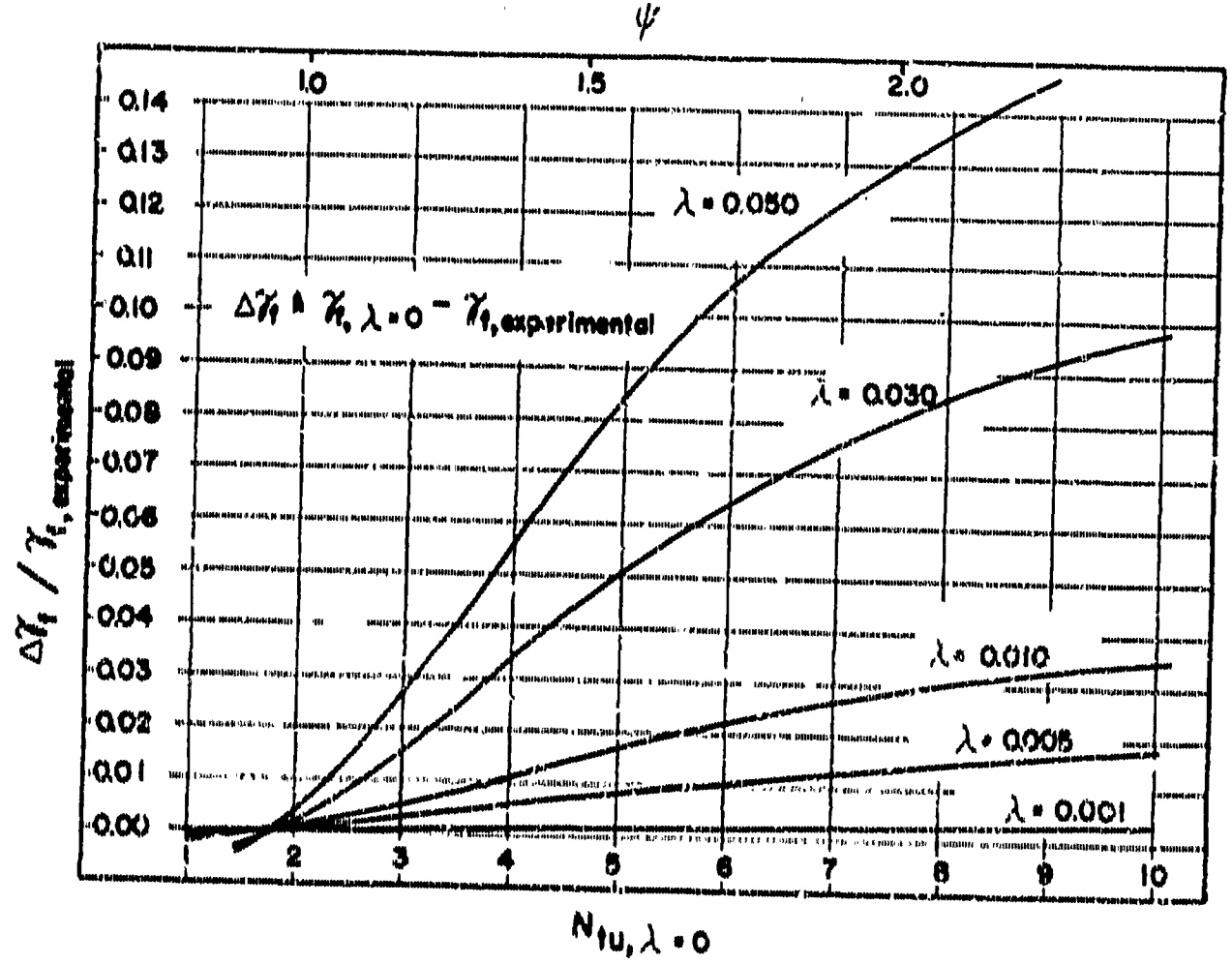

Figure 7.2 Influence of wall longitudinal conduction on the experimental phase shift.

and

$$\bar{m}_w^* = \frac{1}{N_{tu}} \left\{ \left(1 - \frac{1}{\epsilon_3}\right) \left[\exp(-\epsilon_3 N_{tu}) - 1\right] \sin\left(\frac{\theta^*}{\Psi}\right) + \epsilon_4 \left(1 + \frac{N_{tu}}{2}\right) \cos\left(\frac{\theta^*}{\Psi}\right) \right\} \tag{7.13}$$

where

$$\epsilon_3 = \frac{1 + \frac{N_{tu}}{2}}{\Psi + 1 + \frac{N_{tu}}{2}} \tag{7.14}$$

$$\epsilon_4 = \frac{\exp\left\{ - \left[\frac{1 + \frac{N_{tu}}{2}}{\Psi + 1 + \frac{N_{tu}}{2}} \right] N_{tu} \right\} - 1}{1 + \frac{N_{tu}}{2}} \tag{7.15}$$

The phase shift for the fluid downstream of the test core ($Z = N_{tu}$) is plotted as the $\lambda = \infty$ line in Figs. V-2 through V-5; the amplitude attenuation is plotted as the $\lambda = \infty$ line in Figs. V-6 through V-9.

Bell and Katz [2] in 1949 derived an expression for the amplitude attenuation of the fluid response with infinite wall longitudinal conduction, for $N_{tu} \leq 2$. Considering the case where $N_{tu} = 2$ and $\Psi = 1$, the calculated amplitude attenuation is 0.4158. Using Eq. (7.12) with the same parameters, produces an amplitude attenuation of 0.453. The disagreement between the above results is believed to be caused by differing idealizations used in the respective analysis. The analysis in [2] considers the effects of fluid thermal capacitance, and uses a mathematical approximation to calculate the results. The analysis included here in Appendix V, considers fluid thermal capacitance to be very small (as it is in situations involving a gas) but uses no mathematical approximations. It is believed the mathematical approximation used in [2] accounts for the difference in the results.

7.3 Guidelines for Using the Periodic Technique

Temperature measurement uncertainty is considered to be the largest source of error in the periodic technique. Therefore the testing should

be done in a manner that will minimize the sensitivity of the technique to this uncertainty. A temperature uncertainty analysis is included in Appendix VI. The analysis shows that the sensitivity of the periodic technique, both the amplitude attenuation and the phase shift methods, are functions of N_{tu} and $\frac{1}{\gamma}$. For a given N_{tu}, there exists an $\frac{1}{\gamma}$ which will produce the best test results (least uncertainty in the heat transfer results for an uncertainty in temperature measurement). If an appropriate value of $\frac{1}{\gamma}$ is selected and used in testing, the uncertainty in heat transfer results can be held at about 3 percent, for a 1 percent of the inlet amplitude uncertainty in temperature measurement. The values of $\frac{1}{\gamma}$, recommended for testing, and the method to be used to reduce the data, are shown in Fig. 7.3. This figure is a key one for use in setting-up the experimental periods of oscillation. From the figure and the analysis of Appendix VI, the following recommendations are made:

1. $N_{tu} < 1$, use the amplitude attenuation method with $\frac{1}{\gamma} < 0.2$.
2. $1 \leq N_{tu} \leq 7$, use the phase shift method with $0.8 < \frac{1}{\gamma} < 1.3$.
3. $N_{tu} \geq 7$, use the amplitude attenuation method with $\frac{1}{\gamma} > 2.9$.

7.4 Sensitivity of the Heat Transfer Results to Errors in Test Core Physical Properties

The periodic transient technique requires that the matrix physical properties such as density ρ_w, specific heat c_w, and thermal conductivity k_w be known. In the periodic technique $\frac{1}{\gamma}$ is calculated from experimentally obtained amplitude attenuation D_f and phase shift γ_f.

From an uncertainty analysis, included in Appendix VI, N_{St} and N_R were found to be individually sensitive to errors in ρ_w[1]. But because of compensating effects, the j--N_R characteristic is not affected by the errors in solid density (true only for $j \propto 1/N_R$).

---

[1] ρ_w, the wall density, influences the Reynolds No. indirectly through its use in establishing porosity (flow area) gravimetrically. See Eq. (VI-9).

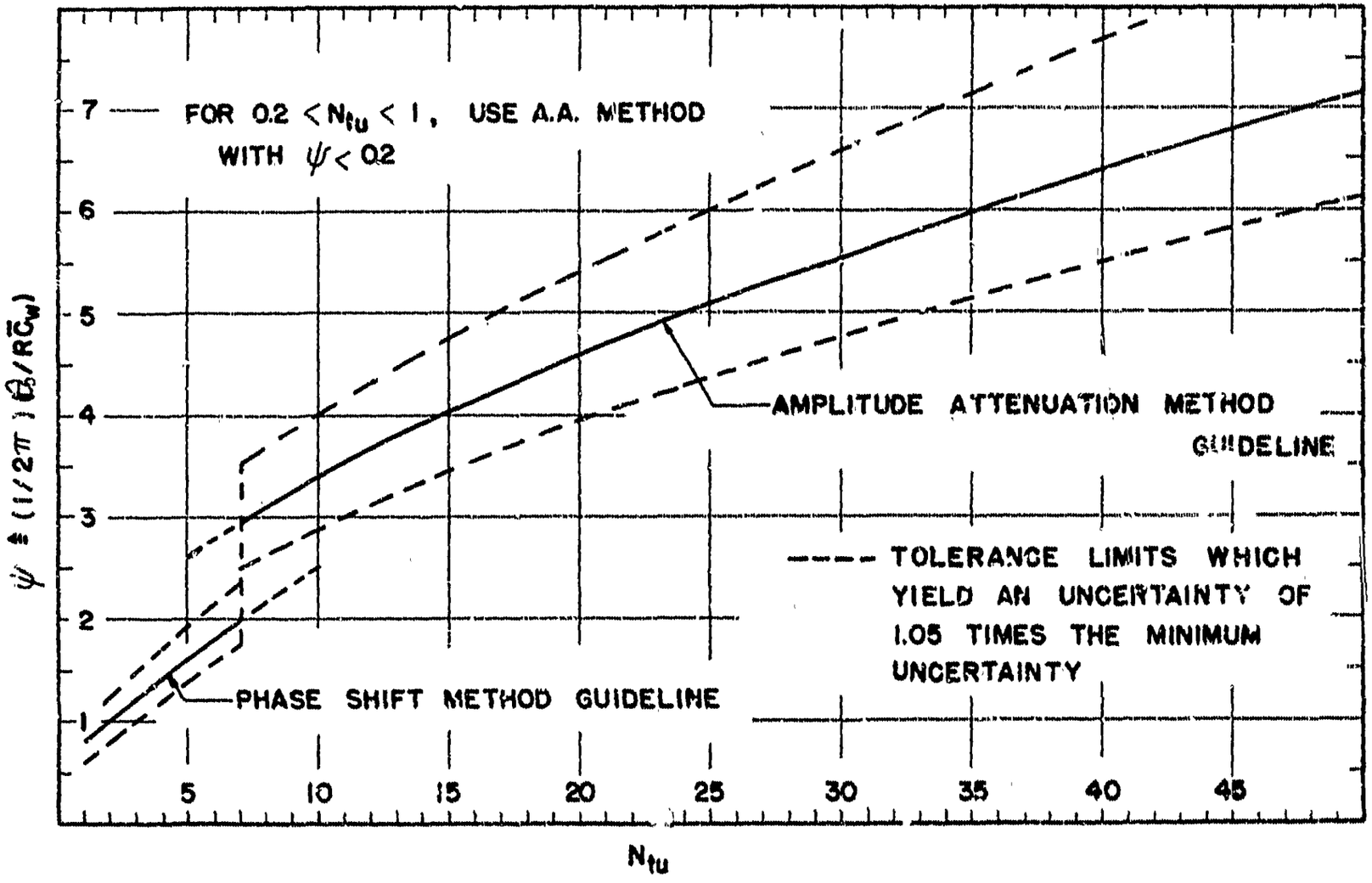

Figure 7.3 Recommended Nondimensional Periods for Best Test Accuracy.

An error in core specific heat does affect the heat transfer results, but not the Reynolds number. The analysis in Appendix VI shows that the magnitude of sensitivity of the heat transfer results to errors in core specific heat is dependent on the test parameter $\frac{}{}$. The sensitivity is plotted in Fig. VI-1. The figure shows that if the periodic technique is used as recommended in Section 7.3, the sensitivity for the amplitude attenuation method is

$$\frac{d\, N_{tu}/N_{tu}}{d\, c_w/c_w} \approx 2 \qquad (7.16)$$

and for the phase shift method is

$$\frac{d\, N_{tu}/N_{tu}}{d\, c_w/c_w} \approx 0.7 \qquad (7.17)$$

The periodic technique then is very sensitive to inaccuracy in the solid specific heat.

The periodic technique is about as sensitive to wall longitudinal conduction effects as the maximum slope single-blow technique. Wall longitudinal conduction effects must be considered for $\lambda\, N_{tu} > 0.01$. Generally the effect on heat transfer results is less than 10 percent. Therefore an uncertainty in solid conductivity k_w of 10 percent, would produce only about a one percent uncertainty in heat transfer results.

7.5 Experimental Apparatus

The periodic technique uses much of the same equipment as the single-blow transient technique. The wind tunnel test rig, originally described by Wheeler [5], has been modified as described mainly in Section 2 and Appendix I. For the periodic technique the FUNCTION SWITCH is set on P (this corresponds to the P position of SW_2, SW_3, SW_4, and SW_5 in Fig. 2.3). A cyclically varying resistor (mechanical drive) is connected to the heater control using the external PERIODIC INPUT plug. This resistor consists of two resistors in series: a variable resistor used to adjust the zero-level (minimum value) of the total resistance and a

log-taper variable resistor which is driven by the cam on a small variable speed electric motor. The result is a periodic variation in electrical resistance which is transformed by the heater control into a periodic variation of the input of electrical power to the airstream heater wires. Two small electric motors are used to cover a 100:1 range of period-of-oscillation, θ_o. One motor has a torque of 52 in. lbs. and a speed range corresponding to $7.5 < \theta_o < 150$ sec. The other motor has a torque of 4.0 in. lbs. and a speed range corresponding to $1.5 < \theta_o < 10$ sec.

The resulting airstream temperature does not have a pure sinusoidal temperature variation. This requires the use of a Fourier analysis of the temperature waveforms to extract the fundamental. To illustrate how closely the input temperature waveform resembles a simple sinusoidal wave, the test run for Core 510, Appendix VII, with $N_R = 226$ is considered here. The amplitude spectrum (i.e. $\sqrt{A_n^2 + B_n^2}$) normalized to the first harmonic is listed in Table 7.1:

Table 7.1

AMPLITUDE SPECTRUM OF THE INPUT
TEMPERATURE WAVE, NORMALIZED
TO THE FIRST HARMONIC, w = 312 lbs/hr

Harmonic	Magnitude
1	1.000
2	0.093
3	0.066
4	0.028

Clearly there is a fair approximation of a simple one-harmonic sinusoidal temperature wave input.

A single channel, Honeywell Electronik 19, Lab Recorder, is used to obtain both the upstream and downstream temperature records. To do this, the recorder is connected to the upstream thermocouples for at least one period θ_o, and then quickly switched to the downstream thermocouples for at least one period. Using the switching point as the starting point

for the downstream record and "backtracking" one period for the upstream starting point, the two close-to-simultaneous temperature waves, required in the data reduction program of Appendix VII, are obtained.

The thermocouple systems for the upstream and downstream each consisted of four series thermocouples using a room temperature mercury bath as the cold junction. A room temperature cold junction was used so that the 0-2 millivolt scale on the recorder could be used with a maximum deflection with no zero offset required. The temperature amplitude was held at about 10°F for the fluid entering the test core.

The period of oscillation θ_o was measured with a stopwatch and a count of the mechanical drive cycles on the variable resistor.

7.6 Results of Testing Core 510

7.6.1 Description of the Test Surface - The surface tested was Core No. 510 (Corning Designation L-2012). It is a glass-ceramic surface with straight triangular passages. The core serves a dual purpose. First it is a new surface of the 1000 cells/in^2 class and provides basic heat transfer and flow friction information. Second it was tested using the periodic technique and the single-blow technique (maximum slope method) and provides a direct comparison of the two techniques. The surface geometry and core weight are described in Table 7.2:

Table 7.2

CORE 510 SURFACE GEOMETRY AND WEIGHT

Cell count, N	910 cells/in^2
Porosity, p	0.716
Hydraulic Diameter, $4r_h$	1.693 (10^{-3} ft)
Area density, α	1691 ft^2/ft^3
Cell height/width, d*	0.622
$L/4r_h$	134.5
Core Mass, M	0.657 lbm

7.6.2 Test Results - The heat transfer and flow friction test results are plotted in Fig. 7.4 and are listed in Table VII-5. The figure demonstrates the very good agreement between the aided single-blow technique (maximum slope) and the periodic technique. The periodic technique was used for $2.6 < N_{tu} < 36.6$. This range in N_{tu} was not possible for the maximum slope method because it is limited to $N_{tu} > 5$. The effects of wall longitudinal conduction on the periodic technique heat transfer results are shown only for the high N_{tu} (low N_R) test points. The rest of the test points were virtually unaffected by the wall longitudinal conduction. The friction factor results are not dependent on the type of transient test technique used since testing for f involves only steady-state. A summary of the basic flow friction and heat transfer data for Core 510, taken from the smoothed curves of Fig. 7.4, is listed in Table 7.3.

Heat transfer results, j, are about 25 percent lower than theoretically predicted results for equilateral triangular tubes, with a constant heat flux boundary condition. This disagreement is believed to be caused primarily by a combination of passage nonuniformity in the matrix, non-triangular shape of the passages (two-thirds of the corners are well rounded), and the heat transfer boundary condition used in the theory not being well duplicated in testing. Friction factor results, f, are about 13 percent lower than the theory for equilateral triangular passages. In this case the disagreement is believed to be caused by passage non-uniformity and non-triangular shape; friction factor is not affected by the heat transfer boundary condition. A more detailed analysis of the above effects will be presented in a future report.

Fig. 7.5 demonstrates how well the guidelines from Section 7.3 were followed in the Core 510 tests. The experimental values of $\frac{}{}$ are plotted for the corresponding values of N_{tu}. The figure shows that the experimental values of the nondimensional period $\frac{}{}$ were all within the tolerance limits of Fig. 7.3.

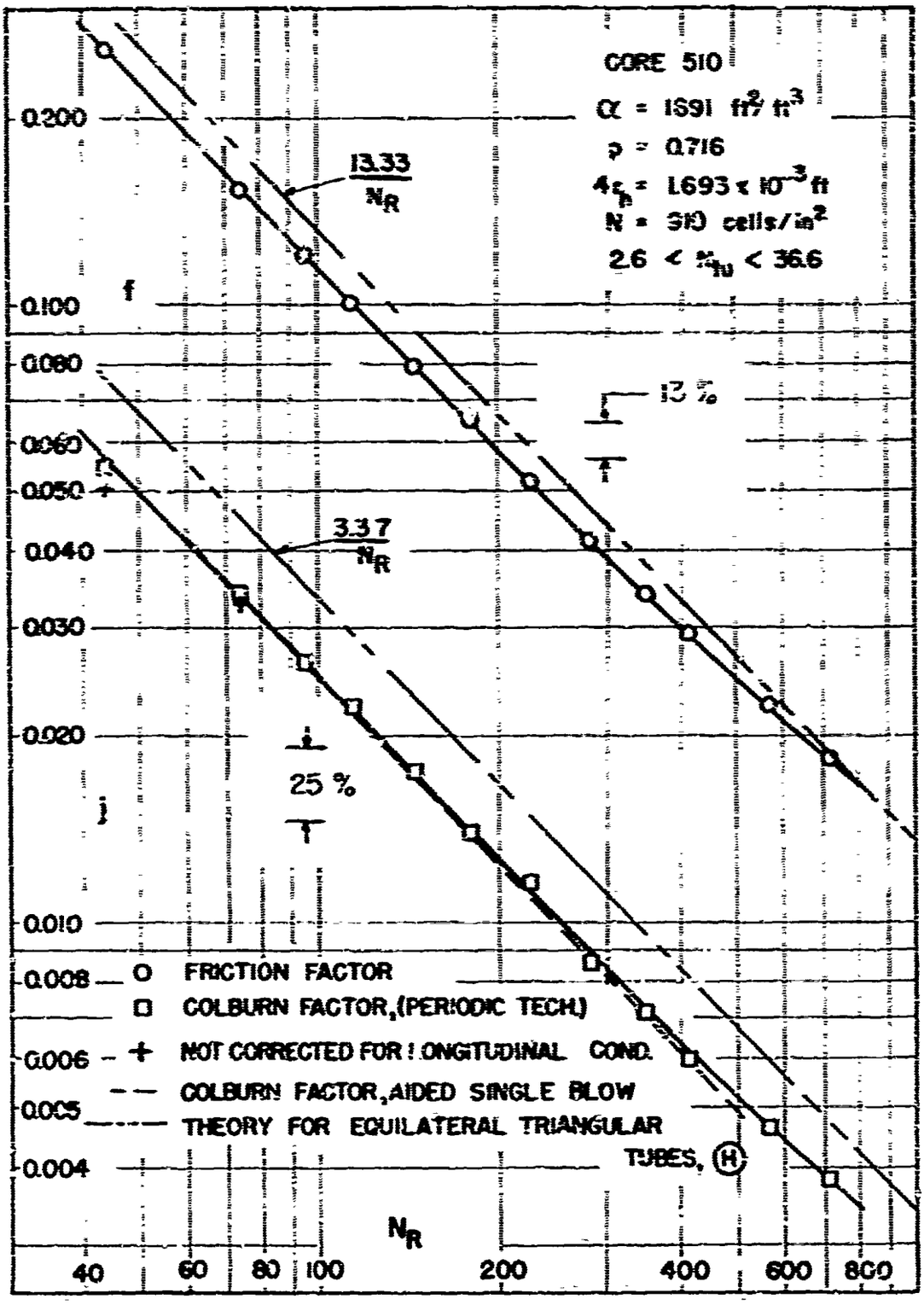

Figure 7.4 Core 510 Surface Characteristics (compared with the fully-developed laminar flow theory for equilateral-triangular passages).

Table 7.3

SUMMARY OF BASIC HEAT TRANSFER AND FLOW FRICTION CHARACTERISTICS FOR CORE 510

N_{Re}	j	f
900	.0031	.0154
750	.0039	.0186
500	.0052	.0246
400	.0064	.0300
300	.0084	.0392
200	.0126	.0581
150	.0166	.077
100	.0249	.114
80	.0312	.143
60	.0413	.190
40	.0620	.283

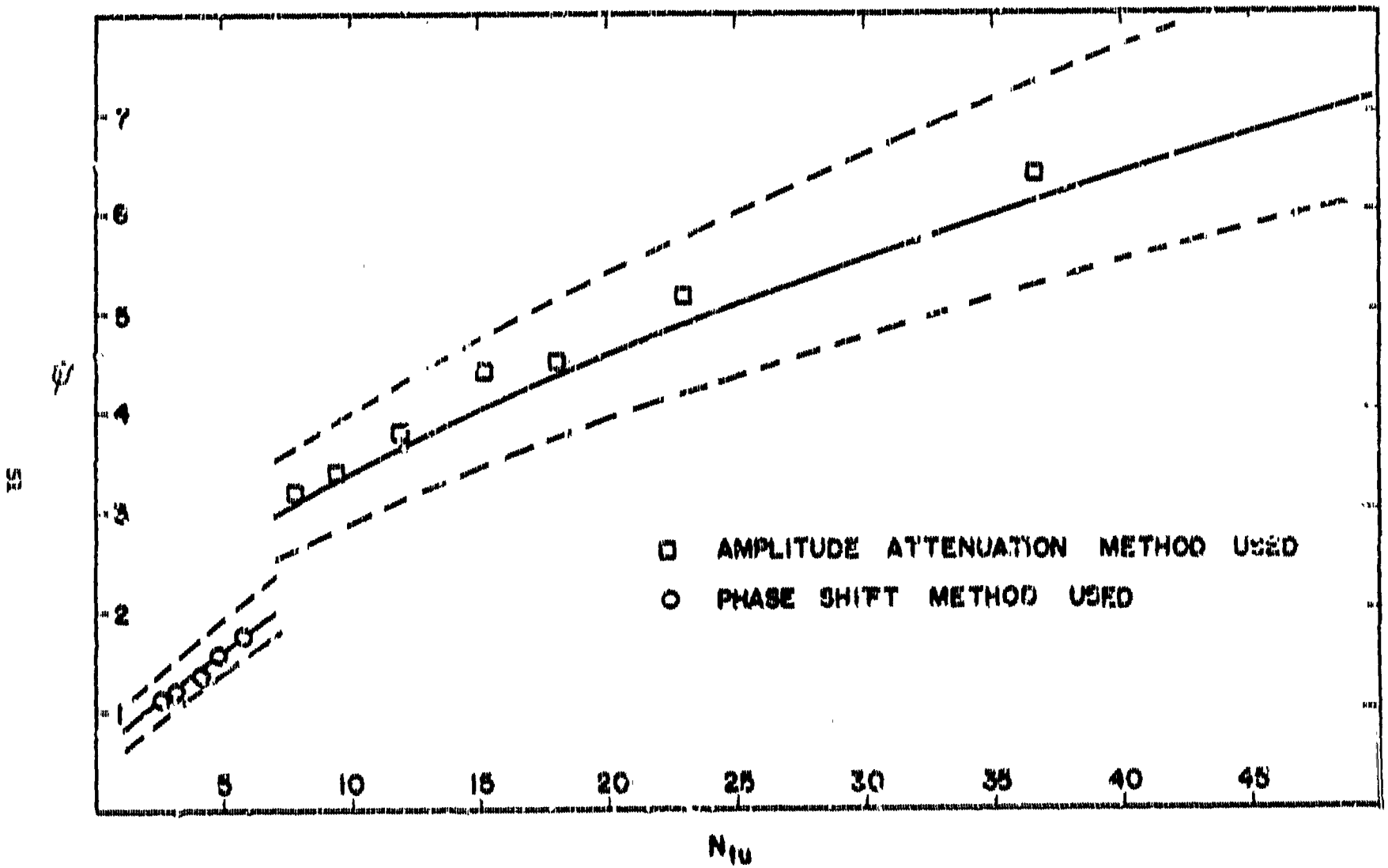

Figure 7.5 Core 510 Experimental Adherance to the Guidelines for Testing (Found Also in Figure 7.3).

8. COMPARING THE PERIODIC TECHNIQUE WITH THE MAXIMUM-SLOPE METHOD

8.1 Periodic Technique

The periodic technique has several advantages:

1. It has a wide useful test range, $0.5 \leq N_{tu} \leq 50$ (may be useful for even higher values of N_{tu}).
2. It is conceptually rather simple. This is shown in the analysis to obtain the finite wall longitudinal conduction effects.
3. It is basically an integral technique and does not require extracting derivatives from experimental measurements.
4. Analytical response curves are not required since the heat transfer results are computed in the data reduction.
5. Computing time is short; each run requires about 1 second on an IBM 360/67.
6. Periodic temperature waves are easier to generate experimentally than step functions. The considerable design effort included in Sections 3, 4, 5, and 6 could be eliminated by using the periodic technique.

Disadvantages of the periodic technique are:

1. It requires two temperature records.
2. A digital computer is required, especially for the Fourier analysis and the iterative steps used in accounting for wall longitudinal conduction.
3. About 30 to 50 data points must be read from each temperature record and this information prepared for the computer, requiring about 30 minutes per run.
4. A suitable period of oscillation, θ_o, must be determined approximately, prior to testing.

8.2 Single-Blow Technique, Maximum-Slope Method

Advantages of the maximum-slope method include:

1. It is easy and fast to use. The experimental temperature records may be evaluated and prepared for the computer in about 15 minutes per run.
2. Computing time is short, about 0.1 seconds per run on an IBM 360/67. Moreover, the computations can be "hand checked" quite readily.
3. It has good accuracy for $5 < N_{tu} < 50$.

Disadvantages of the maximum-slope method are:

1. It requires an experimental step-change in airstream temperature which is difficult to achieve. If a reasonably good step-change is not used in testing, an additional correction must be applied to the experimental results to account for this.
2. Sensitivity to experimental uncertainties becomes very large in the $0.5 \leq N_{tu} \leq 5$ range, limiting use of the method to $N_{tu} > 5$.
3. Conceptually, the method is complicated. Analytical response curves are required in the data reduction.
4. Experimental derivatives are required.

8.3 Similarities

The periodic technique and the maximum slope method are very similar in the following ways:

1. Only one fluid is used.
2. Matrix surfaces can be tested.
3. No wall temperature measurement is needed.
4. High effectiveness cores can be tested.

5. Wall longitudinal conduction effects on test results are about equal.

6. Sensitivities to uncertainty in core specific heat are about equal for $10 < N_{tu} < 50$.

9. CONCLUSIONS AND RECOMMENDATIONS

9.1 Conclusions

1. The heater control, designed and constructed as a part of this project, functions satisfactorily. The time constant of the heater system is reduced by from 60 percent at 100 lbm/hr to 40 percent at 1000 lbm/hr. Some of the other desirable features of the heater control are: solid-state device with no maintenance required, small size and economical, control by a small resistor, flexibility in application to systems requiring more power by just changing the silicon control rectifiers, and cyclic temperature control possibility.

2. Using the fast response heater system (aided) caused the heat transfer results to be higher by an average of 3.8 percent, for the four glass-ceramic cores tested.

3. Guidelines for using the periodic technique were extended so it now can be used in the range $0.2 < N_{tu} < 50$. Use at $N_{tu} > 50$ was not considered, but should present no special problems.

4. The periodic technique was generalized to account and correct for the effects of wall longitudinal conduction. The magnitude of the corrections was found to be about as large as for the maximum-slope method.

5. The periodic technique was used for $2.6 < N_{tu} < 36.6$. Very good agreement was demonstrated with the maximum-slope results obtained using the fast response heater system.

6. As demonstrated by the above agreement, both the periodic and the maximum-slope techniques give good results when properly applied.

9.2 Recommendations

1. A fast response heater system is required in the maximum slope method. A heater control circuit, such as presented in this report, is recommended as a means to achieve the fast response.

2. The periodic technique is recommended as the overall best transient technique to use. A wide N_{tu}-test range as well as an easily generated temperature wave are two major advantages.

3. To resolve the differences between the change in heat transfer results obtained experimentally in this project due to a sharper input step-change, and the analytical predictions of [3,11], the following are recommended:

   a. Perform maximum-slope tests, intentionally using an extremely slow-response heater system. This would allow easy and accurate measurements of the input temperature function and would produce large effects on the heat transfer results.

   b. Use a geometrically uniform test core to eliminate possible effects of passage nonuniformity on results.

4. The effect of a non-simple-sinusoidal input wave on heat transfer results using the periodic technique should be determined. One way to experimentally obtain a more regular sinusoidal wave is by placing a low-N_{tu} matrix in the airstream between the heaters and the test core. The matrix would serve to damp out higher harmonics.

5. The sensitivity of the periodic technique to nonuniform flow distribution in the test matrix should be analyzed.

APPENDIX I

GENERAL TEST RIG INFORMATION

Specifications of the Test Rig (see also Fig. 2.1)

Table II-1

STANFORD TRANSIENT TEST RIG SPECIFICATIONS

Inlet: Bellmouth with a pack of screens and an egg-crate flow straightener. A fan is used to mix the air before entering the inlet.

Heaters: Four banks of 0.003 in. dia. alumel wire with

a. Maximum heat generation rate - 2.37 Btu/sec (= 2500 watts)
b. Electrical resistance - 5 ohms
c. Thermal capacitance - 1.8×10^{-4} Btu/°F

Heater Control: Solid-state device with

a. Single-blow capability - $100 < w < 1000$ lbm/hr, aided $\Delta T_\infty \gtrsim 15°F$
b. Periodic capability - $50 < w < 1000$ lbm/hr, amplitude $\approx 10°F$
   1. Large Motor - $7.5 <$ Period < 150 sec
   2. Small Motor - $1.5 <$ Period < 10 sec

Test Section: Plexiglass drawer capable of accepting a test core of 3.25 in. x 3.25 in. x up to 4.0 in. long.

Temperature Sensors: Copper-constantan thermocouples

a. Inlet - 1 junction, 28 gage, ice reference.
b. Orifice - 1 junction, 28 gage, ice reference.
c. Upstream - 4 junctions, 0.002 in. dia. wire, ice or mercury bath references.
d. Downstream - 4 junctions, 0.002 in. dia. wire; ice or mercury bath or incoming inlet air references.

Pressure Sensors: Vertical and inclined manometers reading inches of water. Taps are located upstream and downstream of the test core and at 1-D and $\frac{1}{2}$-D from the orifice plate.

Flow Meter: Sharp-edged ASME orifice, two plates, No. 1 - 1.301 in. dia., No. 2 - 2.201 in. dia., pipe diameter - 3.06 in.

Blower: 1000 lbm/hr at 70 in. of water static pressure rise.

Pitot Tube: Standard pitot-static tube, 0.1 in. OD. A recession in the test rig wall is provided for stowage during heat transfer tests.

Circuit Layout of the Heater Control

The heater control consists of three main sections, assembled in sequence and enclosed in an aluminum box. The sections are: front panel Fig. I-1, firing-circuit board Fig. I-2, and power board Fig. I-3. Schematic diagrams for the banks of capacitors C_2 and C_3 are shown in Fig. I-4.

Operating Instructions for the Heater Control

FAST RESPONSE SINGLE-BLOW

1. Set air flow rate.
2. Adjust C_2 and C_3 according to Table I-2.
3. Set R_2 and R_5 to 0.
4. Turn SW_1 to ON.
5. Set FUNCTION SWITCH to U.
6. Adjust R_2 for about 20°F tempature rise using airstream thermocouples.
7. Set FUNCTION SWITCH to D.
8. Adjust R_5 for about 5°F temperature rise using the thermocouples.
9. Switching FUNCTION SWITCH alternately from D to U to D etc. will produce the required fast response Step-Up and Step-Down in airstream temperature entering the test core.

NORMAL SINGLE-BLOW

1. Set FUNCTION SWITCH to N.
2. Switching SW_1 from ON to OFF to ON etc. will produce a regular response step-change in airstream temperature. Only R_2 is used to control the upper temperature level.

PERIODIC

1. Set FUNCTION SWITCH to P.
2. Turn SW_1 to OFF.
3. Plug in the variable resistor with zero-level resistor at zero.
4. Rotate cam to minimum resistance position.
5. Turn SW_1 to ON.
6. Adjust zero-level resistor for about 20°F rise in airstream temperature.
7. Rotate cam and note temperature amplitude fluctuation.
8. If necessary adjust the amplitude using the cam mounted resistor and repeat steps 4 through 7 until the desired temperature wave is obtained.
9. The period of oscillation is adjusted using the motor speed control.

Table I-2

CAPACITOR SETTINGS

w (lbm/hr)	C_2 Position	C_3 Position
100	1.0	1.5
130	1.5	2.0
160	2.0	2.5
200	2.5	3.0
250	3.0	3.5
320	3.5	4.0
400	4.0	4.5
500	4.5	5.0
630	5.0	5.0
800	5.5	5.5
1000	6.0	6.0

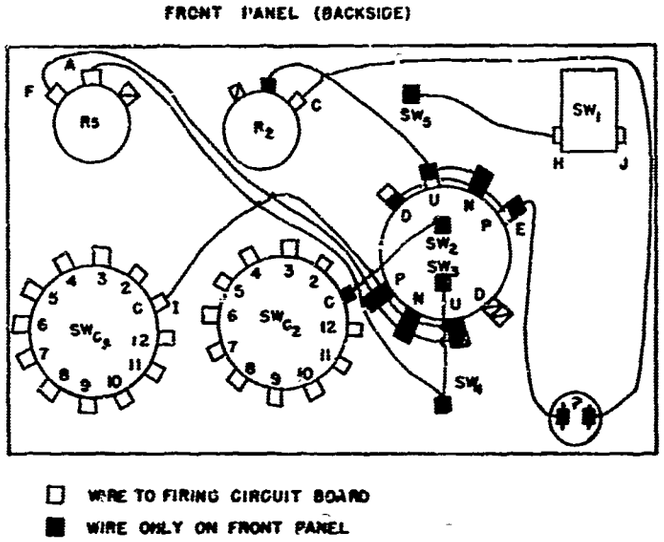

Figure I-1 Backside of the Heater Control Front Panel (showing position of controls and wiring connections).

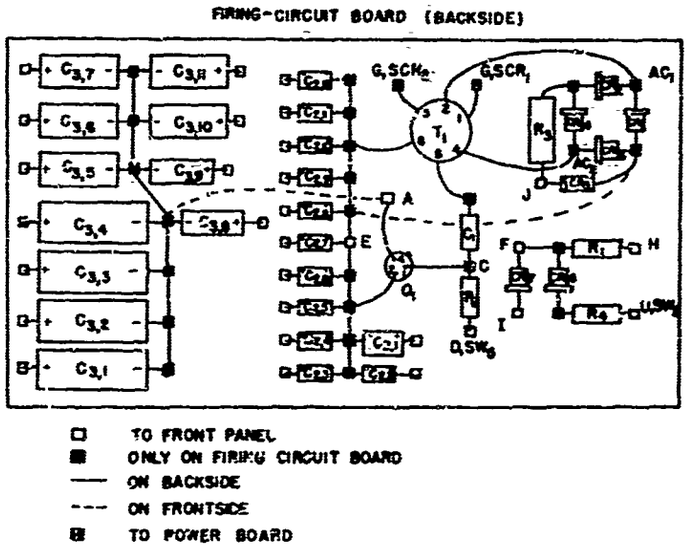

Figure I-2 Heater Control Firing Circuit Board (showing position of circuit elements and wiring connections).

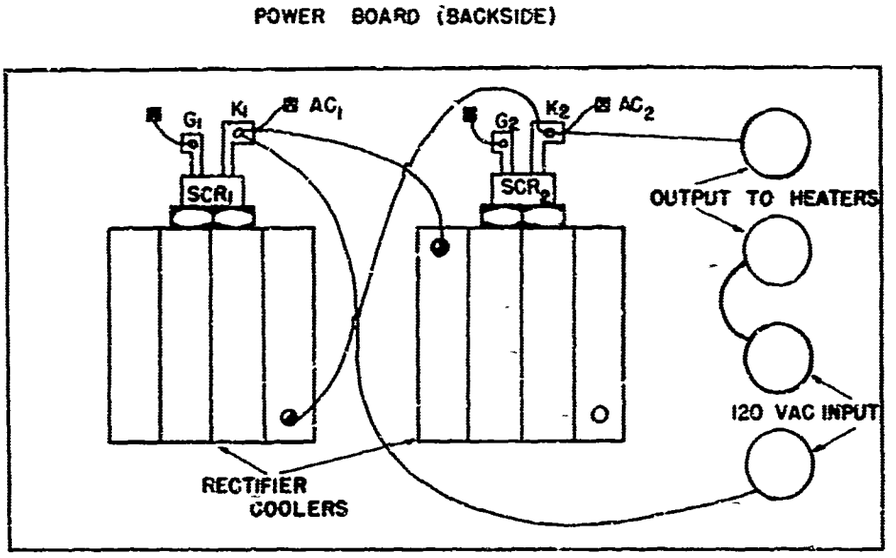

Figure I-3 Heater Control Power Board (showing input and output connection terminals and SCR coolers)

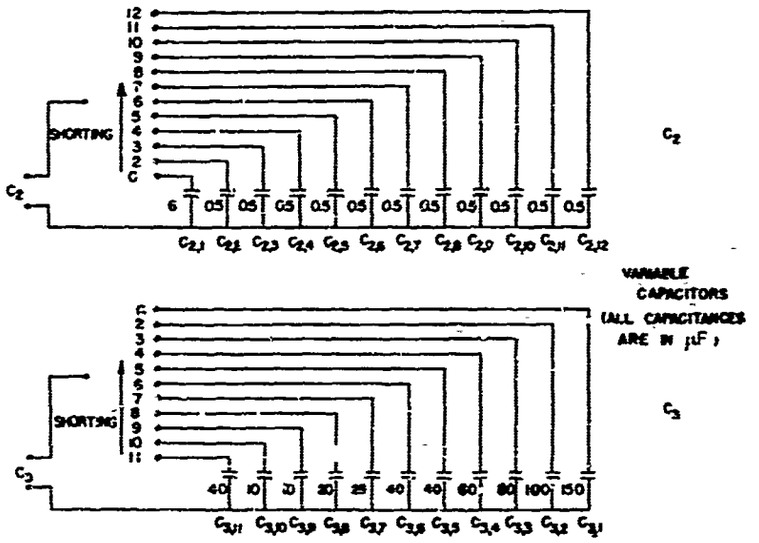

Figure I-4 Schematic Diagrams of Banks of Capacitors C_2 and C_3.

APPENDIX II

HEATER THERMAL CIRCUIT PARAMETERS AND ZCAP INPUT

Thermal Resistance

The air film convective thermal resistance of the heater wires is defined as

$$R_H \triangleq \frac{1}{(hA)_H}$$

The total surface area of the wires, of length 4 heaters x 56 passes x 3.25 inch/pass and dia. 0.003 inches, is

$$A_H = L_H \pi D_H = \frac{\pi \times .003 \times 4 \times 56 \times 3.25}{144} = 0.0476 \text{ ft}^2$$

The surface average convection heat transfer coefficient of the wire h_H can be determined using data presented by McAdams [9]. In the reference, N_{Nu} is plotted versus N_R for air flowing normal to single cylinders. For example, consider the air flow rate of 590 lbm/hr. The Reynolds number is calculated:

$$N_R \triangleq \frac{D_H G}{\mu} = \frac{.003 \times 590 \times 12}{3.25^2 \times 3600 \times 145 \times 10^{-7}} = 38.5$$

From the N_{Nu} versus N_R graph

$$N_{Nu} \triangleq \frac{h_H D_H}{k} \approx 3.1$$

Air viscosity and thermal conductivity used in the N_R and N_{Nu} calculations are taken from [10], using a film temperature of 200°F. Then

$$h_H = \frac{3.1 \times 0.0182 \times 12}{0.003} = 226 \frac{\text{Btu}}{\text{hr-ft}^2\text{-°F}}$$

and

$$R_H = \frac{3600}{226 \times 0.0476} = 336 \frac{sec-°F}{Btu}$$

The above calculations have been repeated for other flow rates to obtai the curve in Fig. 3.2.

Thermal Capacitance

Values used for the physical properties of the alumel heater wire are [13]

$$\rho_H = 544 \text{ lbm/ft}^3$$

$$c_H = 0.11 \frac{Btu}{lbm-°F}$$

The total capacitance can be calculated:

$$C_H = \frac{\pi D_H^2}{4} (Lc\rho)_H = \frac{3.14 \times 0.003^2 \times 56 \times 3.25 \times 544 \times 0.11}{1728}$$

$$= 1.77 \times 10^{-4} \frac{Btu}{°F}$$

ECAP Input

The ECAP [9] equivalent circuit for the thermal circuit in Fig. 3. is given in Fig. II-1. Nodes and positive current directions are assig by the figure. The ECAP input for the case where $w = 590$ lbm/hr, considered in Appendix III, is listed in Table II-1. Current-source values on the I1 card are for the step-up case with $C_2 = 10.1$ pF. This is discussed more in Appendix III.

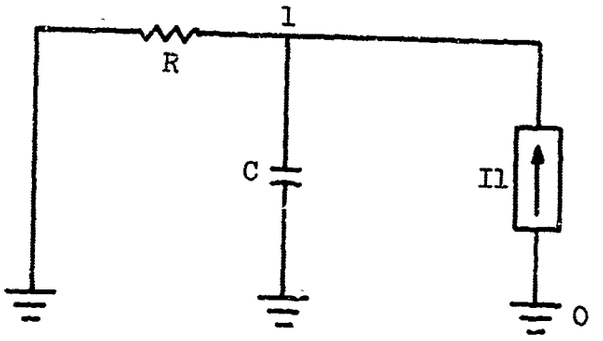

Figure II-1 ECAP Representation of the Thermal Circuit

Table II-1

ECAP PROGRAM INPUT SAMPLE

```
      TRANSIENT ANALYSIS
C  W=590 LBM/HR      C2=10.1 MFD
B1     N(0,1), C=1.77E-04
B2     N(1,0),R=336.
I1     (5),2.37,2.10,1.85,1.64,1.46,1.32,1.21,1.13,1.05,
      *0.99,0.93,0.89,0.86,0.84,0.81,0.80,0.79,0.78,0.78
       TIME STEP=0.001
       OUTPUT INTERVAL=10
       FINAL TIME=0.25
       PRINT,NV,CA
       EXECUTE
```

APPENDIX III

STEP-UP CIRCUIT ANALYSIS

Technique Used

The key elements in the heater control circuit of Fig. 2.3 can be approximated by Fig. III-1:

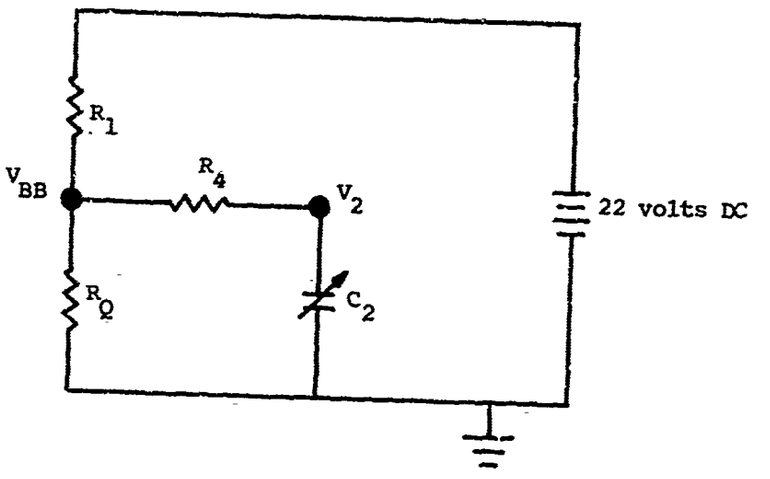

Figure III-1 Approximation of the Heater Control Circuit, Step-Up Case

To analyze the circuit in Fig. 2.3 a means is needed to obtain the interbase voltage V_{BB} or the UJT as a function of time. The circuit in Fig. III-1 makes this possible by simplifying the calculations. The 22-volt DC voltage source is equivalent to the voltage developed across zener diode CR_5. Interbase resistance ($I_E = 0$) is denoted by R_Q. The value used for R_Q in the design calculations was 5910 ohms.

The circuit equations written on a nodal basis are

Node at V_{BB}

$$\frac{22-V_{BB}}{R_1} + \frac{0-V_{BB}}{R_Q} + \frac{V_2-V_{BB}}{R_4} = 0 \qquad \text{(III-1)}$$

Node at V_2

$$\frac{V_{BB}-V_2}{R_4} + C_2 \frac{d(0-V_2)}{d\theta} = 0 \qquad \text{(III-2)}$$

Solving Eqs. (III-1) and (III-2) for V_{BB} yields

$$V_{BB} = 20.6 - 8.7 \exp(-\eta\theta) \qquad \text{(III-3)}$$

where

$$\eta \triangleq \frac{\frac{1}{R_1} + \frac{1}{R_Q}}{\frac{C_2 R_4}{\sigma}\left[\frac{1}{R_1} + \frac{1}{R_Q} + \frac{1}{R_4}\right]}$$

The quantity σ is a correction applied to the value of C_2 to account for the chopped voltage applied to the firing circuit, see Fig. 2.4. A chopped voltage exists across the firing circuit (R_3 or CR_5) because the voltage collapses during conduction by the SCR's. Fig. III-2 shows how the effective heater control output voltage varies with the phase angle (triggering time). The values in the figure are from a simple heating-effect analysis of a sinusoidal voltage wave, with a peak absolute value of 170 volts. Figure III-2 also defines the triggering time θ_s, used in the following definition:

$$\sigma \triangleq \frac{\theta_{s,\ \text{Initial Condition}} + \theta_{s,\ \text{steady-state}}}{2 \times 0.00833} \qquad \text{(III-5)}$$

σ can be regarded as an average portion of real time during which capacitor C_2 is being charged by the blocking effect of the SCR's.

Interbase voltage V_{BB} may now be calculated as a function of real time using Eqs. (III-3), (III-4), and (III-5). Trials are made and the results examined to determine C_2. C_2 is a function of air flow rate, hence the variable notation in Fig. III-1.

Having obtained $V_{BB}(\theta)$, the firing voltage V_p may be calculated. The relation used is given by the manufacturer [7] for UJT 2N2646 as typically

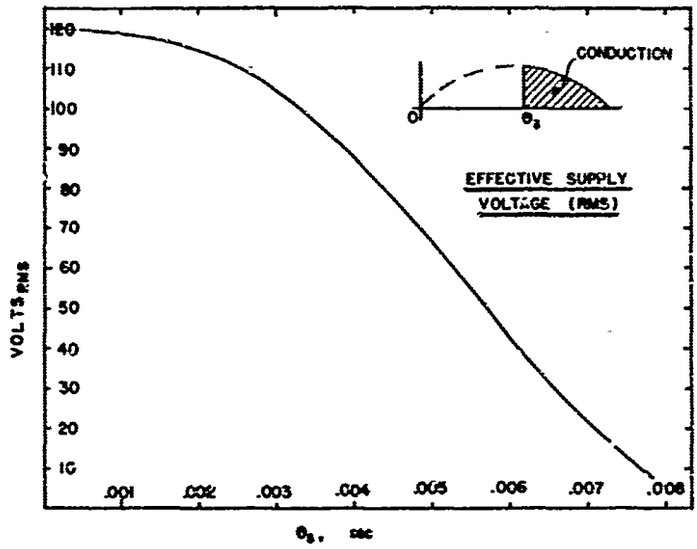

Figure III-2 Effective Heater Control Output Voltage Variation with Triggering Time

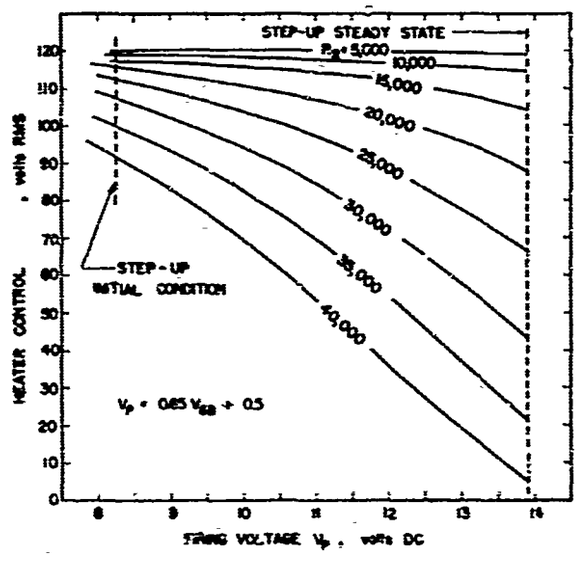

Figure III-3 Heater Control Output Voltage

$$V_p(\theta) = 0.65\ V_{BB}(\theta) + 0.5 \qquad \text{(III-6)}$$

Fig. III-3 provides the output voltage of the heater control as a function of the firing voltage V_p and the steady-state resistor value R_2. It is a key one in the circuit analysis. Knowing the steady-state heater power required, the value for R_2 may be found by first using Fig. 3.3 to get the steady-state voltage output required of the heater control. Next, Fig. III-3 is used to determine the value of R_2 on the steady-state line corresponding to that heater control voltage.

Sample Calculation

An intermediate air flow rate of $w = 590$ lbm/hr is chosen for this example with $C_2 = 10.1\ \mu F$. The heater power for steady-state operation is

$$q_o = wc_p \Delta T_\infty = \frac{590 \times 0.24 \times 20}{3600} = 0.787\ \frac{Btu}{sec}$$

The steady-state voltage output of the heater control is then found using Fig. 3.3:

$$V_{H,\ Steady\text{-}State} = 64 \text{ volts RMS}$$

and the value of R_2 from Fig. III-3:

$$R_2 = 26{,}000 \text{ ohms}$$

Fig. III-3 can also be used to find the initial voltage applied to the heaters. From the figure

$$V_{H,\ Initial} = 112 \text{ volts RMS}$$

with a corresponding power generation rate of 2.37 Btu/sec.

Fig. III-2 is used to find the initial-condition and steady-state triggering times, θ_s, used in the calculation of σ. Using Eq. (III-5)

$$\sigma = \frac{0.00235 + 0.00512}{2 \times 0.00833} = 0.45$$

and from Eq. (III-4) the value of η is calculated

$$\eta = \frac{\frac{1}{390} + \frac{1}{5910}}{\frac{10.1 \times 10^{-6} \times 500}{0.45}\left[\frac{1}{390} + \frac{1}{5910} + \frac{1}{500}\right]} = 51.4 \text{ sec}^{-1}$$

Using this value for η in Eq. (III-3), the calculating equation for $V_{BB}(\theta)$ is

$$V_{BB}(\theta) = 20.6 - 8.7 \exp(-51.4\ \theta)$$

A time step of 0.005 sec. was selected for the calculations of input voltage to the heaters. At the first time step $\theta = 0.005$ sec

$$V_{BB}(0.005) = 20.6 - 8.7 \exp(-51.4 \times 0.005) = 13.9 \text{ volts}$$

and

$$V_p = 0.65 \times 13.9 + 0.5 = 9.6 \text{ volts}$$

From Fig. III-3, with $R_2 = 26{,}000$ ohms and $V_p = 9.6$ volts, the heater voltage may be obtained:

$$V_H(0.005) = 105 \text{ volts RMS}$$

Fig. 3.3 is next used to find the heater power generated:

$$q_o(0.005) = 2.10 \frac{\text{Btu}}{\text{sec}}$$

The value for time θ is now increased to 0.01 sec. and the series of calculations beginning with $V_{BB}(\theta)$ is repeated. The results are plotted in Fig. III-4 for four values of C_2, covering the design range of interest.

Each curve in Fig. III-4 may be used as input for the ECAP program, discussed briefly in Section 3.3 and Appendix II. Response curves, calculated using ECAP, are shown in Fig. III-5 for the four values of C_2. The influence of C_2 on the results is very apparent and $C_2 = 10.1\ \mu F$ was selected for use in the circuit.

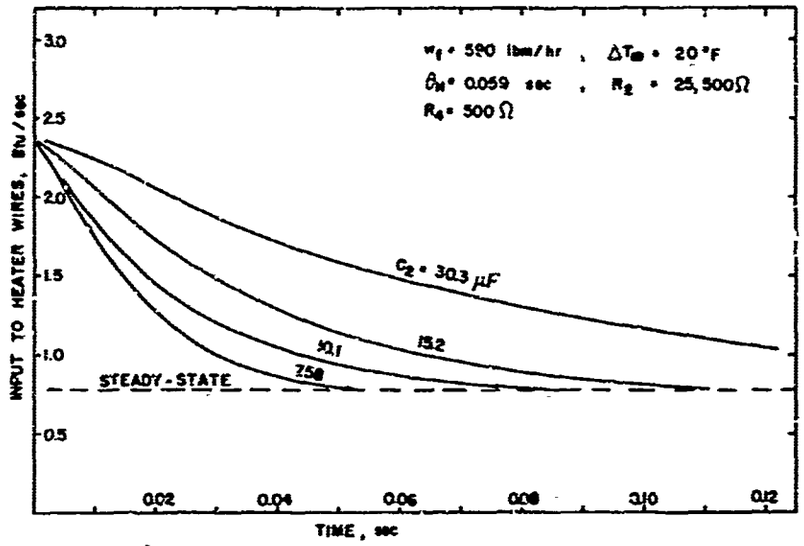

Figure III-4 Input to the Heater Wires, w = 590 lbm/hr.

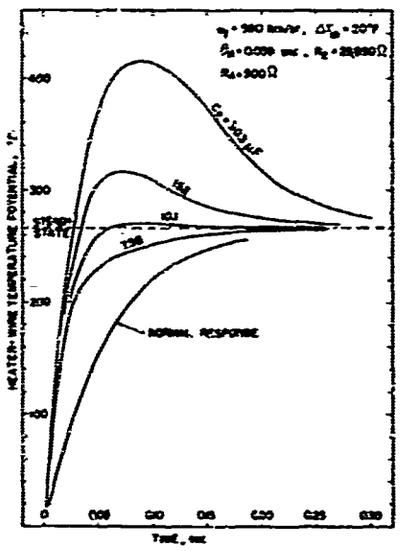

Figure III-5 Response of the Heater Wires Calculated Using ECAP.

The same type of analysis was done at air flow rates of 100 lbm/hr and 1000 lbm/hr. The respective values for C_2 were selected on the basis of resulting closest approach to a step-change in airstream temperature. Values of C_2 to be used at intermediate air flow rates were determined by interpolation.

APPENDIX IV

STEP-DOWN CIRCUIT ANALYSIS

The key elements in the heater control circuit of Fig. 2.3 can be approximated by Fig. IV-1:

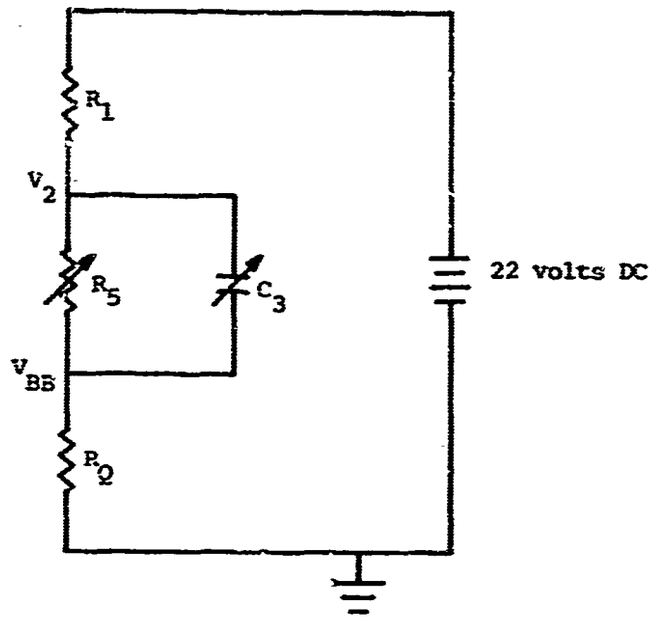

Figure IV-1 Approximation of the Heater Control Circuit, Step-Down Case

As in the step-up case, to analyze the circuit in Fig. 2.3 a means is needed to obtain the interbase voltage V_{BB} on the UJT as a function of time. The circuit in Fig. IV-1 simplifies the calculations. The 22-volt DC voltage is equivalent to the voltage developed across zener diode CR_5. Interbase resistance (with $I_E \approx 0$) is denoted by R_Q. The value used for R_Q in the design calculations was 5910 ohms. Variable resistor R_5 is used to adjust the steady-state voltage ($\Delta T \approx 5°F$) output to the heaters in the step-down mode of operation.

The circuit equations written on a nodal basis are

Node at V_{BB}

$$\frac{0-V_{BB}}{R_Q} + \frac{V_2-V_{BB}}{R_5} + C_3 \frac{d(V_2-V_{BB})}{d\theta} = 0 \qquad \text{(IV-1)}$$

Node at V_2

$$\frac{22-V_2}{R_1} + \frac{V_{BB}-V_2}{R_5} + C_3 \frac{d(V_{BB}-V_2)}{d\theta} = 0 \qquad \text{(IV-2)}$$

Solving Eqs. (IV-1) and (IV-2) for V_{BB} yields:

$$V_{BB}(\theta) = \left[20.6 - \left(\frac{22}{\frac{R_5}{R_Q} + \frac{R_1}{R_Q} + 1}\right)\right] \exp(-\eta\theta) + \left[\frac{22}{\frac{R_5}{R_Q} + \frac{R_1}{R_Q} + 1}\right] \qquad \text{(IV-3)}$$

where

$$\eta \triangleq \frac{\frac{1}{R_Q} + \frac{R_1}{R_5 R_Q} + \frac{1}{R_5}}{\frac{C_3}{\sigma}\left(\frac{R_1}{R_Q} + 1\right)}$$

σ is defined and discussed in Appendix III. However, for the step-down case the initial condition corresponds to $q_o = 0$ and the steady-state condition to $\Delta T_\infty \approx 5°F$. Therefore, Eq. (III-5) becomes

$$\sigma = 0.5 + \frac{\theta_{s,\ \text{steady-state}}}{2 \times 0.00833} \qquad \text{(IV-4)}$$

As steady-state is approached, the exponential term in Eq. (IV-3) vanishes, allowing calculation of R_5. The steady-state heat generation rate is

$$q_o = wc_p\Delta \qquad \text{(IV-5)}$$

Fig. 3.3 is used to convert this into heater voltage. Fig. III-3 is then entered at the curve for $R_2 = 40{,}000$ ohms to obtain the firing voltage V_p, hence $V_{BB,\ \text{steady-state}}$ using

$$V_{BB} = \frac{V_P - 0.5}{0.65}$$

From Eq. (IV-3)

$$R_5 = R_Q \left(\frac{22}{V_{BB,\,steady\text{-}state}} - \frac{R_1}{R_Q} - 1 \right) \qquad \text{(IV-6)}$$

All the parameters in Eq. (IV-3) having been evaluated, the interbase voltage V_{BB} can now be calculated as a function of time. A process very similar to the step-up case in Appendix III is used to calculate heater-wire temperature. The curve for R_2 = 40,000 ohms in Fig. III-3 is used for all air flow rates in the step-down mode; the variable resistor R_2 has been replaced by a fixed resistor R_6.

APPENDIX V

DERIVATIONS FOR THE PERIODIC TECHNIQUE

In this appendix, a segment of an idealized heat exchanger, Fig. V-1, is analyzed to arrive at the differential and integral equations which govern the bulk fluid temperature and the wall temperature in the heat exchanger. The conservation of energy; conservation of mass, the conductive and convective rate equations, and the equation of state are used in the analysis. Three cases are considered: the wall longitudinal conduction is zero (as treated in [4]), the wall longitudinal conduction is finite, and the wall longitudinal conduction is infinite. In all cases the radial thermal conductivity is considered as infinite.

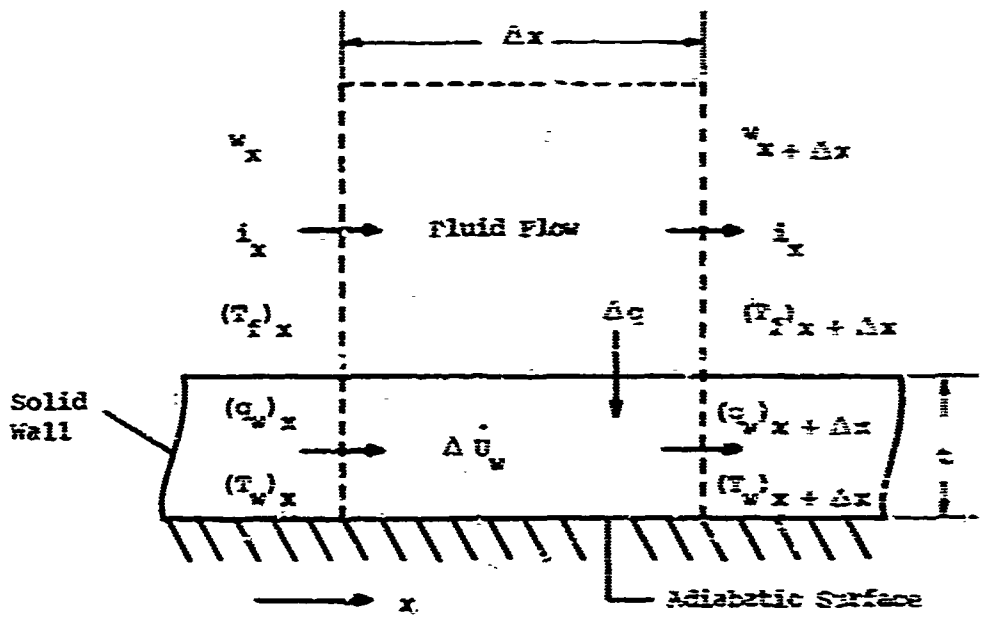

Figure V-1. Segment of an Idealized Heat Exchanger

The following idealizations are made:

1. The temperatures T_w of the wall, and T_f of the fluid, are functions of time θ and distance x only.

2. The system is overall adiabatic.
3. Wall and fluid properties are constant.
4. The fluids are considered to be low velocity gases at constant pressure, and the enthalpy and internal thermal energy can be treated as functions of temperature using the specific heat property.
5. There is no longitudinal heat conduction in the fluid.
6. Fluid thermal capacitance is neglected relative to the wall capacitance $\tilde{C}_w$. This was considered in [4] and shown to be negligible in situations involving a gas.
7. The fluid has steady-flow.

Derivation of Equations

The conservation of energy applied to the solid wall segment of unit depth normal to Fig. V-1 can be stated by the following equation. At any instant of time θ

$$(q_w)_{x+\Delta x} - (q_w)_x + \Delta q + \Delta \dot{U}_w = 0 \qquad \text{(V-1)}$$

The conduction and convection rate equations for q_w and Δq respectively are:

$$q_w = -k_w t \frac{\partial T_w}{\partial x} \qquad \text{(V-2)}$$

$$\Delta q = \int_x^{x+\Delta x} h(T_f - T_w)\, dx \qquad \text{(V-3)}$$

The energy storage term for the wall is

$$\Delta \dot{U}_w = \int_x^{x+\Delta x} (\rho c t)_w \frac{\partial T_w}{\partial \theta}\, dx \qquad \text{(V-4)}$$

Eqs. (V-1) through (V-4) can be combined and after applying the theorem of the mean and passing to the limit ($\Delta x \to 0$), the following equation is obtained:

$$-k\frac{\partial}{\partial x}\left(t\frac{\partial T_w}{\partial x}\right) - h(T_f-T_w) + (\rho ct)_w \frac{\partial T_w}{\partial \theta} = 0 \qquad \text{(V-5)}$$

The conservation of energy applied to the fluid system in Fig. V-1 can be stated by the following equation. At any instant of time θ

$$(wi)_{x+\Delta x} - (wi)_x + \Delta q = 0 \qquad \text{(V-6)}$$

Eqs. (V-3) and (V-6) can be combined and after applying the theorem of the mean and passing to a limit ($\Delta x \to 0$), the following equation is obtained:

$$\frac{\partial}{\partial x}(wi) + h(T_f-T_w) = 0 \qquad \text{(V-7)}$$

For a perfect gas

$$\frac{\partial i}{\partial x} = c_p \frac{\partial T_f}{\partial x} \qquad \text{(V-8)}$$

Since w is a constant, Eqs. (V-7) and (V-8) are combined and become

$$wc_p \frac{\partial T_f}{\partial x} + h(T_f-T_w) = 0 \qquad \text{(V-9)}$$

The parameters C_f, $\bar{C}_w$, and R are now introduced and are defined by

$$C_f \triangleq wc_p \qquad R \triangleq \frac{1}{hA}$$

$$\bar{C}_w \triangleq (\rho Ac)_w L$$

Eqs. (V-5) and (V-9) become

$$-k_w L \frac{\partial}{\partial x}\left(A_w \frac{\partial T_w}{\partial x}\right) - \frac{T_f - T_w}{R} + \bar{C}_w \frac{\partial T_w}{\partial \theta} = 0 \qquad \text{(V-10)}$$

$$C_f \frac{\partial T_f}{\partial x} + \frac{T_f - T_w}{RL} = 0 \qquad \text{(V-11)}$$

The above Eqs. (V-10) and (V-11) apply even for variable A_w, R, $\bar{C}_w$, and C_f. These will be considered constant and the following definitions are introduced:

$$x^* \triangleq \frac{x}{L} \qquad \theta^* \triangleq \frac{\theta}{RC_w}$$

$$RC_f \triangleq \frac{1}{N_{tu}} \qquad \lambda \triangleq \frac{k_w A_w}{LC_f} \tag{V-12}$$

$$T_f^* \triangleq \frac{T_f - T_m}{\Delta T_o} \qquad T_w^* \triangleq \frac{T_w - T_m}{\Delta T_o}$$

$$Z = N_{tu}\, x^*$$

where T_m is the mean temperature about which the system oscillates and ΔT_o is the amplitude of T_f at the inlet. T_f^* and T_w^* are the nondimensional temperatures and θ^* is the nondimensional time. The nondimensional space coordinate is Z. Then Eqs. (V-10) and (V-11) become:

$$T_f^* - T_w^* = \frac{\partial T_w^*}{\partial \theta^*} - \lambda\, N_{tu} \frac{\partial^2 T_w^*}{\partial Z^2} \tag{V-13}$$

$$T_f^* - T_w^* = -\frac{\partial T_f^*}{\partial Z} \tag{V-14}$$

Solution For Wall Longitudinal Conduction Zero ($\lambda = 0$)

When the wall longitudinal conduction parameter $\lambda\left(\triangleq \frac{k_w A_w}{LC_f}\right)$ approaches zero, the last term in Eq. (V-13) becomes negligible and the equations of interest are

$$T_f^* - T_w^* = \frac{\partial T_w^*}{\partial \theta^*} \tag{V-15}$$

$$T_f^* - T_w^* = -\frac{\partial T_f^*}{\partial Z} \tag{V-14}$$

The boundary condition is

$$T_f^*(0,\theta^*) = \sin 2\pi \frac{\theta}{\theta_o} = \sin \frac{\theta^*}{\Psi} \qquad \text{(V-16)}$$

with the definition

$$\Psi \triangleq \frac{1}{2\pi} \frac{\theta_o}{R\bar{C}_w} \qquad \text{(V-17)}$$

The parameter Ψ is a nondimensional period of oscillation and $R\bar{C}_w$ is the heat exchanger wall time constant. The solutions of interest are the particular solutions which result after all the initial condition effects have damped out. The solutions as given in [4] are

$$T_f^* = \exp\left(\frac{-Z}{1+\Psi^2}\right)\left\{\sin\left(\frac{\theta^*}{\Psi} - \frac{Z}{1+\Psi^2}\right)\right\} \qquad \text{(V-18)}$$

$$T_w^* = \frac{\Psi}{\sqrt{1+\Psi^2}} \exp\left(\frac{-Z}{1+\Psi^2}\right)\left\{\sin\left(\frac{\theta^*}{\Psi} - \frac{\Psi}{1+\Psi^2} Z - \beta\right)\right\} \qquad \text{(V-19)}$$

where $\beta \triangleq \tan^{-1} \frac{1}{\Psi}$ (V-20)

For the <u>fluid</u>:

$$\text{Amplitude Attenuation} = D_f = \exp\left(\frac{-Z}{1+\Psi^2}\right) \qquad \text{(V-21)}$$

and

$$\text{Phase Shift} = \gamma_f = \frac{\Psi}{1+\Psi^2} Z \qquad \text{(V-22)}$$

The amplitude attenuation and the phase shift of the fluid at $x^* = 1$ or $Z = N_{tu}$ are plotted in Figs. V-2 through V-9.

For the <u>wall</u>:

$$\text{Amplitude Attenuation} = D_w = \frac{\Psi}{\sqrt{1+\Psi^2}} \exp\left(\frac{-Z}{1+\Psi^2}\right) = \frac{\Psi}{\sqrt{1+\Psi^2}} D_f \qquad \text{(V-23)}$$

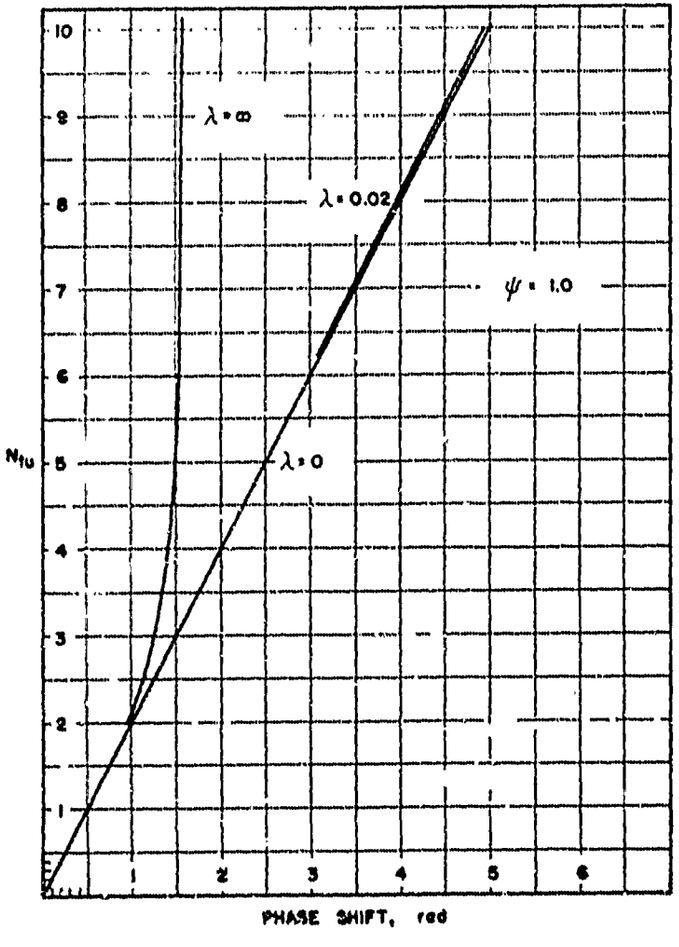

Figure V-2 Phase Shift for the Fluid Temperature Response, $x^* = 1$, $\psi = 1.0$.

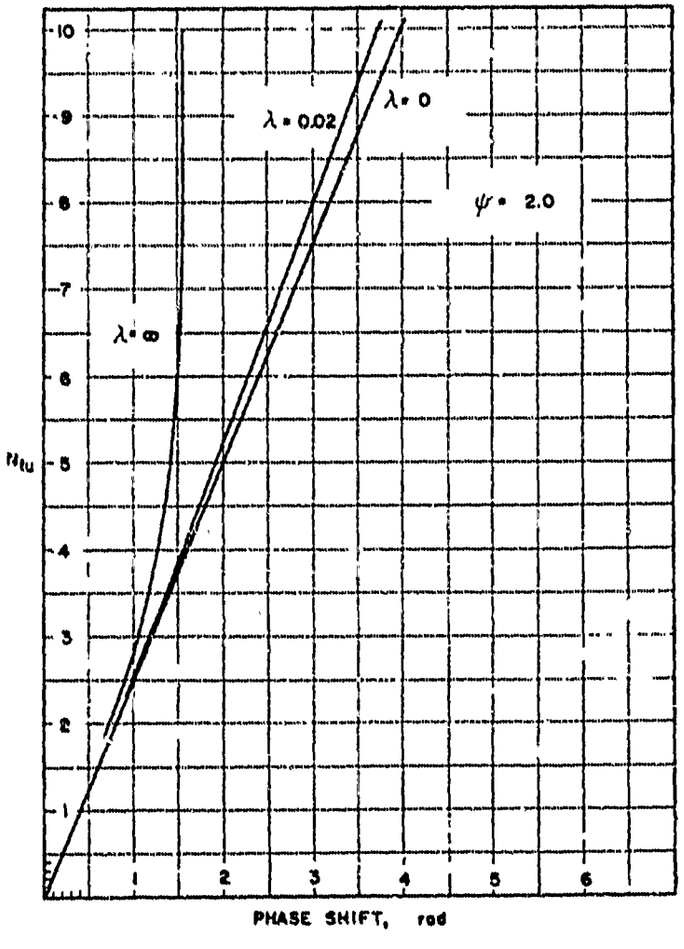

Figure V-3 Phase Shift for the Fluid Temperature Response, $x^* = 1$, $\psi = 2.0$.

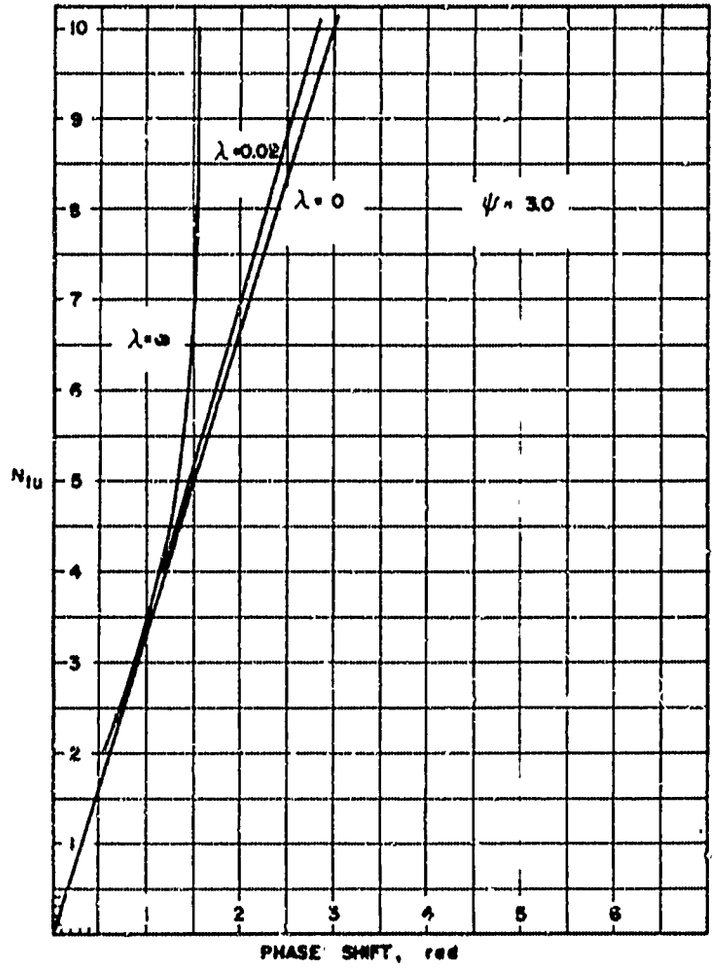

Figure V-4 Phase Shift for the Fluid Temperature Response, $x^* = 1$, $\psi = 3.0$.

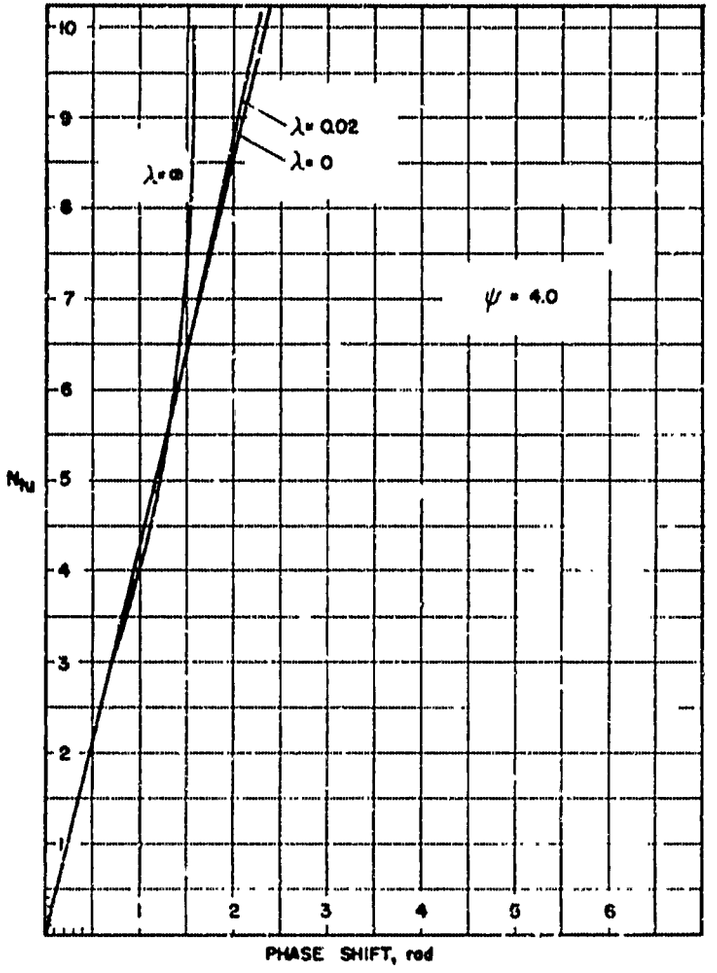

Figure V-5 Phase Shift for the Fluid Temperature Response, $x^* = 1$, $\psi = 4.0$.

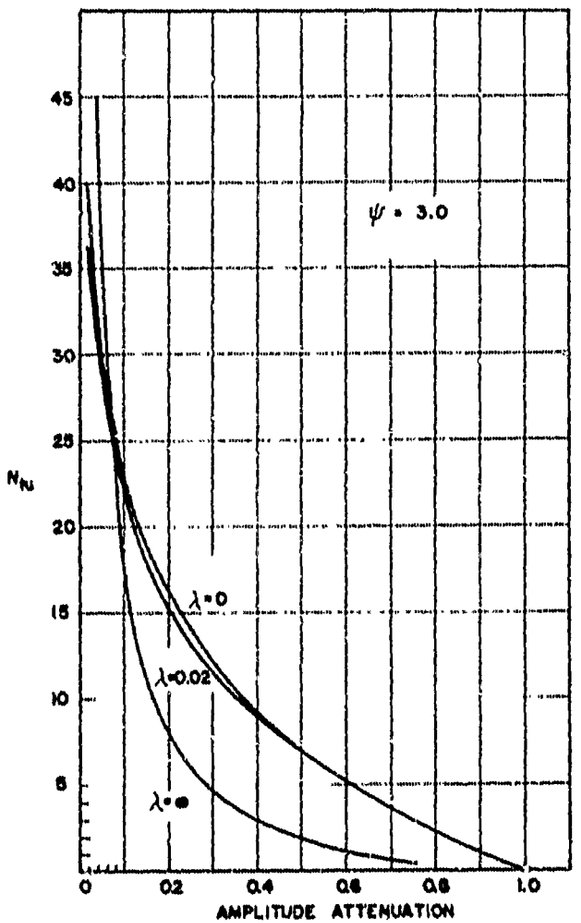

Figure V-6 Amplitude Attenuation for the Fluid Temperature Response, $x^* = 1$, $\psi = 3.0$.

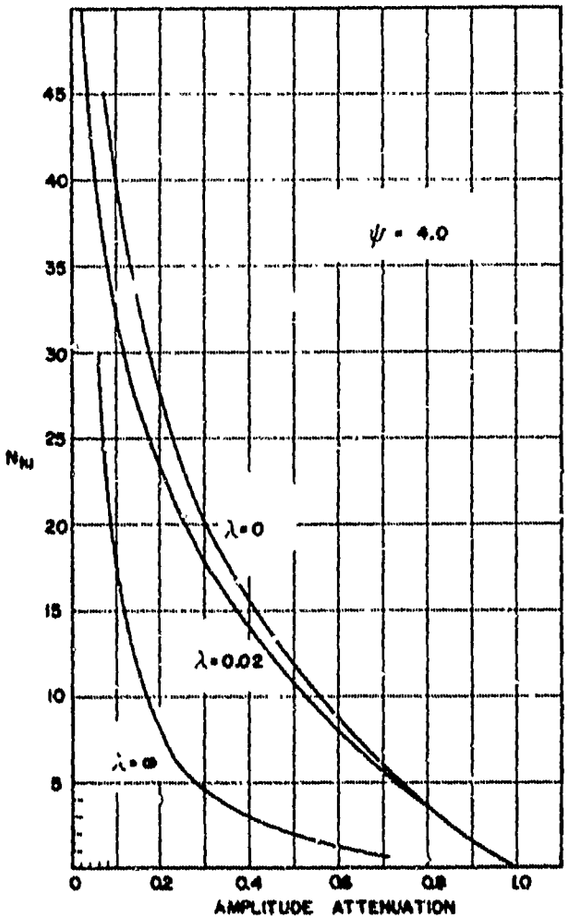

Figure V-7 Amplitude Attenuation for the Fluid Temperature Response, $x^* = 1$, $\psi = 4.0$.

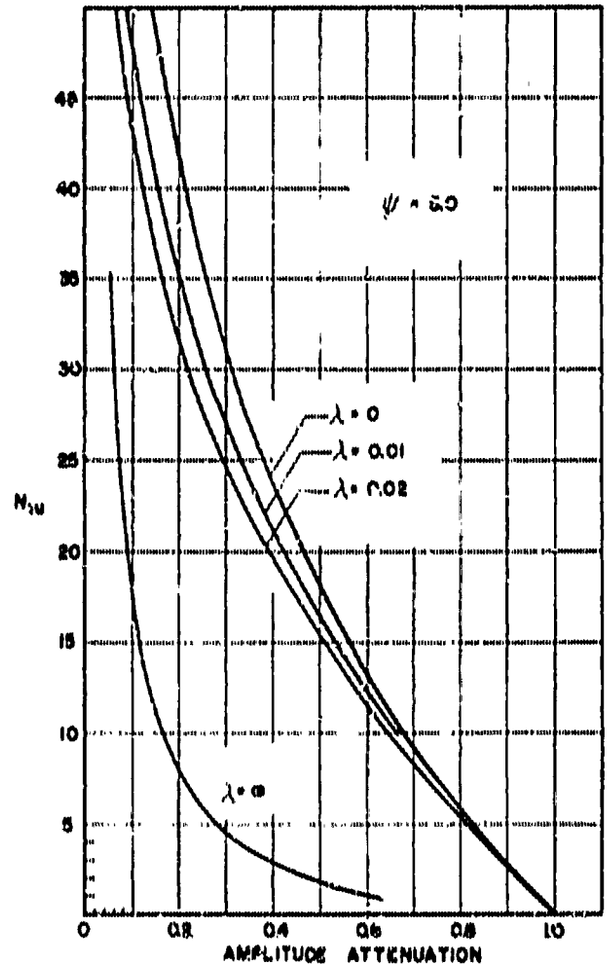

Figure V-8 Amplitude Attenuation for the Fluid Temperature Response, $x^* = 1$, $\psi = 5.0$.

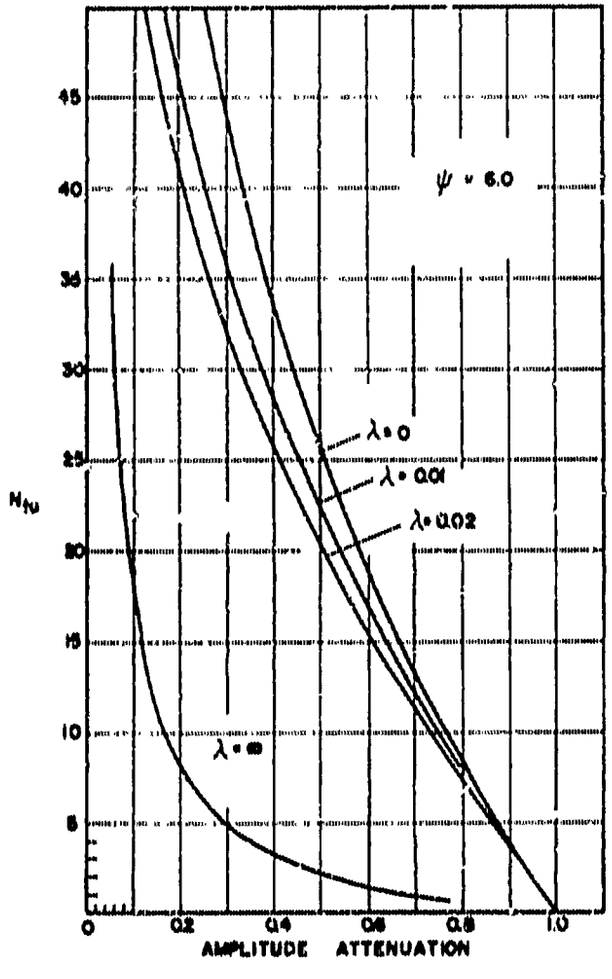

Figure V-9 Amplitude Attenuation for the Fluid Temperature Response, $x^* = 1$, $\psi = 6.0$.

and

$$\text{Phase Shift} \triangleq \gamma_w = \frac{\psi}{1+\psi^2} 2 + \beta = \gamma_f + \tan^{-1}\frac{1}{\psi} \qquad \text{(V-24)}$$

The recommended values for ψ to use in actual tests using fluid temperature measurement, are derived in Appendix VI and are presented in Fig. 7.3 for $0.2 < N_{tu} < 50$.

Solution For Wall Longitudinal Conduction Finite

In this case the last term of Eq. (V-13) is not neglected, and the equations of interest are Eqs. (V-13) and (V-14):

$$T_f^* - T_w^* = \frac{\partial T_w^*}{\partial \theta^*} - \lambda N_{tu} \frac{\partial^2 T_w^*}{\partial Z^2} \qquad \text{(V-13)}$$

$$T_f^* - T_w^* = -\frac{\partial T_f^*}{\partial Z} \qquad \text{(V-14)}$$

The boundary condition is unchanged. The solutions are

$$T_f^* = \exp(-\epsilon_1 Z)\ \sin\left\{\left(\frac{\theta^*}{\psi} - \epsilon_2 Z\right)\right\} \qquad \text{(V-25)}$$

$$T_w^* = \exp(-\epsilon_1 Z)\ \left\{(1-\epsilon_1)\ \sin\left(\frac{\theta^*}{\psi} - \epsilon_2 Z\right) - \epsilon_2 \cos\left(\frac{\theta^*}{\psi} - \epsilon_2 Z\right)\right\} \qquad \text{(V-26)}$$

where ϵ_1 and ϵ_2 are functions of ψ and λN_{tu} only, and must satisfy the following set of equations:

$$\epsilon_1 = \frac{\epsilon_2}{\psi} - \lambda N_{tu}\left(-\epsilon_1^3 + \epsilon_1^2 + 3\epsilon_1\epsilon_2^2 - \epsilon_2^2\right) \qquad \text{(V-27)}$$

$$\epsilon_2 = \frac{1-\epsilon_1}{\psi} - \lambda N_{tu}\left(\epsilon_2^3 - 3\epsilon_1^2\epsilon_2 + 2\epsilon_1\epsilon_2\right) \qquad \text{(V-28)}$$

The constants ϵ_1 and ϵ_2 have been calculated and are tabulated in Tables V-1 and V-2. The fortran subroutine CONDCT, presented in Appendix VII, was used to generate these tables. The subroutine CONDCT uses the

Table V-1

CONSTANT ϵ_1 IN THE SOLUTION FOR THE PERIODIC TECHNIQUE WITH FINITE WALL LONGITUDINAL CONDUCTION

ψ	λN_{tu}							
	0	0.001	0.005	0.010	0.050	0.100	0.500	1.000
0.2	0.9615	0.9616	0.9617	0.9618	0.9629	0.9642	0.9767	0.9974
0.4	0.8621	0.8621	0.8621	0.8621	0.8623	0.8625	0.8588	0.7989
0.6	0.7353	0.7352	0.7347	0.7342	0.7296	0.7232	0.6506	0.5498
0.8	0.6098	0.6095	0.6087	0.6076	0.5988	0.5875	0.5000	0.4242
1.0	0.5000	0.4998	0.4988	0.4975	0.4877	0.4758	0.4008	0.3457
1.2	0.4096	0.4096	0.4087	0.4076	0.3989	0.3889	0.3313	0.2912
1.4	0.3378	0.3377	0.3370	0.3361	0.3294	0.3218	0.2799	0.2506
1.6	0.2809	0.2808	0.2803	0.2797	0.2750	0.2697	0.2404	0.2191
1.8	0.2358	0.2358	0.2355	0.2351	0.2321	0.2287	0.2091	0.1939
2.0	0.2000	0.2000	0.1998	0.1996	0.1979	0.1959	0.1838	0.1733
2.2	0.1712	0.1712	0.1711	0.1710	0.1703	0.1694	0.1628	0.1560
2.4	0.1479	0.1479	0.1479	0.1479	0.1478	0.1477	0.1453	0.1413
2.6	0.1289	0.1289	0.1289	0.1290	0.1294	0.1298	0.1305	0.1288
2.8	0.1131	0.1131	0.1132	0.1133	0.1140	0.1148	0.1178	0.1179
3.0	0.1000	0.1000	0.1001	0.1002	0.1012	0.1022	0.1069	0.1083
3.2	0.0890	0.0890	0.0891	0.0892	0.0903	0.0915	0.0974	0.0999
3.4	0.0796	0.0796	0.0798	0.0799	0.0811	0.0824	0.0891	0.0925
3.6	0.0716	0.0717	0.0718	0.0719	0.0731	0.0745	0.0818	0.0858
3.8	0.0648	0.0648	0.0649	0.0651	0.0663	0.0676	0.0753	0.0799
4.0	0.0588	0.0589	0.0590	0.0591	0.0603	0.0617	0.0695	0.0745
4.2	0.0536	0.0537	0.0538	0.0539	0.0551	0.0565	0.0644	0.0697
4.4	0.0491	0.0491	0.0493	0.0494	0.0505	0.0519	0.0598	0.0653
4.6	0.0451	0.0452	0.0453	0.0454	0.0465	0.0478	0.0556	0.0613
4.8	0.0416	0.0416	0.0417	0.0419	0.0429	0.0442	0.0519	0.0576
5.0	0.0385	0.0385	0.0386	0.0387	0.0397	0.0409	0.0485	0.0543
5.2	0.0357	0.0357	0.0358	0.0359	0.0369	0.0380	0.0454	0.0512
5.4	0.0332	0.0332	0.0333	0.0334	0.0343	0.0354	0.0426	0.0484
5.6	0.0309	0.0309	0.0310	0.0311	0.0320	0.0331	0.0401	0.0458
5.8	0.0289	0.0289	0.0290	0.0291	0.0299	0.0310	0.0377	0.0434
6.0	0.0270	0.0270	0.0271	0.0272	0.0280	0.0290	0.0356	0.0412
6.2	0.0254	0.0254	0.0255	0.0256	0.0263	0.0273	0.0336	0.0391
6.4	0.0238	0.0239	0.0239	0.0240	0.0248	0.0257	0.0318	0.0372
6.6	0.0224	0.0225	0.0225	0.0226	0.0233	0.0242	0.0301	0.0354
6.8	0.0212	0.0212	0.0213	0.0213	0.0220	0.0228	0.0285	0.0337
7.0	0.0200	0.0200	0.0201	0.0202	0.0208	0.0216	0.0271	0.0322
7.2	0.0189	0.0189	0.0190	0.0191	0.0197	0.0205	0.0258	0.0307
7.4	0.0179	0.0179	0.0180	0.0181	0.0187	0.0194	0.0245	0.0294
7.6	0.0170	0.0170	0.0171	0.0172	0.0177	0.0184	0.0234	0.0281
7.8	0.0162	0.0162	0.0162	0.0163	0.0169	0.0175	0.0223	0.0269
8.0	0.0154	0.0154	0.0155	0.0155	0.0160	0.0167	0.0213	0.0258
8.2	0.0147	0.0147	0.0147	0.0148	0.0153	0.0159	0.0203	0.0247
8.4	0.0140	0.0140	0.0140	0.0141	0.0146	0.0152	0.0195	0.0237
8.6	0.0133	0.0134	0.0134	0.0135	0.0139	0.0145	0.0186	0.0228
8.8	0.0127	0.0128	0.0128	0.0129	0.0133	0.0139	0.0179	0.0219
9.0	0.0122	0.0122	0.0122	0.0123	0.0127	0.0133	0.0171	0.0211
9.2	0.0117	0.0117	0.0117	0.0118	0.0122	0.0127	0.0164	0.0203
9.4	0.0112	0.0112	0.0112	0.0113	0.0117	0.0122	0.0158	0.0195
9.6	0.0107	0.0107	0.0108	0.0108	0.0112	0.0117	0.0152	0.0188
9.8	0.0103	0.0103	0.0104	0.0104	0.0108	0.0112	0.0146	0.0182

Table V-2

CONSTANT ϵ_2 IN THE SOLUTION FOR THE PERIODIC TECHNIQUE WITH FINITE WALL LONGITUDINAL CONDUCTION

ψ	λN_{tu}							
	0	0.001	0.005	0.010	0.050	0.100	0.500	1.000
0.2	0.1923	0.1923	0.1924	0.1926	0.1936	0.1949	0.2057	0.2191
0.4	0.3448	0.3449	0.3454	0.3460	0.3509	0.3572	0.4199	0.5247
0.6	0.4412	0.4413	0.4420	0.4428	0.4493	0.4573	0.5086	0.5147
0.8	0.4878	0.4879	0.4883	0.4888	0.4925	0.4964	0.5000	0.4705
1.0	0.5000	0.5000	0.5000	0.5000	0.4995	0.4983	0.4714	0.4309
1.2	0.4918	0.4917	0.4914	0.4909	0.4873	0.4824	0.4409	0.3975
1.4	0.4730	0.4728	0.4723	0.4716	0.4661	0.4594	0.4123	0.3694
1.6	0.4494	0.4493	0.4486	0.4479	0.4417	0.4343	0.3865	0.3453
1.8	0.4245	0.4244	0.4237	0.4229	0.4167	0.4094	0.3633	0.3244
2.0	0.4000	0.3998	0.3992	0.3985	0.3926	0.3857	0.3425	0.3062
2.2	0.3767	0.3766	0.3760	0.3753	0.3699	0.3636	0.3237	0.2900
2.4	0.3550	0.3549	0.3544	0.3538	0.3489	0.3432	0.3068	0.2755
2.6	0.3351	0.3349	0.3345	0.3339	0.3296	0.3245	0.2914	0.2625
2.8	0.3167	0.3166	0.3163	0.3158	0.3119	0.3074	0.2775	0.2507
3.0	0.3000	0.2999	0.2996	0.2991	0.2958	0.2917	0.2647	0.2399
3.2	0.2847	0.2846	0.2843	0.2839	0.2810	0.2774	0.2529	0.2300
3.4	0.2707	0.2706	0.2704	0.2700	0.2674	0.2642	0.2421	0.2209
3.6	0.2579	0.2578	0.2576	0.2573	0.2550	0.2522	0.2322	0.2125
3.8	0.2461	0.2461	0.2459	0.2456	0.2435	0.2410	0.2229	0.2048
4.0	0.2353	0.2352	0.2351	0.2348	0.2330	0.2308	0.2143	0.1975
4.2	0.2253	0.2253	0.2251	0.2249	0.2233	0.2213	0.2064	0.1908
4.4	0.2161	0.2161	0.2159	0.2157	0.2143	0.2125	0.1989	0.1844
4.6	0.2076	0.2075	0.2074	0.2073	0.2060	0.2043	0.1920	0.1785
4.8	0.1997	0.1996	0.1995	0.1994	0.1982	0.1967	0.1855	0.1729
5.0	0.1923	0.1923	0.1922	0.1920	0.1910	0.1897	0.1794	0.1677
5.2	0.1854	0.1854	0.1853	0.1852	0.1843	0.1831	0.1736	0.1628
5.4	0.1790	0.1790	0.1789	0.1788	0.1780	0.1769	0.1682	0.1581
5.6	0.1731	0.1730	0.1730	0.1729	0.1721	0.1711	0.1631	0.1537
5.8	0.1674	0.1674	0.1673	0.1673	0.1665	0.1656	0.1583	0.1495
6.0	0.1622	0.1621	0.1621	0.1620	0.1613	0.1605	0.1537	0.1455
6.2	0.1572	0.1572	0.1571	0.1571	0.1565	0.1557	0.1494	0.1417
6.4	0.1525	0.1525	0.1525	0.1524	0.1518	0.1511	0.1454	0.1381
6.6	0.1481	0.1481	0.1481	0.1480	0.1475	0.1468	0.1415	0.1347
6.8	0.1439	0.1439	0.1439	0.1438	0.1434	0.1428	0.1378	0.1314
7.0	0.1400	0.1400	0.1399	0.1399	0.1395	0.1389	0.1343	0.1283
7.2	0.1363	0.1363	0.1362	0.1362	0.1358	0.1353	0.1309	0.1253
7.4	0.1327	0.1327	0.1327	0.1326	0.1323	0.1318	0.1278	0.1225
7.6	0.1293	0.1293	0.1293	0.1293	0.1289	0.1285	0.1247	0.1197
7.8	0.1261	0.1261	0.1261	0.1261	0.1257	0.1253	0.1218	0.1171
8.0	0.1231	0.1231	0.1230	0.1230	0.1227	0.1223	0.1190	0.1146
8.2	0.1202	0.1202	0.1201	0.1201	0.1198	0.1195	0.1164	0.1122
8.4	0.1174	0.1174	0.1174	0.1173	0.1171	0.1167	0.1138	0.1099
8.6	0.1147	0.1147	0.1147	0.1147	0.1144	0.1141	0.1114	0.1076
8.8	0.1122	0.1122	0.1122	0.1121	0.1119	0.1116	0.1091	0.1055
9.0	0.1098	0.1098	0.1097	0.1097	0.1095	0.1092	0.1068	0.1034
9.2	0.1074	0.1074	0.1074	0.1074	0.1072	0.1069	0.1047	0.1015
9.4	0.1052	0.1052	0.1052	0.1051	0.1050	0.1047	0.1026	0.0995
9.6	0.1030	0.1030	0.1030	0.1030	0.1028	0.1026	0.1006	0.0977
9.8	0.1010	0.1010	0.1010	0.1009	0.1008	0.1006	0.0987	0.0959

Newton-Raphson method [16] to find the roots ϵ_1 and ϵ_2 and can be used to calculate ϵ_1 and ϵ_2 for intermediate values of $\frac{1}{\psi}$ and λN_{tu} not provided by the tables. It is entered by means of the fortran CALL statement, see Appendix VII. For the fluid

$$\text{Amplitude Attenuation} = D_z = \exp(-\epsilon_1 Z) \qquad \text{(V-29)}$$

and

$$\text{Phase Shift} = \gamma_z = \epsilon_2 Z \qquad \text{(V-30)}$$

When $\lambda = 0$

$$\epsilon_1 = \frac{1}{1 + \frac{1}{\psi}^2} \quad \text{and} \quad \epsilon_2 = \frac{\frac{1}{\psi}}{1 + \frac{1}{\psi}^2}$$

Solution For Wall Longitudinal Conduction Infinite

As the wall longitudinal conduction parameter λ becomes very large $(\lambda \to \infty)$, the temperature T_w of the wall becomes only a function of time θ. The temperature T_f of the fluid, remains a function of both time θ and distance x. Then Eqs. (V-5) and (V-9) become

$$-h(T_f - T_w) + (\rho c t)_w \frac{dT_w}{d\theta} = 0 \qquad \text{(V-31)}$$

$$wc_p \frac{\partial T_f}{\partial x} + h(T_f - T_w) = 0 \qquad \text{(V-32)}$$

The conservation of energy applied to the solid wall segment of unit depth normal to Fig. V-1, can be stated by the following equation:

$$-h \int_0^L (T_f - T_w)\,dx + L(\rho c t)_w \frac{dT_w}{d\theta} = 0 \qquad \text{(V-33)}$$

The conservation of energy applied to the fluid system in Fig. V-1 can be stated:

$$wc_p \int_0^L \frac{\partial T_f}{\partial x}\,dx + h \int_0^L (T_f - T_w)\,dx = 0 \qquad \text{(V-34)}$$

Introducing some of the nomenclature of Eqs. (V-12), Eqs. (V-33) and (V-34) become:

$$-\frac{1}{N_{tu}}\int_{o}^{N_{tu}} T_f^* \, dZ + T_w^* + \frac{dT_w^*}{d\theta^*} = 0 \qquad \text{(V-35)}$$

$$\frac{1}{N_{tu}}\int_{o}^{N_{tu}} \frac{\partial T_f^*}{\partial Z} \, dZ + \frac{1}{N_{tu}}\int_{o}^{N_{tu}} T_f^* \, dZ - T_w^* = 0 \qquad \text{(V-36)}$$

The solutions are

$$T_f^* = \exp\left(-\epsilon_3 Z\right) \sin\left(\frac{\theta^*}{\Psi}\right) + \frac{\epsilon_4 Z}{N_{tu}} \cos\left(\frac{\theta^*}{\Psi}\right) \qquad \text{(V-37)}$$

$$T_w^* = \frac{1}{N_{tu}}\left\{\left(1-\frac{1}{\epsilon_3}\right)\left[\exp\left(-\epsilon_3 N_{tu}\right) - 1\right] \sin\left(\frac{\theta^*}{\Psi}\right) + \epsilon_4\left(1+\frac{N_{tu}}{2}\right)\cos\left(\frac{\theta^*}{\Psi}\right)\right\} \qquad \text{(V-38)}$$

where

$$\epsilon_3 = \frac{1 + \frac{N_{tu}}{2}}{\Psi + 1 + \frac{N_{tu}}{2}} \qquad \text{(V-39)}$$

$$\epsilon_4 = \frac{\exp\left\{-N_{tu}\left[\frac{1 + \frac{N_{tu}}{2}}{\Psi + 1 + \frac{N_{tu}}{2}}\right]\right\} - 1}{1 + \frac{N_{tu}}{2}} \qquad \text{(V-40)}$$

The phase shift of the fluid for $\lambda = \infty$ at $x^* = 1$ is presented in Figs. V-2 through V-5. The amplitude attenuation of the fluid for $\lambda = \infty$ at $x^* = 1$ is presented in Figs. V-6 through V-9.

Figs. V-10, V-11, and V-12 show what is happening to both the fluid temperature T_f^*, and the wall temperature T_w^*, as functions of time $\frac{\theta^*}{\Psi}$, space x^*, and wall longitudinal conduction λ. Fig. V-10 shows the time-varying temperatures at the heat exchanger matrix exit ($x^* = 1$). The

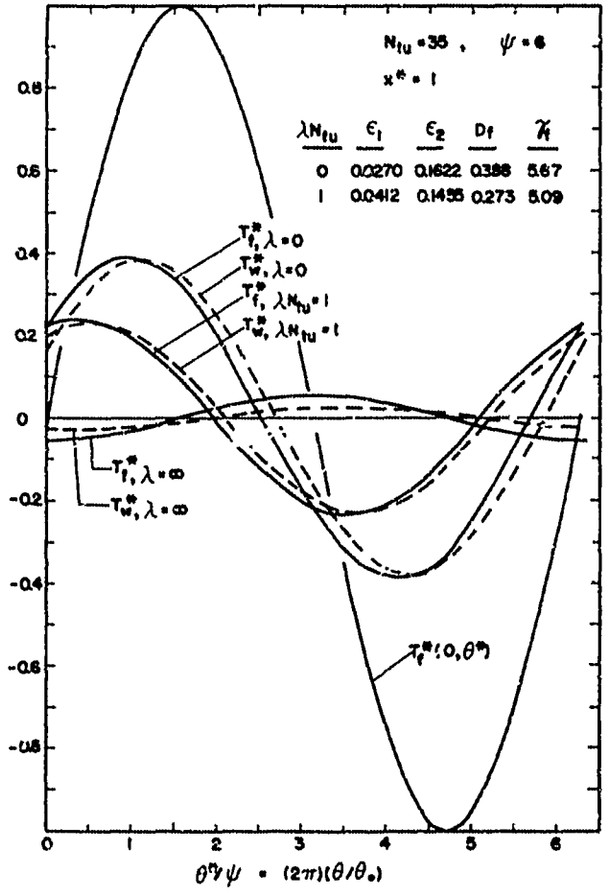

Figure V-10 Sample of the Time-Varying Temperatures at the Test Matrix Exit, $x^* = 1$.

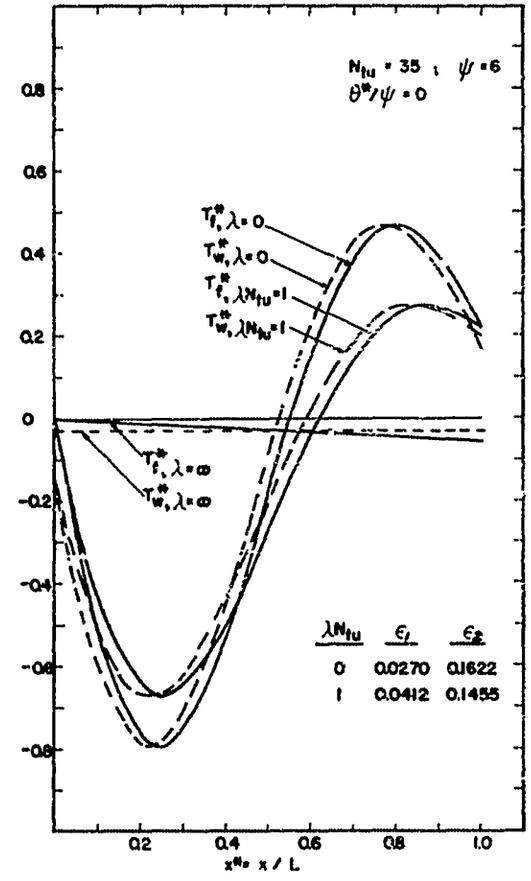

Figure V-11 Sample of the Temperature Profile Along the Test Matrix Longitudinal Axis at Time, $\frac{\theta^*}{\psi} = 0$.

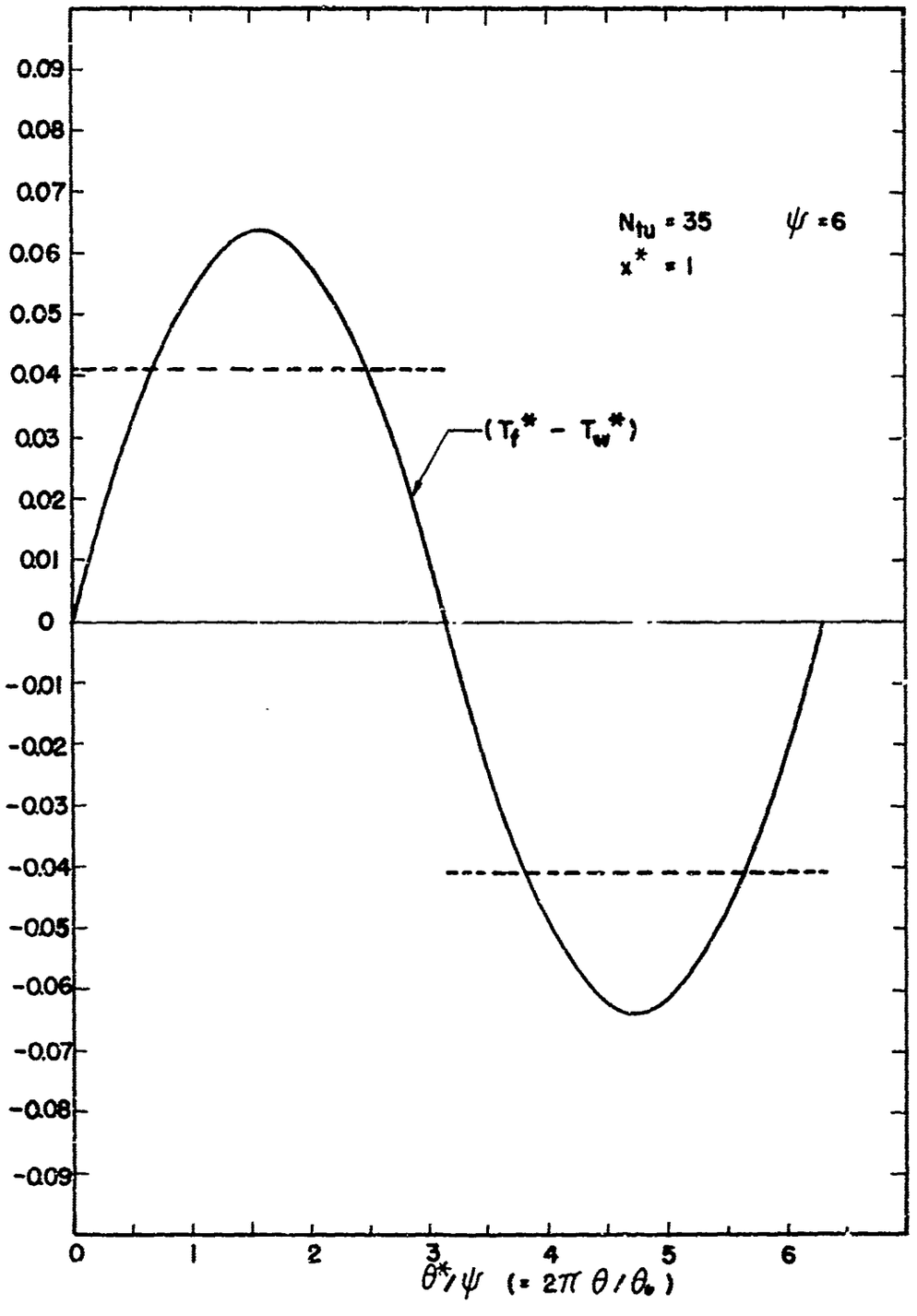

Figure V-12 Sample of the Time Varying Temperature Difference $(T_f^* - T_w^*)$ at the test matrix exit, $x^* = 1$. (The plot is phase-shifted in time to appear as a sinusoidal curve beginning at zero.)

changes in amplitude attenuation and phase shift due to longitudinal conduction effects can be seen. Fig. V-11 shows the wall and fluid temperatures along the longitudinal axis of the core at time $\theta^* = 0$. Again the effects of longitudinal conduction can be seen, however in this case the amplitude attenuation change and the phase shift change cannot be read directly. Fig. V-12 shows the temperature difference between the fluid and the wall for the ($\lambda = 0$) case. The difference is a direct measure of heat flux to and from the wall. Because it is small and creates an illusion, it is difficult to read this difference from the $\lambda = 0$ curve in Fig. V-10. A dotted line representing the constant heat flux boundary condition is superimposed on the figure. It shows that the periodic technique tends toward the constant heat flux boundary condition. Results of testing are therefore not expected to agree fully with theoretical predictions using the constant heat flux boundary condition.

APPENDIX VI

ERROR ANALYSIS FOR THE PERIODIC TECHNIQUE

The periodic transient technique requires accurate measurement of temperature variation upstream and downstream of the core. Matrix physical properties such as density ρ_w, specific heat c_w, and thermal conductivity k_w must also be known. The objective of this appendix is to show how uncertainties in the temperature measurements and in the core physical properties may affect the heat transfer test results (the j--N_R curves).

Fluid Temperature Measurement, Sinusoidal Case

The solution for the fluid temperature when wall longitudinal conduction is zero ($\lambda = 0$) is given by Eq. (V-18). At $x^* = 1$ this equation becomes

$$T_f^* = \exp\left(\frac{-N_{tu}}{1 + \psi^2}\right)\left\{\sin\left(\frac{\theta^*}{\psi} - \frac{\psi}{1 + \psi^2}\, N_{tu}\right)\right\} \qquad \text{(VI-1)}$$

Amplitude Attenuation Method - The amplitude attenuation method compares the amplitude of the temperature wave downstream of the test core with the input wave upstream of the core. At $x^* = 1$ the amplitude attenuation from Eq. (VI-1) is

$$D_f = \exp\left(\frac{-N_{tu}}{1 + \psi^2}\right) \qquad \text{(IV-2)}$$

Experimentally this is arrived at by recording the upstream and downstream temperature waves and selecting the maximum and minimum values on the waves. If the outlet amplitude, called ΔT_{f2}, has an error, the following result is obtained from Eq. (VI-2):

$$\frac{\Delta T_{f2}}{\Delta T_o} = \exp\left(\frac{-N_{tu}}{1 + \psi^2}\right) \qquad \text{(VI-3)}$$

and

$$\frac{dh/h}{\delta\Delta T_{f2}/\Delta T_o} = \exp\left(\frac{N_{tu}}{1+\psi^2}\right)\left[\frac{(\psi^2+1)^2}{N_{tu}(\psi^2-1)}\right] \qquad \text{(VI-4)}$$

Note the singularity in Eq. (VI-4), for $\psi = 1$ the amplification factor goes to ∞.

Phase Shift Method - The phase shift method compares the phase of the temperature wave downstream of the test core with the input wave upstream of the core. At $x^* = 1$, the phase shift from Eq. (VI-1) is

$$\nu_f = \frac{\psi}{1+\psi^2} N_{tu} \qquad \text{(VI-5)}$$

Experimentally the phase shift is arrived at by determining what portion of the input wave length (considered as 2π radians) has been shifted by passage of the fluid through the test core. If the outlet temperature, called $T_{f2'}$ has an error, the following result is obtained from Eq. (VI-1):

$$\frac{T_{f2} - T_m}{\Delta T_o} = D_f \left\{\sin\left(\frac{\theta^*}{\psi} - \frac{\psi}{1+\psi^2} N_{tu}\right)\right\} \qquad \text{(VI-6)}$$

Noting that the phase shift is measured at

$$\frac{\theta^*}{\psi} = \frac{\psi}{1+\psi^2} N_{tu} \qquad \text{(VI-7)}$$

it follows that

$$\frac{dh/h}{\delta T_{f2}/\Delta T_o} = \frac{1}{D_f}\left[\frac{(\psi^2+1)^2}{-2\,N_{tu}\,\psi}\right] \qquad \text{(VI-8)}$$

For a given N_{tu}, one may evaluate the right-hand sides of Eqs. (VI-4) and (VI-8) for various values of ψ. The best experimental value of ψ (with least resulting uncertainty) and the best method (amplitude

attenuation or phase shift) may be selected and used in testing. Fig. 7.3 is an operationally convenient plot showing the values of Ψ and the method to use for values of $0.2 < N_{tu} < 50$. This figure is a plot of Ψ versus N_{tu} and the best test method that will yield the minimum uncertainty for the heat transfer coefficient is noted on the graph. The magnitude of this uncertainty is about 3 percent on h for a $dT_{f2}/\Delta T_o$ magnitude of 1 percent.

Test Core Physical Properties

The periodic transient technique requires that the matrix physical properties such as density ρ_w, specific heat c_w, and thermal conductivity k_w be known. The technique calculates the parameter Ψ from experimentally obtained D_f and γ_f, using Eqs. (VII-17) and (VII-18).

Density of the Core Solid Material - The laboratory technique used for calculating the core porosity p is to measure the core mass M, the frontal area A_{fr}, the flow length L, and use the following Eq. (VI-9):

$$p = \frac{A_c}{A_{fr}} = 1 - \frac{M}{A_{fr} L \rho_w} \qquad \text{(VI-9)}$$

The sensitivity of the N_{St} to uncertainty in ρ_w may be found using

$$N_{St} \triangleq \frac{h}{Gc_p} = \frac{A_c}{A} \Psi \omega^* \qquad \text{(VI-10)}$$

where

$$\frac{A_c}{A} = \frac{p}{\alpha L} \qquad \text{(VI-11)}$$

For the revised Bayley Model [15]

$$\frac{A_c}{A} = \frac{\sqrt{p}}{\eta L} \qquad \text{(VI-12)}$$

where η is a constant based on observed or measured cell characteristics such as cell count or cell shape. Combining Eqs. (VI-9), (VI-10), and (VI-12) and differentiating yields

$$\frac{dN_{St}}{N_{St}} = \frac{dj}{j} = \frac{1 - p}{2p} \frac{d\rho_w}{\rho_w} \qquad \text{(IV-13)}$$

The sensitivity of N_R to uncertainties in ρ_w may be found using

$$N_R \triangleq \frac{4r_h G}{\mu} = \frac{4 L G}{\mu} \frac{A_c}{A} \qquad \text{(IV-14)}$$

Combining Eqs. (VI-12) and (VI-14) and differentiating yields

$$\frac{dN_R}{N_R} = \frac{-(1-p)}{2p} \frac{d\rho_w}{\rho_w} \qquad \text{(IV-15)}$$

For the case of fully developed laminar flow in tubes, with the constant heat flux or constant wall temperature boundary condition, and a fixed geometry, the Nusselt number is constant and

$$N_{Nu} \triangleq \frac{h4r_h}{k} = N_{St} N_R N_{Pr} \qquad \text{(IV-16)}$$

The relationship between j and N_R has the form

$$j = \frac{E}{N_R} \qquad \text{(VI-17)}$$

where E depends on the cross section geometry and the boundary condition, and

$$\frac{d_j}{j} = \frac{dE}{E} - \frac{dN_R}{N_R} \qquad \text{(VI-18)}$$

Combining Eqs. (VI-13), (VI-15), and (VI-18) produces

$$\frac{dE}{E} = 0 \qquad \text{(VI-19)}$$

This means the j--N_R characteristic is not sensitive to uncertainties in ρ_w, even though j and N_R if considered individually are.

Specific Heat of the Core Solid Material - The core specific heat c_w will affect only the heat transfer results, j, of the periodic technique. Flow friction results and Reynolds number are not affected. Differentiating Eq. (VI-10) yields

$$\frac{dN_{St}}{N_{St}} = \frac{d\psi}{\psi} + \frac{d\varpi^*}{\varpi^*} \qquad \text{(VI-20)}$$

From the definition of ϖ^* ($\triangleq 2\pi\tilde{C}_w/C_f\theta_o$)

$$\frac{d\varpi^*}{\varpi^*} = \frac{dc_w}{c_w} \qquad \text{(VI-21)}$$

For the amplitude attenuation method, the equation used for computing ψ is Eq. (VII-17). Using Eq. (VII-17) in Eq. (VI-20) yields:

$$\frac{dN_{St}/N_{St}}{dc_w/c_w} = 1 + \frac{1+\psi^2}{2\psi^2} \pm \frac{1+\psi^2}{4\psi^3}\left[\left(\frac{1+\psi^2}{2\psi}\right)^2 - 1\right]^{-1/2} \qquad \text{(VI-22)}$$

(The plus sign is used for $\psi > 1$, the minus sign for $\psi < 1$.)

For the phase shift method, ψ is computed using Eq. (VII-18). Combining Eq. (VII-18) and Eq. (VI-20) produces:

$$\frac{dN_{St}/N_{St}}{dc_w/c_w} = 1 - \frac{1}{2}\sqrt{\frac{1}{1+\psi^2}} \qquad \text{(VI-23)}$$

The sensitivities in Eqs. (VI-22) and (VI-23) are plotted in Fig. VI-1 for $0 < \Psi < 10$, $\lambda = 0$, and no temperature measurement error.

For the maximum slope method [12] with $\lambda = 0$

$$\frac{dN_{St}/N_{St}}{dc_w/c_w} \approx 2.2$$

for the range $N_{tu} > 10$.

Thermal Conductivity of the Core Solid Material - The solid wall thermal conductivity affects only the heat transfer results, through the wall longitudinal conduction parameter λ. For the periodic technique, this affect must be taken into consideration if $\lambda N_{tu} > 0.01$ (For $\lambda N_{tu} = 0.01$, the influence on amplitude attenuation and phase shift is less than 1 percent). Generally the magnitude of the wall longitudinal conduction effect on heat transfer results is less than 10 percent. Therefore an uncertainty in solid thermal conductivity k_w of 10 percent, hence in λ also, would produce only about a 1 percent uncertainty in heat transfer results.

Consider for example the actual test point for Core 510 which had the largest $\lambda N_{tu} = 0.091$. If the effect of longitudinal conduction was completely ignored, the heat transfer result would be 6.9 percent in error. Under the same test conditions, the maximum slope method would have been 7.1 percent in error if the longitudinal conduction effect was completely ignored. Therefore the periodic technique is about as sensitive as the maximum slope single-blow technique to wall longitudinal conduction effects.

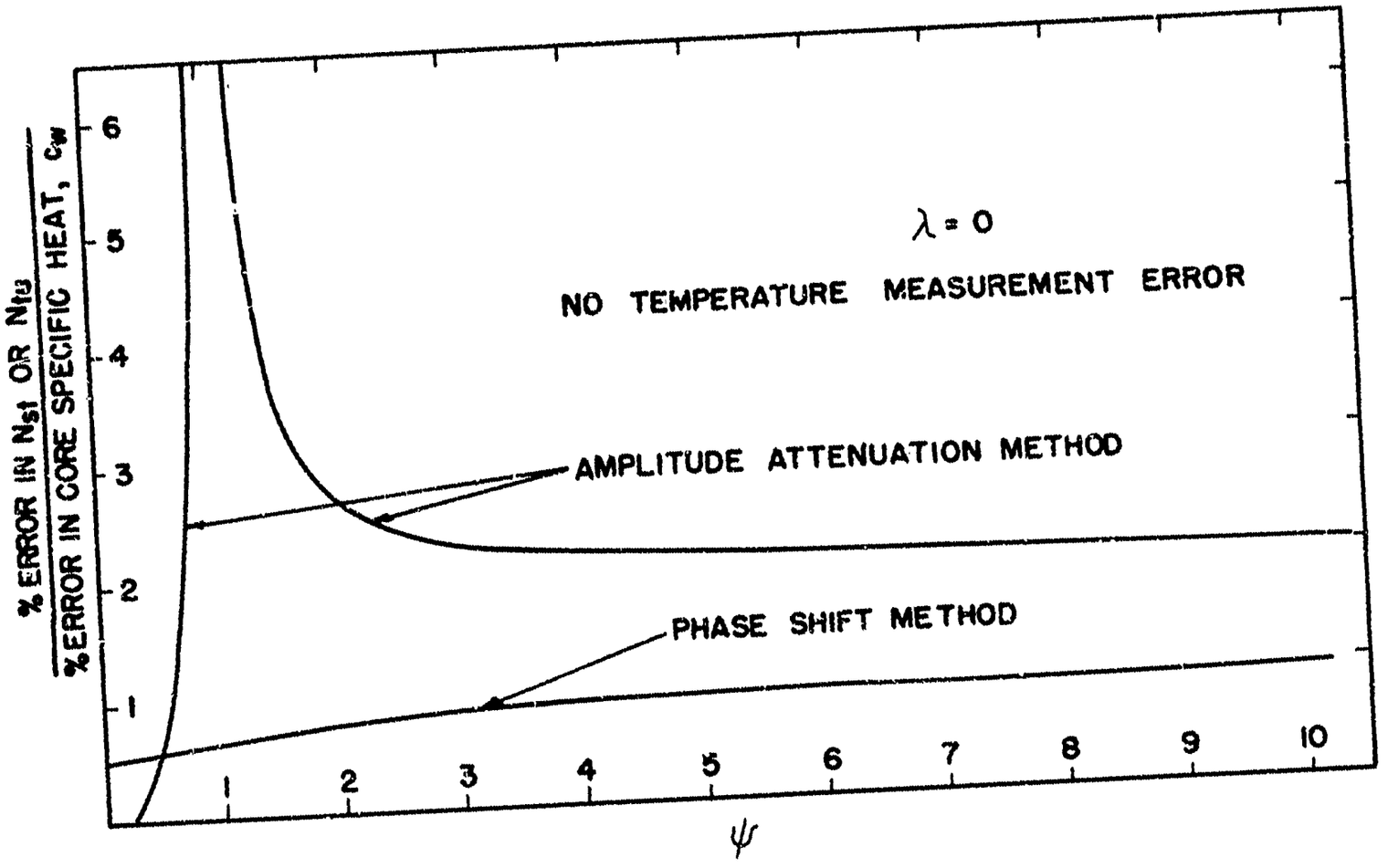

Figure VI-1 Error in N_{St} or N_{tu} Relative to an Error in Core Specific Heat (with no temperature measurement error).

APPENDIX VII

DATA REDUCTION

Single-Blow Technique

The computer program used is as described by Wheeler in [5]. Physical properties, such as specific heat, thermal conductivity, and density of the core solid material were taken from [15] and are (for room temperature conditions)

$$\rho_w = 141 \text{ lbm/ft}^3$$
$$c_w = 0.200 \text{ Btu/(lbm °F)}$$
$$k_w = 0.42 \text{ Btu/(hr ft °F)}$$

The physical properties of air used in the data reduction program are from Bureau of Standards Sources [10] and the humidity corrections are made in accordance with the method described by Shah [17].

The maximum slope method is used in this program. In nondimensional form the maximum slope is

$$\text{Max. Slope} = MS = \frac{\bar{C}_w \times 3600}{C_f \times (DTAU)}$$

DTAU is the time (sec.) required for the nondimensional temperature to change its full value, 1.0, at the maximum rate of change. The average of four runs at a single flow rate (two step-up and two step-down) is used. The longitudinal conduction parameter λ is also required to establish N_{tu}. A graphical and tabular presentation of N_{tu} as a function of Max. Slope and λ is given by [12]. The computer program incorporates this in the form of a "look-up" table.

Nomenclature for the computed data is presented in Table VII-1. Single-blow heat transfer test result listings are provided for cores 505A, 505B, 505C, and 510 in Table VII-2 for both the aided and the unaided cases. The flow friction results are virtually identical for

the aided and unaided cases. Flow friction results for core 505A may be found in [15]. Flow friction results for core 510 are included with the periodic results in this appendix.

Table VII-1

NOMENCLATURE FOR SINGLE-FLOW HEAT TRANSFER RESULTS

W	Flowrate, lbm/hr
G	Mass Velocity, lbm/(hr ft^2)
TBA	Average core inlet temperature, °F
DTAU	The time required for the nondimensional temperature to change its full value, 1.0, at the maximum rate of change, sec
LAMBDA	λ, heat transfer longitudinal conduction parameter, dimensionless
MAX SLOPE	Maximum slope, dimensionless
NTU	N_{tu}, dimensionless
NST	N_{St}, Stanton Number, dimensionless
J	Colburn j factor $N_{St}N_{Pr}^{2/3}$, dimensionless
NR	Reynolds Number

Table VII-2

SINGLE-FLOW TRANSIENT TEST DATA

HEAT TRANSFER RESULTS

CORE 505A AIDED

HYDRAULIC DIA = 0.002472 FT FRONTAL AREA = 10.569 SQIN FLOW LENGTH = 2.998 IN
POROSITY = 0.794 ALPHA = 1285.0 SQFT/CFT
CORE MASS = 0.534 LBM CORE SP HT = 0.200 BTU/LB-F
CORE COND = 0.42 BTU/HR-FT-F COND AREA = 2.18 SQIN

RUN	W LB/HR	G LB/HR-SQFT	TBA DEG.F	DTAU SEC	LAMBDA	MAX SLOPE	NTU	NST	J	NR
2	[illegible]	1720.	93.7	13.90	0.0010	1.175	14.75	0.0414	0.0329	93.4
4	[illegible]	2265.	93.7	11.58	0.0008	1.040	12.84	0.0318	0.0253	123.0
6	[illegible]	2780.	93.6	10.32	0.0006	0.951	10.96	0.0261	0.0208	150.9
8	401.1	3652.	90.0	9.09	0.0005	0.870	8.66	0.0214	0.0170	188.4
10	248.9	4271.	89.6	8.04	0.0004	0.794	7.05	0.0174	0.0139	233.2
12	315.5	5413.	89.0	7.01	0.0003	0.719	5.57	0.0138	0.0110	295.8
14	390.3	5870.	89.0	6.10	0.0003	0.651	4.33	0.0107	0.0085	379.5
16	488.1	8376.	89.6	5.48	0.0002	0.594	3.33	0.0082	0.0066	457.4

CORE 505A NOT AIDED

HYDRAULIC DIA = 0.002472 FT FRONTAL AREA = 10.569 SQIN FLOW LENGTH = 2.998 IN
POROSITY = 0.794 ALPHA = 1285.0 SQFT/CFT
CORE MASS = 0.534 LBM CORE SP HT = 0.200 BTU/LB-F
CORE COND = 0.42 BTU/HR-FT-F COND AREA = 2.18 SQIN

RUN	W LB/HR	G LB/HR-SQFT	TBA DEG.F	DTAU SEC	LAMBDA	MAX SLOPE	NTU	NST	J	NR
1	101.0	1733.	92.1	13.94	0.0010	1.129	15.37	0.0380	0.0303	94.3
3	132.4	2273.	91.9	11.78	0.0008	1.019	12.28	0.0304	0.0242	123.7
5	162.1	2781.	92.5	10.52	0.0006	0.932	10.11	0.0250	0.0199	151.3
7	202.3	3472.	88.5	9.26	0.0005	0.849	8.20	0.0203	0.0161	189.9
9	249.1	4275.	86.3	8.10	0.0004	0.788	6.92	0.0171	0.0136	233.9
11	315.5	5414.	87.9	7.14	0.0002	0.706	5.32	0.0132	0.0105	296.3
13	401.2	6884.	87.2	6.13	0.0003	0.646	4.25	0.0105	0.0084	77.2
15	488.0	8375.	88.1	5.45	0.0002	0.598	3.39	0.0084	0.0067	458.3

CORE 505B AIDED

HYDRAULIC DIA = 0.002472 FT FRONTAL AREA = 10.621 SQIN FLOW LENGTH = 1.986 IN
POROSITY = 0.794 ALPHA = 1285.0 SQFT/CFT
CORE MASS = 0.354 LBM CORE SP HT = 0.200 BTU/LB-F
CORE COND = 0.42 BTU/HR-FT-F COND AREA = 2.19 SQIN

RUN	W LB/HR	G LB/HR-SQFT	TBA DEG.F	DTAU SEC	LAMBDA	MAX SLOPE	NTU	NST	J	NR
2	99.0	1691.	91.2	11.16	0.0016	0.954	10.68	0.0399	0.0317	92.1
4	129.5	2212.	91.9	9.60	0.0012	0.847	8.17	0.0305	0.0242	120.4
6	161.3	2754.	92.2	8.42	0.0010	0.776	6.67	0.0249	0.0198	149.9
8	201.4	3422.	93.2	7.49	0.0008	0.702	5.25	0.0196	0.0156	186.0
10	245.0	4183.	93.1	6.62	0.0007	0.650	4.31	0.0161	0.0128	227.4
12	314.0	5361.	92.6	5.70	0.0005	0.589	3.23	0.0121	0.0096	291.6

CORE 505B NOT AIDED

HYDRAULIC DIA = 0.002472 FT FRONTAL AREA = 10.621 SQIN FLOW LENGTH = 1.986 IN
POROSITY = 0.794 ALPHA = 1285.0 SQFT/CFT
CORE MASS = 0.354 LBM CORE SP HT = 0.200 BTU/LB-F
CORE COND = 0.42 BTU/HR-FT-F COND AREA = 2.19 SQIN

RUN	W LB/HR	G LB/HR-SQFT	TBA DEG.F	DTAU SEC	LAMBDA	MAX SLOPE	NTU	NST	J	NR
1	99.8	1704.	90.1	11.18	0.0016	0.928	10.04	0.0375	0.0298	93.0
3	129.8	2218.	90.4	9.59	0.0012	0.820	7.58	0.0283	0.0226	120.9
5	161.3	2755.	91.1	8.61	0.0010	0.759	6.23	0.0236	0.0188	150.1
7	200.5	3424.	91.7	7.49	0.0008	0.702	5.24	0.0198	0.0158	186.5
9	244.9	4182.	91.8	6.64	0.0007	0.648	4.28	0.0160	0.0127	227.7
11	313.9	5360.	91.1	5.72	0.0005	0.590	3.05	0.0114	0.0091	292.1

Table VII-2 cont'd.

SINGLE-BLOW TRANSIENT TEST DATA

HEAT TRANSFER RESULTS

CORE 505C AIDED

HYDRAULIC DIA = 0.002472 FT FRONTAL AREA = 10.212 SQIN FLOW LENGTH = 0.996 IN
POROSITY = 0.794 ALPHA = 1285.0 SQFT/CFT
CORE MASS = 0.171 LBM CORE SP HT = 0.200 BTU/LB-F
CORE COND = 0.42 BTU/HR-FT-F CCND AREA = 2.10 SQIN

RUN	W LB/HR	G LB/HR-SQFT	TBA DEG.F	DTAU SEC	LAMBDA	MAX SLOPE	NTU	NST	J	NR
2	98.8	1754.	88.1	7.29	0.0031	0.709	5.35	0.0399	0.0317	96.0
4	134.0	2381.	88.3	6.01	0.0023	0.633	4.01	0.0298	0.0238	130.2
6	165.2	2934.	88.8	5.31	0.0019	0.582	3.08	0.0229	0.0182	160.4
8	199.5	3542.	89.6	4.68	0.0015	0.547	********	********	********	193.5

CORE 505C NOT AIDED

HYDRAULIC DIA = 0.002472 FT FRONTAL AREA = 10.212 SQIN FLOW LENGTH = 0.996 IN
POROSITY = 0.794 ALPHA = 1285.0 SQFT/CFT
CORE MASS = 0.171 LBM CORE SP HT = 0.200 BTU/LB-F
CORE COND = 0.42 BTU/HR-FT-F CCND AREA = 2.10 SQIN

RUN	W LB/HR	G LB/HR-SQFT	TBA DEG.F	DTAU SEC	LAMBDA	MAX SLOPE	NTU	NST	J	NR
1	100.0	1776.	86.5	7.34	0.0031	0.693	5.10	0.0379	0.0302	97.5
3	134.3	2385.	87.2	6.11	0.0023	0.672	3.80	0.0283	0.0225	130.7
5	165.3	2935.	87.0	5.45	0.0018	0.567	********	********	********	160.8
7	199.7	3567.	88.1	4.71	0.0015	0.542	********	********	********	194.1

CORE NO. CORE 510 (AIDED) DATA TAKEN ON 14 JUL 72 DATA TAKEN BY JHS

HYDRAULIC DIA = 0.001656 FT POROSITY = 0.7142 FRONTAL AREA = 10.365 SQIN KC = 1.06
FLOW LENGTH = 2.994 INCH ALPHA = 1691.0 SQFT/CFT FREE-FLOW AREA = 7.421 SQIN KE =-0.44
CORE MASS = 0.6560 LBM CORE SP HT = 0.200 BTU/LB-F COND AREA = 2.945 SQIN
CORE COND = 0.42 BTU/HR-FT-F

RUN	W LB/HR	G LB/HR-SQFT	TBA DEG.F	DTAU SEC	LAMBDA	MAX SLOPE	NTU	NST	J	NR
1	93.6	1753.	97.74	14.320	0.0016	1.311	21.27	0.03055	0.03147	72.5
3	133.7	2494.	93.00	12.230	0.0012	1.176	17.30	0.03233	0.02573	96.6
5	159.8	3080.	96.33	11.230	0.0010	1.097	14.43	0.02482	0.02135	114.5
7	201.6	3417.	96.78	9.670	0.0008	1.002	11.44	0.02207	0.01757	145.6
9	256.4	4537.	92.56	8.510	0.0006	0.934	9.43	0.01753	0.01395	184.9
11	313.8	5053.	91.81	7.640	0.0005	0.815	7.50	0.01503	0.01109	227.2
13	356.2	7461.	90.76	6.795	0.0004	0.731	5.80	0.02074	0.00858	288.7
15	499.7	9464.	91.26	5.960	0.0003	0.674	4.74	0.00682	0.00702	357.7
17	617.5	12021.	90.26	5.150	0.0003	0.613	3.44	0.00681	0.00542	449.4

CORE NO. CORE 510 (UNAIDED) DATA TAKEN ON 15 JUL 72 DATA TAKEN BY JHS

HYDRAULIC DIA = 0.001656 FT POROSITY = 0.7142 FRONTAL AREA = 10.365 SQIN KC = 1.06
FLOW LENGTH = 2.994 INCH ALPHA = 1691.0 SQFT/CFT FREE-FLOW AREA = 7.421 SQIN KE =-0.56
CORE MASS = 0.6560 LBM CORE SP HT = 0.200 BTU/LB-F COND AREA = 2.945 SQIN
CORE COND = 0.42 BTU/HR-FT-F

RUN	W LB/HR	G LB/HR-SQFT	TBA DEG.F	DTAU SEC	LAMBDA	MAX SLOPE	NTU	NST	J	NR
2	99.6	1929.	91.73	15.099	0.0016	1.135	21.06	0.03036	0.03115	72.0
4	134.9	2549.	91.49	12.489	0.0012	1.161	16.31	0.03331	0.02413	97.2
6	159.3	3066.	95.43	11.430	.0010	1.077	13.36	0.02574	0.02350	115.0
8	201.7	3914.	92.76	9.840	0.0008	0.925	11.18	0.02077	0.01652	145.9
10	254.9	4965.	90.55	8.590	0.0006	0.844	8.93	0.01671	0.01330	184.9
12	314.6	6103.	93.09	7.730	0.0005	0.806	7.26	0.01349	0.01024	228.1
14	391.3	7609.	93.48	6.860	0.0004	0.773	5.76	0.01070	0.00853	286.4
16	497.1	9477.	92.44	6.095	0.0003	0.666	4.50	0.00837	0.00666	353.8
18	620.3	12066.	88.76	5.267	0.0003	0.603	3.64	0.00644	0.00512	460.0

Periodic Technique - Heat Transfer Calculations

The measured inlet and outlet temperature variations ($x^* = 0$ and 1) of the fluid are processed using Eqs. (V-29) and (V-30)

$$D_f = \exp(-\epsilon_1 N_{tu}) \qquad \text{(V-29)}$$

$$Y_f = \epsilon_2 N_{tu} \qquad \text{(V-30)}$$

to determine the heat transfer performance. The terms ϵ_1 and ϵ_2 are listed in Tables V-1 and V-2 as functions of ψ and λN_{tu}.

Since the inlet and outlet temperature waves are not in general pure sine waves, the analysis of Appendix V is modified using Fourier Series to account for this. If only the first harmonic is considered, a general periodic temperature variation at the test core inlet can be represented by:

$$T_f(0,\theta) = \frac{B_o}{2} + A \sin\frac{2\pi}{\theta_o}\theta + B \cos\frac{2\pi}{\theta_o}\theta \qquad \text{(VII-1)}$$

where

$$A = \frac{2}{\theta_o}\int_o^{\theta_o} T_f(0,\theta)\, \sin\frac{2\pi}{\theta_o}\theta \, d\theta \qquad \text{(VII-2)}$$

$$B = \frac{2}{\theta_o}\int_o^{\theta_o} T_f(0,\theta)\, \cos\frac{2\pi}{\theta_o}\theta \, d\theta \qquad \text{(VII-3)}$$

$$T_m = \frac{B_o}{2} = \frac{1}{\theta_o}\int_o^{\theta_o} T_f(0,\theta)\, d\theta \qquad \text{(VII-4)}$$

The measured periodic response of the fluid ($x^* = 1$) can be represented in like manner by:

$$T_f(x^* = 1, \theta) = \frac{b_o}{2} + a \sin\frac{2\pi}{\theta_o}\theta + b \cos\frac{2\pi}{\theta_o}\theta \qquad \text{(VII-5)}$$

where

$$a = \frac{2}{\theta_o} \int_o^{\theta_o} T_f(x^* = 1, \theta) \sin\frac{2\pi}{\theta_o}\theta \, d\theta \qquad \text{(VII-6)}$$

$$b = \frac{2}{\theta_o} \int_o^{\theta_o} Tf(x^* = 1, \theta) \cos\frac{2\pi}{\theta_o}\theta \, d\theta \qquad \text{(VII-7)}$$

$$T_m = \frac{b_o}{2} = \frac{1}{\theta_o} \int_o^{\theta_o} T_f(x^* = 1, \theta) \, d\theta \qquad \text{(VII-8)}$$

Eqs. (VII-4) and (VII-8) serve as an experimental check on the adiabatic behavior of the test section from $x^* = 0$ to $x^* = 1$.

The above analysis is similar to that in [4] where the higher harmonics were also considered. However, the higher harmonics have no value in the heat transfer calculations, so they are deleted from this analysis.

The Fourier Coefficients in Eqs. (VII-2), (VII-3), (VII-6), and (VII-7) can be numerically determined using the Trapezoidal Rule. The temperatures, $T_f(0,\theta)$ and $T_f(x^* = 1,\theta)$, must be known simultaneously as functions of time for at least one period θ_o; this may be done graphically. Each period θ_o of these two wave functions is divided into (K-1) equal intervals with K data points. The first data point is considered as at $\theta/\theta_o = 0$ and the last as at $\theta/\theta_o = 1$. However the first point may occur at any point in real time on the wave function records, keeping it simultaneous for both the upstream and downstream records. The two temperature wave records are used in Eqs. (VII-2), (VII-3), (VII-6), and (VII-7) to obtain the Fourier Coefficients. This is done numerically using the following approximation (Trapezoidal Rule) with B as an example:

$$T_f(0,\vartheta) \approx T_f\left(0,\frac{\theta_o}{K-1}(i-1)\right) \triangleq T_{fi}(x^* = 0) \quad i = 1,2,\ldots,K \tag{VII-9}$$

$$B = \frac{1}{K-1}\left[\frac{y_1}{2} + y_2 + \ldots + y_{K-1} + \frac{y_k}{2}\right] \tag{VII-10}$$

where

$$y_i = T_{fi} \cos\left[2\pi\left(\frac{i-1}{K-1}\right)\right] \quad i = 1,2,\ldots,K \tag{VII-11}$$

Other Fourier Coefficients (A, a, and b) can be calculated in like manner by using the appropriate temperature record in Eq. (VII-9) and the associated trig function in Eq. (VII-11).

The number of data points, K, typically ranged from 30 to 50 for the results included in this appendix on Core 510. This makes the Trapezoidal Rule reasonably accurate. The number K can be either even or odd.

The temperature records were obtained with one Honeywell Electronik 19 Single-Channel Lab Recorder. To obtain the upstream and downstream temperature records, the recorder was connected to the upstream thermocouples for at least one period θ_o and then quickly switched to the downstream set for at least one period. Using the switching time as the starting point for the downstream record and then "backtracking" one period for the upstream starting point, two simultaneous wave traces were obtained.

The Fourier Coefficients are used to determine the <u>experimental</u> amplitude attenuation and phase shift as follows [4]:

$$\text{Amplitude Attenuation} = D_{f,expr} = \frac{\sqrt{a^2 + b^2}}{\sqrt{A^2 + B^2}} \tag{VII-12}$$

$$\text{Phase Shift} = \gamma_{f,expr} = \tan^{-1}\left(\frac{\frac{a}{b} - \frac{A}{B}}{1 + \frac{aA}{bB}}\right) \tag{VII-13}$$

These relationships are combined with Eqs. (V-29) and (V-30) to obtain

$$\exp(-\epsilon_1 N_{tu}) = \frac{\sqrt{a^2 + b^2}}{\sqrt{A^2 + B^2}} \qquad \text{(VII-14)}$$

$$\epsilon_2 N_{tu} = \tan^{-1}\left(\frac{\frac{a}{b} - \frac{A}{B}}{1 + \frac{aA}{bB}}\right) \qquad \text{(VII-15)}$$

Since ϵ_1 and ϵ_2 are complicated functions of $\dot{\psi}$ and λN_{tu} and

$$N_{tu} = \dot{\psi}\,\frac{\dot{C}_w}{C_f}\,\frac{2\pi}{\theta_o} \triangleq \dot{\psi}\omega^* \qquad \text{(VII-16)}$$

the above equations cannot be solved explicitly. For the case where $\lambda = 0$, using the amplitude attenuation obtained experimentally and $\epsilon_1 = 1/(1 + \dot{\psi}^2)$, Eq. (VII-14) can be solved for $\dot{\psi}$:

$$\dot{\psi} = \frac{\omega^*/2}{\ln\left(\frac{1}{D_{f,expr}}\right)} \pm \left\{\left[\frac{\omega^*/2}{\ln\left(\frac{1}{D_{f,expr}}\right)}\right]^2 - 1\right\}^{1/2} \qquad \text{(VII-17)}$$

(The plus sign is used for $\dot{\psi} > 1$, the minus sign for $\dot{\psi} < 1$.) Using the phase shift obtained experimentally and $\epsilon_2 = \dot{\psi}/(1 + \dot{\psi}^2)$, Eq. (VII-15) can be solved for $\dot{\psi}$:

$$\dot{\psi} = \frac{1}{\left[\frac{\omega}{\gamma_{f,expr}} - 1\right]^{1/2}} \qquad \text{(VII-18)}$$

A heat transfer performance parameter, N_{tu}, can now be calculated using Eq. (VII-16)

$$N_{tu} = \dot{\psi}\omega^* \qquad \text{(VII-16)}$$

These values for $\dot{\psi}$ and N_{tu} are only fully applicable if $\lambda N_{tu} = 0$. However, they are the initial values to use when entering Tables V-1 and V-2 to obtain approximate values for ϵ_1 and ϵ_2. The experimental amplitude attenuation $D_{f,expr}$ and phase shift $\gamma_{f,expr}$ can now be modified as follows to obtain corrected values that are closer to D_f and γ_f for $\lambda N_{tu} = 0$:

$$D_{f,mod} = D_{f,expr}\left[\frac{\Delta D_f}{D_{f,expr}} + 1\right] \qquad \text{(VII-19)}$$

where

$$\Delta D_f \triangleq D_{f,\lambda=0} - D_{f,expr} \qquad \text{(VII-20)}$$

and

$$\frac{\Delta D_f}{D_{f,expr}} = \frac{\exp\left(\frac{-N_{tu}}{1+\dot{\psi}^2}\right)}{\exp(-\epsilon_1 N_{tu})} - 1 \qquad \text{(VII-21)}$$

$$\gamma_{f,mod} = \gamma_{f,expr}\left[\frac{\Delta\gamma_f}{\gamma_{f,expr}} + 1\right] \qquad \text{(VII-22)}$$

where

$$\Delta\gamma_f \triangleq \gamma_{f,\lambda=0} - \gamma_{f,expr} \qquad \text{(VII-23)}$$

and

$$\frac{\Delta\gamma_f}{\gamma_{f,expr}} = \frac{\frac{\dot{\psi}}{1+\dot{\psi}^2}}{\epsilon_2} - 1 \qquad \text{(VII-24)}$$

The $D_{f,mod}$ and $\gamma_{f,mod}$ can now be used in Eqs. (VII-17) and (VII-18) to obtain new approximations for $\dot{\psi}$ and hence N_{tu}. The whole procedure can be carried through as often as needed to obtain the desired accuracy. $D_{f,mod}$ and $\gamma_{f,mod}$ converge rapidly to $D_{f,\lambda=0}$ and $\gamma_{f,\lambda=0}$. For example, in the calculations for Core 510, only two iteration cycles were used at most by the computer program; the third iteration cycle produced a change in D_f of less than 0.1 percent of $D_{f,expr}$. The total

change was 6.4 percent of $D_{f,expr}$. This is a process ideally suited to a high-speed digital computer.

Other heat transfer parameters can now be calculated using:

$$N_{tu} = \psi \omega^*$$

$$R\bar{C}_w = \frac{1}{2\pi} \frac{\theta_o}{\psi} \qquad \text{(VII-25)}$$

$$N_{St} \triangleq \frac{h}{Gc_p} = \frac{A_c}{A} \psi \omega^*$$

$$j \triangleq N_{St} N_{Pr}^{2/3}$$

The total surface area A used in the calculation of N_{St} and f, requires that the passage geometry be known. A model is used for the purpose of calculating α from more readily measurable quantities including porosity p, cell count N cells/in^2, and the cell height to width ratio d^*. The model used for Core 510, Table VII-5, is the "Revised Triangular Bayley" model [15]:

$$\alpha = 2\sqrt{pN}\ \frac{\sqrt{d^{*2} + 1} + 1}{\sqrt{d^*}} \qquad \text{(VII-26)}$$

The total area may be calculated using

$$A = \alpha L A_{fr} \qquad \text{(VII-27)}$$

The hydraulic radius, used in N_R, is defined as [14]

$$r_h = L\frac{A_c}{A} = \frac{p}{\alpha} \qquad \text{(VII-28)}$$

Friction Factor Calculations

The relation used for the calculation of the friction factor is from [14]:

$$f = \frac{A_c v_1}{A v_m}\left[\frac{\Delta P_c \times 2g_c}{G^2 v_1} - \left(K_c + 1 - p^2\right) - 2\left(\frac{v_2}{v_1} - 1\right) + \left(1 - p^2 - K_e\right)\frac{v_2}{v_1}\right] \qquad \text{(VII-29)}$$

where the subscript 1 indicates $x^* = 0$ and 2 indicates $x^* = 1$ and

$$v_m = (v_1 + v_2)/2 \qquad \text{(VII-30)}$$

The temperature used in the calculation of v_m is the time-mean temperature of the fluid leaving the heat exchanger, $T_m(x^* = 1)$.

Periodic Technique-Computer Program for Data Reduction

The data reduction program used in the periodic technique to calculate the heat transfer and flow friction characteristics is described in this section. The program is written in the Fortran IV language and was used on an IBM 360/67 computer. It is based on [4] but has been extensively refined. The program has been successfully used for a test range of $0.4 < N_{tu} < 36.6$. It is designed to be used where one temperature record is taken upstream of the heat exchanger test core and the other is taken downstream of the core. The program is not sensitive to the point in real time used as a starting point, but the upstream and downstream records must occur simultaneously.

Input Formats and Nomenclature

Input is in the form of data sets. A data set consists of test core parameters (Cards 1 through 3) followed by individual run information (Cards 4 through 8) all using the same set of core parameters. Any number of data sets may be run in series.

Card 1 This card contains the overall test identification in columns 1 through 76. A nonzero digit in column 80 is also required. This card serves a dual purpose. It initiates a new data set, and it causes a summary of the previous data set results to be listed should one exist.

Card 2 This card contains the test core parameters and geometry information for the series of test runs that follow. Each entry should contain a decimal point. The columns allotted, variable names, definitions, and dimensions are as follows:

Col. 1-8 ALF - core alpha, ft^2/ft^3
9-16 POR - core porosity
17-24 AFR - core frontal area, in^2
25-32 LENGTH - core flow length, in
33-40 WT - core weight, lbm
41-48 SPHT - core specific heat, Btu/(lbm °F)
49-56 KC - core K_c
57-64 KE - core K_c
65-72 COND - core conductivity, Btu/(hr ft °F)

Card 3 This card contains the dry bulb temperature and the wet bulb temperature for use in calculating the airstream humidity. Each entry should contain a decimal point.

Col. 1-8 TDB - dry bulb temperature, °F
9-16 TWB - wet bulb temperature, °F

Card 4 This card contains the individual test run description in columns 1 through 76. Column 80 is left blank.

Card 5

Col. 1-2 N - number of temperature points which are read for each temperature record in this test. No decimal point is needed, but right adjust.

9-16 RJ - reference junction level in millivolts for a copper-constantan thermocouple with an ice bath.

17-24 PERIOD - the period θ_o of the individual test run, sec.

Card 5

Col. 1-30 T(I) - ten of the upstream temperature data points which are read off the upstream record. As many of these cards are used as is required. Three columns are allowed for each temperature reading in microvolts, with no decimal point required, but each entry must be right justified in its 3 columns.

Card 7 This card is similar to Card 6, except downstream temperature readings in microvolts are entered.

Card 8 This card contains fluid flow rate information for each individual test run. Decimal points are required in all entries except IORF.

Col. 1 IORF - number of orifice plate used. Orifice plate number 1 is 1.301 inches in diameter and number 2 is 2.201 inches in diameter.

2-8 HEAD - orifice pressure drop, in. water

9-16 DROP - core pressure drop, in. water

17-24 BAR - ambient pressure, barometer, in. mercury

25-32 PC - depression of core inlet pressure below ambient, in. water

33-40 PO - depression of orifice inlet pressure below ambient, in. water

To compute more than one test run with the same core, Cards 4 through 8 are repeated as often as required. If the core is changed, Cards 1 through 3 must again be used. At the end of all runs, a blank card with a nonzero digit in column 80 is used to cause a summary of the last data set to be printed.

A Fortran Source Listing of the Periodic Transient Technique Data Reduction Program is presented in Table VII-3.

Additional Information on the Use of the Periodic-Test-Technique Data Reduction Program

The program consists of three parts: the main program, the subroutine CONVRS, and the subroutine CONDCT. The Main Program does the bulk of the calculations and all of the input/output. Subroutine CONVRS converts thermocouple voltage to degrees Fahrenheit. Subroutine CONDCT calculates ϵ_1 and ϵ_2 using inputs of ϕ and λN_{tu}.

A constant, CHART is included in the program as a scale factor. It provides flexibility and convenience in the type of recorder used in the thermocouple voltage input Cards 6 and 7 and the number of thermocouples used. Ultimately the scale factor is used:

$$T_{actual} = T_{input} \times CHART$$

Physical properties of the solid core material and the physical properties of air used in the periodic data reduction are identical to those described in this appendix under the Single-Blow Technique.

Description of Subroutine CONDCT

The subroutine CONDCT, Table VII-3, calculates ϵ_1 and ϵ_2 for values of ϕ and λN_{tu} and is used in the solution for the periodic technique with finite wall longitudinal conduction, Eqs. (V-25) and (V-26). It is entered by means of a fortran CALL statement. A description of the parameters in the SUBROUTINE statement follows:

LNTU - product λN_{tu}
P - nondimensional period ϕ
OED - ϵ_1 for $\lambda = 0$ or $1/(1 + \phi^2)$
OET - ϵ_2 for $\lambda = 0$ or $\phi/(1 + \phi^2)$
EO - ϵ_1 used in Eqs. (V-25) and (V-26)
ET - ϵ_2 used in Eqs. (V-25) and (V-26)

```
      C
      C     PERIODIC TRANSIENT TEST TECHNIQUE DATA REDUCTION PROGRAM
      C
      1     REAL LENGTH,NTU,NTUA,KC,KE,MU ,LAMBDA,LNTU
      2     DIMENSION ALPH(19),BET(19)
      3     DIMENSION BF(150),AF(150),B(11,2),A(11,2),MM(11),T(150)
      4     DIMENSION AW(20),IG(20),NR(20),PE(20),PSA(20),ANTA(20),ARC(20),AST
           1PR(20),SPSS(20),SNTA(20),SRC(20),SSTPRR(20),AAR(20)  ,ALAM(20)
      5     PR=0.710
      6     TCON=0.0
      7     CHART=0.5
      8     NC=0
      9     BAR=0.0
      C
      C     READING THE TEST CORE PARAMETERS
      C
     10  1  READ(5,69) ALPH, INACT
     11  69 FORMAT(19A4,3X,I1)
     12     IF(INACT.EQ.0) GO TO 3
     13     IF(NC.NE.0) GO TO 46
     14  46 DO 47 JO=1,19
     15  47 BET(JO)=ALPH(JO)
     16     READ(5,480,END=60)ALF,POR,AFR,LENGTH,WT,SPHT,KC,KE ,COND
     17     AWALL=AFR*(1.0-POR)/144.
     18     AC=POR*AFR
     19     READ(5,460)TDB,TWB
     20     CW=WT*SPHT
     21     AT=ALF*AFR*LENGTH/1728.
     22     STP=(AC/AT)*PR**(2./3.)/144.
     23     NC=0
     24     GO TO 1
      C
      C     READING THE DATA FOR EACH INDIVIDUAL TEST CASE
      C
     25  3  READ(5,481)N,RJ,PERIOD
     26     NC=NC+1
     27     DO 2 L=1,2
     28     READ(5,580)(T(I),I=1,N)
     29     GO TO (41,42),L
     30  41 WRITE(6,488)
     31     WRITE(6,54) ALPH
     32  54 FORMAT(1X,19A4/)
     33     WRITE(6,487)
     34     GO TO 26
     35  42 WRITE(6,489)
     36  26 CONTINUE
     37     WRITE(6,482)(J,T(J),J=1,N)
     38     RJT=RJ
      C
      C     CONVERTING MILLIVOLTS TO DEGREES F
      C
     39     DO 19 I=1,N
     40     T(I)=T(I)*CHART+32
     41  19 CALL CONVRS(T(I),TCON)
     42     CALL CONVRS(RJT,TCON)
     43     WRITE(6,482)(J,T(J),J=1,N)
     44     WRITE(6,499)
     45     DSIG=1./FLOAT(N-1)
     46     PI=3.1415926
```

```
      C
      C     FINDING THE FOURIER COEFFICIENTS
      C
   47       DO 21 NN=1,11
   48       SIG=0.0
   49       N1=NN-1
   50       N2=N-1
   51       BR=2.*PI*SIG*FLOAT(N1)
      C
      C     TRAPEZOIDAL RULE INTEGRATION
      C
   52       AF(1)=T(1)*SIN(BR)/2.0
   53       BF(1)=T(1)*COS(BR)/2.0
   54       DO 30 J=2,N
   55       SIG=SIG+DSIG
   56       BR=2.0*PI*SIG*FLOAT(N1)
   57       AF(J)=T(J)*SIN(BR)
   58    30 BF(J)=T(J)*COS(BR)
   59       AF(N)=AF(N)/2.
   60       BF(N)=BF(N)/2.
   61       B(NN,L)=0.0
   62       A(NN,L)=0.0
   63       DO 40 K=1,N
   64       B(NN,L)=B(NN,L)+BF(K)
   65    40 A(NN,L)=A(NN,L)+AF(K)
   66       B(NN,L)=B(NN,L)/(0.5*FLOAT(N2))
   67    21 A(NN,L)=A(NN,L)/(0.5*FLOAT(N2))
   68       DO 27 KI=1,33
   69    27 NN(KI)=KI-1
   70       WRITE(6,495)(NN(I),A(I,L),I=1,11)
   71       WRITE(6,496)(NN(I),B(I,L),I=1,11)
   72       WRITE(6,510)
   73    2  CONTINUE
   74       TMEAN=B(1,2)/2.
   75       MU=0.0425+(5.1E-05)*(TMEAN-40.3)+1.E-07*(TMEAN-40.3)**2
      C
      C     CALCULATING THE FLOW PARAMETERS
      C
   76       READ(5,560)IORF,HEAD,DROP,BAR,PC,PO
   77       WRITE(6,509)BAR,RJT,TCON,TMEAN,TDB,TWB,ALF,KC,KE,MT
   78       P1=BAR*70.73-PC*5.204
   79       P2=P1-DROP*5.204
   80       P3=P1-PO*5.204
   81       P4=P3-HEAD*5.204
   82       X=(P3-P4)/P3
   83       T1=459.67+TMEAN
      C
      C     DENSITY CORRECTION FACTORS
      C
   84       H=0.0196919-0.000679526*TWB+  8.91667E-06*TWB**2-0.000232*
           1(TDB-TWB)
   85       XV=(1.0+1.607*H)/(1.0+H)
      C
      C     SPECIFIC HEAT OF AIR
      C
   86       CP=(0.87*H+1.000)*0.24
   87       V1=(XV*53.34*T1)/P1
   88       V2=V1*P1/P2
   89       V3=V1*P1/P3
   90       V4=V1*P1/P4
```

```
      C
      C     SSLECTING THE PROPER FLOW COEFFICIENTS
      C
   91       GO TO (11,22),IORF
   92    11 CF=0.6053
   93       BETA=0.4252
   94       DIAO=1.30
   95       DC=0.0127
   96       GO TO 50
   97    22 CF=0.7100
   98       BETA=0.7193
   99       [illegible]
  100       [illegible]
  101    50 [illegible]  (41+0.35*BETA**4)*X/1.4
  102       WH=359.*CF*(DIAO**2)*SQRT(HEAD/V3)*Y
  103       RD=48.*WH/(PI*DIAO*MU)
  104       CF=CF+DC*(1.0E+04/RD)**0.5
  105       WH=359.*CF*(DIAO**2)*SQRT(HEAD/V3)*Y
  106       WS=WH/3600.
  107       LAMBDA=COND*AWALL*12./(LENGTH*WH*CP)
  108   560 FORMAT(I1,F7.2,5E8.2)
  109       DH=4.*AC*LENGTH/(AT*1728.)
  110       NREYNO=WH*DH*144.0/(MU*AC)
  111       WRITE(6,510)
  112       WRITE(6,505)
  113       WRITE(6,506)
  114       WRITE(6,507)
  115       G=WH*144.0/AC
      C
      C     CALCULATING THE FRICTION FACTOR
      C
  116       VM=(V1+V2)/2.0
  117       GS=WS*144.0/AC
  118       F=((DROP*5.204*2.0*32.2)/(GS**2*V1)-((KC+1.0-POR**2)+2.0*(V2/V1-1.
           10)-(1.0-POR**2-KE)*V2/V1))*AC*V1/(AT*VM*144.0)
  119       PRINT 508,IORF,HEAD,DROP,LAMBDA,WH,AT,AC,AFR,LENGTH,CW,DH,PERIOD,
           1NREYNO,G,F
  120       WRITE (6,510)
  121       WRITE(6,499)
  122       WRITE(6,494)
  123       WRITE(6,499)
  124       WRITE(6,498)
      C
      C     USING THE FOURIER COEFFICIENTS
      C
      C     PHASE SHIFT COMPARISON
      C
  125       DO 24 JJ=1,5
  126       IF(N.EQ.3) GO TO 35
  127       WNS=FLOAT(JJ)*(2.*PI*CN)/(PERIOD*WS*CP)
  128       JK=JJ+1
  129       ERNN=ATAN2((A(JK,2)/B(JK,2)-A(JK,1)/B(JK,1)),(1.+A(JK,
           12)*A(JK,1)/(B(JK,1)*B(JK,2))))
  130       IF((ERNN.GT.0.0).AND.(WNS.GT.3.00)) GO TO 72
  131       IF((ERNN.LT.0.0).AND.(WNS.GT.4.25)) GO TO 71
  132       IF(ERNN.LT.0.0) GO TO 72
  133       GO TO 73
  134    71 ERNN=ERNN+PI
  135    72 ERNN=ERNN+PI
  136    73 CONTINUE
```

```
      NGF=0
      DGF=0.0
      CDGF=0.0
74    GERM=GRMM*DGF
      TERMM=WNS/GERM
      IF(TERMM.LT.(1.0)) GO TO 8
      FEE=1./SQRT(TERMM-1.0)
      RCC=PERIGO/(FLOAT(JJ)*2.*PI*FEE)
      NTU=FEE*WNS
      IF(JJ.NE.1) GO TO 76
      LNTU=LAMBDA*NTU
      CALL CONDCT(LNTU,FEE,OEO,OET,EO,ET)
      DGF=(OET-ET)*KTU
      IF(ABS(CDGF-DGF).LT..001*ERMM) GO TO 76
      CDGF=DGF
      NGF=NGF+1
      GO TO 74
75    CONTINUE
C
C     AMPLITUDE ATTENUATION COMPARISON
C
      NDF=0
      DDF=0.0
      ODDF=0.0
78    ATEN=SQRT((A(JK,2)**2+B(JK,2)**2)/(A(JK,1)**2+B(JK,1)**2))
      BTEN=ATEN*DDF
      TERM=WNS/(2.0*LOG(1.0/BTEN))
      IF(TERM.LT.(1.0)) GO TO 88
      FEP=TERM+SQRT(TERM**2-1.0)
      FEM=TERM-SQRT(TERM**2-1.0)
      FE=FEP
      IF(FEE.LT.1.2.OR.FEMP.GT.PI.AND.ATEN.GT..2)FE=FEM
      NTUA=FE*WNS
      IF(JJ.NE.1) GO TO 77
      LNTU=LAMBDA*NTUA
      CALL CONDCT(LNTU,FE,OEO,OET,EO,ET)
      DDF=EXP(-OEO*NTUA)-EXP(-EO*NTUA)
      IF(ABS(ODDF-DDF).LT..001*ATEN) GO TO 77
      ODDF=DDF
      NDF=NDF+1
      GO TO 78
77    CONTINUE
      RC=PERIOD/(FE*2.*PI*FLOAT(JJ))
      GO TO 89
88    FE=0.0
      RC=0.0
      PER=0.0
      RCC=0.0
89    NTUA=FE*WNS
      STPRR=NTU*STP
      STPR=NTUA*STP
C
C     OUTPUT OF TEST RESULTS
C
      WRITE(6,497)JJ,FE,NTUA,RC,STPR,FEE,NTU,RCC,STPRR,ATEN,ERMM,NDF,NGF
      IF(JJ.NE.1) GO TO 24
35    AW(NC)=WH
      AAF(NC)=F
      IG(NC)=G
      NR(NC)=NREYNO
```

```
      IF(N.EQ.3) GO TO 24
      PE(NC)=PERIOD
      PSA(NC)=FE
      ANTA(NC)=NTUA
      ARC(NC)=RC
      ASTPR(NC)=STPR
      SPSS(NC)=FEE
      SNTA(NC)=NTU
      SRC(NC)=REC
      SSTPRR(NC)=STPRR
      ALAM(NC)=LAMBDA
      GO TO 24
 9    WRITE(6,491)
 24   CONTINUE
      GO TO 1
 48   DO 61 NCT=1,3
      WRITE(6,150)
 150  FORMAT(1H1,33X,'PERIODIC TECHNIQUE EXPERIMENTAL RESULTS'//)
      WRITE(6,51)BET
 51   FORMAT(30X,19A4//)
      WRITE(6,52)DH,AFR,LENGTH,POR,ALF,WT,SPHT,TDB,TWB,BAR,KC,KE,COND
 52   FORMAT(T25,'HYDRAULIC DIA =',F8.5,' FT ',
     1T70,'FRONTAL AREA =',F8.3,' SQIN'/T25,
     2'FLOW LENGTH   =',F8.3,' IN ',T70,'POROSITY      =',
     3F8.3/T25,'ALPHA          =',F8.1,
     4 ' SQFT/CFT',T70,'CORE MASS     =',F8.3,' LBM '/
     5T25,'CORE SP HT     =',F8.3,' BTU/LB-F ',
     6T70,'DRY BULB TEMP=',F8.2,' F'/T25,'WET BULB TEMP =',
     7F8.2,' F',T70,'BAROMETER     =',F8.2,' IN HG '/T25,
     8'KC              =',F8.3,T70,'KE             =',F8.3/
     9T25,'CORE COND.     =',F8.4,' BTU/HR-FT-F'//)
      WRITE(6,300)
      WRITE(6,301)
      WRITE(6,302)
      DO 45 JA=1,NC
 45   PRINT 303,AW(JA),TG(JA),NR(JA),PE(JA),ALAM(JA),PSA(JA),ANTA(JA),AR
     1C(JA), ASTPR(JA),SPSS(JA),SNTA(JA),SRC(JA),SSTPRR(JA),AAF(JA)
 61   CONTINUE
      WRITE(6,488)
      GO TO 46
 300  FORMAT(45X,'AMPLITUDE ATTENUATION',9X,'PHASE SHIFT')
 301  FORMAT(10X,'W',7X,'G',6X,'NR   PERIOD LAMBDA   PSI   NTU   RCW
     1 J    PSI   NTU   RCW     J',7X,'F')
 302  FORMAT(8X,'LB/HR    W/SQFT',9X,'SEC.',23X,'SEC.',21X,'SEC.'/ )
 303  FORMAT(7X,F6.1,2I7,F8.2,1X,F7.4,1X,2(F5.2,F7.2,F6.2,F7.4),F8.4)
 500  FORMAT(1X,F12.4)
 487  FORMAT(1HO,8HUPSTREAM)
 489  FORMAT(1H ,10HDOWNSTREAM)
 488  FORMAT(1H1)
 499  FORMAT(1H )
 494  FORMAT(23X,20HAMPLITUDE COMPARISON,15X, 'PHASE SHIFT COMPARISON
     1       AMPLITUDE ATTENUATION   PHASE  SHIFT')
 496  FORMAT(1X,4HB     ,11(I3,F8.3))
 495  FORMAT(1X,4HA     ,11(I3,F8.3))
 491  FORMAT(1X,17HSOLUTION NOT REAL  )
 480  FORMAT(10E8.4)
 482  FORMAT(10(1X,I3,F7.3))
 481  FORMAT(I2,6X,2E8.4)
 497  FORMAT(18X,I1,2(2F7.3,F7.2,F9.5,5X), 1X,F9.3,10X,F12.3,2I5)
 498  FORMAT(18X,75HN    PSI    NTU     RCW  STPR2/3        PSI    NTU
```

```
     1  ROW  STP82/3                                    )
239  501  FORMAT(F4.1,I4,F6.1,4F5.4,2I2F5.2,F5.1,F7.4)
240  502  FORMAT(6F3.3)
241  510  FORMAT(1X,131(1H=))
242  505  FORMAT(1HO,58X,15HTEST PARAMETERS  )
243  506  FORMAT(1HO,131HORIFICE ORIFICE CORE LAMBDA  AIR    SURFACE  M
     1IN. FLOW  FRONTAL  LENGTH CORE  HYDRAULIC PERIOD REYNOLDS  M
     2ASS  FRICTION       )
244  507  FORMAT(1X ,131H NO.     DROP    DROP          LBS/HR.  AREA
     1  AREA      AREA     NO.   CAP.    DIAMETER  SEC-     NO.   VEL
     2OCITY  FACTOR                )
245  508  FORMAT(1X,I4,F11.2,F?.2,F8.4,F8.3,F9.2,F11.3,F10.3,F8.2,F9.2,F11.4
     1,F9.2,I9,F12.2,F9.4)
246  509  FORMAT(1H ,10HBAROMETER=,F6.2,5X,19HREFERENCE JUNCTION=,F7.3,5X,34
     1H THERMOCOUPLE COMPENSATION FACTOR=, F7.3,5X,15HAIR TEMPERATURE=,F
     28.3/' DRY BULB TEMP =',F6.1,5X,'WET BULB TEMP =',F6.1,5X,'ALPHA =
     3',F7.1,5X,'XC = ',F8.2,5X,'ZE = ',F8.3,5X,'CORE MASS = ',F8.3)
247  60   STOP
249       END


249       SUBROUTINE CONVRT(AT,TCON)
     C
     C    THIS PROGRAM CONVERTS MILLIVOLTS TO DEGREES F
     C
250       DIMENSION V(14)
251       DATA V(1),V(2),V(3),V(4),V(5),V(6),V(7),V(8),V(9),V(10),V(11),V(12
          1),V(13),V(14)/0.171,0.339,0.459,0.832,1.057,1.284,1.517,1.751,1.98
          27,2.225,2.467,2.711,2.958,3.207/
252       AT=AT*(1.0-TCON)
253       J=0
254  88   J=J+1
255       IF(AT.GE.V(J)) GO TO 88
256       AT=(AT-V(J-1))*10.0/(V(J)-V(J-1))+FLOAT(10*(J-2))
257       RETURN
258       END


259       SUBROUTINE CONDCT(LNTU,P,DEO,DET,EO,ET)
     C
     C    THIS ROUTINE CALCULATES E1 AND E2 FOR FINITE WALL
     C    LONGITUDINAL CONDUCTION
     C
260       REAL LNTU,H,K
261       J=0
262       EO=1.0/(1.0+P**2)
263       ET=P*EO
264       DEO=EO
265       DET=ET
266  50   PFOREO=-1.0-LNTU*(-3.0*EO**2+2.0*EO+3.0*ET**2)
267       PFORET=1.0/P-LNTU*(-2.0*ET+6.0*EO*ET)
268       PFTREO=-1.0/P-LNTU*(-6.0*EO*ET+2.0*ET)
269       PFTRET=-1.0-LNTU*(3.0*ET**2-3.0*EO**2+2.0*EO)
270       FO=-EO+ET/P-LNTU*(-EO**3+EO**2-ET**2+3.0*EO*ET**2)
271       FT=(1.0-EO)/P-ET-LNTU*(ET**3-3.0*EO**2*ET+2.0*EO*ET)
272       D=PFOREO*PFTRET-PFTREO*PFORET
273       H=(-FO*PFTRET+FT*PFORET)/D
274       K=(-PFOREO*FT+PFTREO*FO)/D
275       EO=EO+H
276       ET=ET+K
277       J=J+1
278       IF((ABS(H).LT..001*EO).AND.(ABS(K).LT..001*ET)) GO TO 27
279       GO TO 50
280  27   RETURN
281       END
```

The Newton-Raphson method [16] is used to find the roots of Eqs. (V-27) and (V-28). This is an iterative method. Initial guesses used are for $\epsilon_1 = 1/(1 + \psi^2)$ and $\epsilon_2 = \psi/(1 + \psi^2)$, the $\lambda = 0$ case. Convergence is very rapid and iteration is stopped when the correction becomes less than 0.1 percent of ϵ_1 or ϵ_2. This occurred during the third iteration in the extreme case with $\lambda N_{tu} = 3.5$ and $\psi = 6$.

Periodic Technique - Output of Test Results

Two forms of the output are provided by the periodic technique data reduction program. For each run, a basic listing of thermocouple voltage inputs, the corresponding temperatures, the Fourier coefficients, core parameters, and flow rate parameters, along with heat transfer and flow friction results are provided. At the end of each data set, a summary of all the runs for the set is listed. The nomenclature for this listing is given in Table VII-4 and the results of testing Core 510 are presented in Table VII-5.

Table VII-4

NOMENCLATURE FOR PERIODIC TECHNIQUE RESULTS

W	Flowrate, lbm/hr
G	Mass velocity, lbm/(hr ft^2)
NR	Reynolds number, dimensionless
PERIOD	Period of oscillation θ_o, sec.
LAMBDA	λ, heat transfer conduction parameter
PSI	ψ, nondimensional period of oscillation
NTU	N_{tu}, dimensionless
RCW	$R\bar{C}_w$, time constant of the core solid material, sec.
J	Colburn j factor $N_{St}N_{Pr}^{2/3}$, dimensionless
F	Friction factor, f, dimensionless

Note: The parameters PSI, NTU, RCW, and J are presented twice. The first set for the amplitude attenuation method uses Eq. (VII-17) to compute ψ. The second set for the phase shift uses Eq. (VII-18) to compute ψ. Although both are presented for each run, only the results of the recommended method, Fig. 7.3, should be considered useful.

Table VII-5

PERIODIC TECHNIQUE EXPERIMENTAL RESULTS

CORE NO. 510 (CORNING L-20121 16 JUL 70 JHS

HYDRAULIC DIA	= 0.00169 FT	FRONTAL AREA	= 10.248 SQIN
FLOW LENGTH	= 2.734 IN	POROSITY	= 0.716
ALPHA	= 1691.0 SQFT/CFT	CORE MASS	= 0.687 LBM
CORE SP HT	= 0.200 BTU/LB-F	DRY BULB TEMP	= 79.00 F
WET BULB TEMP	= 63.00 F	BAROMETER	= 29.95 IN HG
KC	= 1.060	KE	= -0.560
CORE COND.	= 0.4200 BTU/HR-FT-F		

					AMPLITUDE ATTENUATION					PHASE SHIFT				
W LB/HR	G W/SQFT	NR	PERIOD SEC.	LAMBDA	PSI	NTU	PCH SEC.	J		PSI	NTU	PCH SEC.	J	F
61.8	1190	44	34.60	0.0025	6.36	36.57	0.87	0.0541	3.33	19.13	1.65	0.0283	0.2574	
102.7	1992	74	26.00	0.0015	5.15	22.91	0.83	0.0339	3.42	15.20	1.35	0.0225	0.1538	
130.8	2537	95	23.40	0.0012	4.50	18.09	0.83	0.0267	3.32	13.20	1.13	0.0196	0.1200	
157.8	3062	114	22.54	0.0010	4.41	15.25	0.91	0.0226	3.78	11.67	1.06	0.0173	0.1001	
200.6	3892	145	19.56	0.0008	3.80	11.90	0.82	0.0176	3.05	9.54	1.02	0.0141	0.0791	
248.2	4816	180	17.76	0.0006	3.38	9.47	0.84	0.0139	2.81	7.84	1.00	0.0116	0.0643	
312.1	6055	226	16.00	0.0005	3.19	7.86	0.80	0.0116	2.60	6.60	0.98	0.0098	0.0515	
391.6	7599	284	9.47	0.0004	1.83	6.07	0.82	0.0090	1.76	5.03	0.86	0.0084	0.0413	
485.8	9427	352	8.10	0.0003	1.50	4.65	0.87	0.0069	1.96	4.01	0.84	0.0071	0.0	
572.1	11100	415	7.22	0.0003	1.36	4.06	0.84	0.0060	1.36	4.06	0.84	0.0060	0.0390	
779.7	15129	566	6.12	0.0002	1.38	3.55	0.71	0.0053	1.22	3.14	0.90	0.0046	0.0223	
977.4	18964	711	5.64	0.0002	1.20	2.69	0.79	0.0040	1.14	2.56	0.79	0.0038	0.0184	

Unclassified

Security Classification

DOCUMENT CONTROL DATA - R & D

(Security classification of title, body of abstract and indexing annotation must be entered when the overall report is classified)

Stanford University
Mechanical Engineering Department
Stanford, California 94305

Unclassified

Some Contributions to the Techniques for Testing Compact Heat Exchanger Surfaces

John E. Sunn

December 1970	120	17

Nonr 225(91)

TR No. 74

The distribution of this document is unlimited.

Office of Naval Research
NR-090-342
Washington, D.C. 20360

Two techniques for testing compact heat exchangers are refined. They are the maximum-slope variation of the single-blow transient technique, and the regular periodic technique.

The maximum-slope method is improved by using an electronic control to produce a very fast heater response, thereby generating a sharper step change in airstream temperature. The design method for the electronic control is presented along with an experimental verification of its functi.n. A 40 to 60 percent reduction in the heater system time constant was achieved. This produced an average increase in experimental heat transfer results of 4 percent, for five glass-ceramic matrix surfaces tested.

The periodic technique is improved by establishing guidelines for use over a range $0.2 < N_{tu} < 35.6$. This range was limited by test rig capabilities with respect to air flow rate and heater power, not the test technique. Periodic technique results are compared with maximum-slope method results $3.6 < N_{tu} < 21.3$. The agreement is excellent.

DD Form 1473

Unclassified

Security Classification

14. KEY WORDS	LINK A		LINK B		LINK C	
	ROLE	WT	ROLE	WT	ROLE	WT
Compact heat exchangers, testing techniques						
Periodic technique for testing compact heat exchangers						
Compact heat exchangers, design data						